

Guaranteed Sampling Flexibility for Low-tubal-rank Tensor Completion

Bowen Su

SUBOWEN@MSU.EDU

Department of Mathematics, Michigan State University, East Lansing, MI 48824, USA

Juntao You

JTYOU@SZU.EDU.CN

Institute for Advanced Study, Shenzhen University, Shenzhen 518000, China

HanQin Cai

HQCAI@UCF.EDU

Department of Statistics and Data Science and Department of Computer Science, University of Central Florida, Orlando, FL 32816, USA

Longxiu Huang*

HUANGL3@MSU.EDU

Department of Computational Mathematics, Science and Engineering, Department of Mathematics, Michigan State University, East Lansing, MI 48824, USA.

Abstract

While Bernoulli sampling is extensively studied in tensor completion, t-CUR sampling approximates low-tubal-rank tensors via lateral and horizontal subtensors. However, both methods lack sufficient flexibility for diverse practical applications. To address this, we introduce Tensor Cross-Concentrated Sampling (t-CCS), a novel and straightforward sampling model that advances the matrix cross-concentrated sampling concept within a tensor framework. t-CCS effectively bridges the gap between Bernoulli and t-CUR sampling, offering additional flexibility that can lead to computational savings in various contexts. A key aspect of our work is the comprehensive theoretical analysis provided. We establish a sufficient condition for the successful recovery of a low-rank tensor from its t-CCS samples. In support of this, we also develop a theoretical framework validating the feasibility of t-CUR via uniform random sampling and conduct a detailed theoretical sampling complexity analysis for tensor completion problems utilizing the general Bernoulli sampling model. Moreover, we introduce an efficient non-convex algorithm, the Iterative t-CUR Tensor Completion (ITCURTC) algorithm, specifically designed to tackle the t-CCS-based tensor completion. We have intensively tested and validated the effectiveness of the t-CCS model and the ITCURTC algorithm across both synthetic and real-world datasets.

Keywords: tensor decomposition, tensor completion, tensor Cross-Concentrated Sampling (t-CCS), low-rank tensor approximation, t-CUR decomposition

*. Corresponding author

1. Introduction

A tensor, as a multidimensional generalization of a matrix, provides an intuitive representation for handling multi-relational or multi-modal data such as hyperspectral data [8, 61, 68], videos [35, 48], seismic data [16, 43], and DNA microarrays [40]. However, in real-world scenarios, it is common to encounter situations where only partial observations of the tensor data are available due to unavoidable or unforeseen circumstances. These limitations can stem from factors such as data collection issues or errors made during data entry by researchers. The problem of recovering the missing data by effectively leveraging the available observations is commonly referred to as the Tensor Completion (TC) problem.

The TC problem is inherently complex and often ill-posed [19, 67], necessitating the exploration of various sampling models and completion techniques. A common and crucial assumption for resolving TC is the low-rank structure of the tensor, which has been extensively utilized to enhance TC approaches [3, 35, 64]. However, the concept of tensor rank is not unique and has its own limitations. For example, the CANDECOMP/PARAFAC (CP) rank represents the minimum number of rank-one tensors required to achieve the CP decomposition, involving summations of these tensors [24]. Computing the CP rank—an NP-hard problem—presents difficulties in the recovery of tensors with a low CP rank [30]. Thus, finding the optimal low-CP-rank approximation of the target tensor is still an open problem [67]. Other tensor ranks, such as Tucker [55], Tensor Train [41], tubal [32] and Hierarchical-Tucker [18, 20], to name a few, also play prominent roles in the field, each with its distinct computation and application implications.

In this study, we focus on the low-tubal-rank model for TC. The tubal-rank is defined based on the tensor decomposition known as tensor Singular Value Decomposition (t-SVD), which employs the tensor-tensor product (t-product) [31]. In t-SVD, a tensor is decomposed into the t-product of two orthogonal tensors and an f -diagonal tensor. The tubal-rank is then determined by the number of non-zero singular tubes present in the f -diagonal tensor. Previous research has shown that models based on tubal-rank exhibit superior modeling capabilities compared to other rank-based models, particularly for tensors with fixed orientation or specific spatial-shifting characteristics [44, 62]. In low-tubal-rank TC model, we consider a tensor $\mathcal{T} \in \mathbb{K}^{n_1 \times n_2 \times n_3}$ with tubal-rank r and observed locations in Ω . Our goal is to recover the original tensor \mathcal{T} from the observations on Ω . Mathematically, we formulate the problem as:

$$\min_{\tilde{\mathcal{T}}} \langle \mathcal{P}_\Omega(\mathcal{T} - \tilde{\mathcal{T}}), \mathcal{T} - \tilde{\mathcal{T}} \rangle, \quad \text{subject to tubal-rank}(\tilde{\mathcal{T}}) = r, \quad (1)$$

where $\langle \cdot, \cdot \rangle$ denotes the Frobenius inner product, and \mathcal{P}_Ω is the sampling operator defined by

$$\mathcal{P}_\Omega(\mathcal{T}) = \sum_{(i,j,k) \in \Omega} [\mathcal{T}]_{i,j,k} \mathcal{E}_{i,j,k}, \quad (2)$$

where $\mathcal{E}_{i,j,k} \in \{0, 1\}^{n_1 \times n_2 \times n_3}$ is a tensor with all elements being zero except for the element at the position indexed by (i, j, k) .

For successful recovery, the general setting of an efficient solver for (1) requires the observation set Ω to be sampled entry-wise, fiber-wise, or slab-wise through a certain unbiased stochastic process, including the Bernoulli sampling process as referenced in [47, 49, 52, 56] and the uniform sampling process as referenced in [26, 50, 64]. Although extensive theoretical and empirical studies have been conducted on these sampling settings, their practical applicability is sometimes limited in certain contexts. For instance, in collaborative filtering applications, each dimension of the three order tensor data typically represents users, rated items (such as movies or products), and time, respectively. The unbiased sampling models implicitly assume that all users are equally likely to rate all items over time, a premise that is often unrealistic in real-world scenarios. Let's consider the application of Magnetic Resonance Imaging (MRI) as another example. MRI scans face limitations with certain metal implants and can cause discomfort in prolonged sessions [1].

To address these issues, we propose a generalization of the cross-concentrated sampling model to the TC setting based on the cross-concentrated sampling model for matrix completion [10], termed tensor Cross-Concentrated Sampling (t-CCS). t-CCS enables partial observations on selected horizontal and lateral subtensors, making it more practical in many applications.

1.1 Main contributions

This paper bridges Bernoulli sampling and t-CUR sampling in TC problems by introducing a new sampling model termed tensor Cross-Concentrated Sampling (t-CCS). The main contributions of this work are as follows:

- (i) We extend the matrix cross-concentrated sampling model [10] to tensor setting, termed t-CCS (see Section 3). We establish a sufficient condition for the reliable recovery of low-rank tensors from t-CCS samples. Although our research primarily concentrates on third-order tensors, our theoretical analysis provides a more comprehensive understanding of the underlying principles. While third-order tensors can be flattened into block diagonal matrices, the interdependent sampling properties of the index set prevent the direct application of matrix Chernoff inequalities. Additionally, to the best of our knowledge, no existing tensor completion results based on the tubal rank setting explicitly express numerical constants within their theorem statements, in contrast to matrix completion results such as those detailed in [45, Theorem 1.1]. While typical tensor-related results, such as [64, Theorem 3.1], only imply numerical constants implicitly, our work makes a significant contribution by providing a detailed analysis and explicitly stating these constants (see Section 3.1 for more details).

- (ii) We develop an efficient non-convex solver called Iterative t-CUR Tensor Completion (ITCURTC) for t-CCS-based TC problem in Section 4. Specifically, for a TC problem of size $n_1 \times n_2 \times n_3$, the computational cost per iteration is only $\mathcal{O}(r|I|n_2n_3 + r|J|n_1n_3)$ provided $|I| \ll n_1$, $|J| \ll n_2$.
- (iii) In Section 5, we demonstrate the flexibility of the t-CCS model in sampling and the efficiency of its corresponding algorithm in accurately reconstructing low-tubal-rank tensors, as evidenced by tests on synthetic datasets. We also demonstrate the practicality and real-world utility of the t-CCS model through our ITCURTC algorithm, which effectively balances runtime efficiency and reconstruction quality, making it suitable for applications requiring such a trade-off, as evidenced by extensive numerical experiments on real-world datasets.

1.2 Related work

1.2.1 Tensor completion in tubal-rank setting

[31] introduced the concepts of tensor multi-rank and tubal-rank characterized by t-SVD. Researchers often use a convex surrogate to tubal-rank function augmented with regularization of the tensor nuclear norm (TNN), as discussed in [28, 29, 36, 37, 64, 69]. While a pioneering optimization method featuring TNN was initially proposed to tackle the TC problem in [65], this approach requires minimizing all singular values across tensor slices, which hinders its ability to accurately approximate the tubal-rank function [25, 60]. To address this challenge, various truncated methods have been introduced. Notably, examples include the truncated nuclear norm regularization [25] and the tensor truncated nuclear norm (T-TNN) [60]. Furthermore, [63] introduced a novel strategy for low-rank regularization, focusing on non-local similar patches. However, these tensor completion algorithms are primarily designed based on the Bernoulli sampling model, which often encounters practical limitations in real-world data collection scenarios [17, 42]. In collaborative filtering, where the tensor’s horizontal and lateral slices represent users and rated objects (such as movies and merchandise) over a specific time period, the Bernoulli sampling model implicitly assumes that every user is equally likely to rate any given object. This assumption rarely holds in real-world scenarios. The variability in user preferences and interaction patterns renders this equal-probability assumption unrealistic, thereby compromising the effectiveness of the Bernoulli sampling approach in these contexts.

1.2.2 t-CUR decompositions

The t-CUR decomposition, a self-expressiveness tensor decomposition of a 3-mode tensor, has received significant attention [2, 13, 21, 51]. Specifically, it involves representing a tensor $\mathcal{T} \in \mathbb{K}^{n_1 \times n_2 \times n_3}$ as $\mathcal{T} \approx \mathcal{C} * \mathcal{U} * \mathcal{R}$, with $\mathcal{C} = [\mathcal{T}]_{:,J,:}$ and $\mathcal{R} = [\mathcal{T}]_{I,,:}$ for some $J \subseteq [n_2]$ and $I \subseteq [n_1]$. There exist different versions of \mathcal{U} . Our work focuses on the t-CUR decomposition of the form $\mathcal{T} \approx \mathcal{C} * \mathcal{U}^\dagger * \mathcal{R}$ with $\mathcal{U} = [\mathcal{T}]_{I,J,:}$, and conditions

for exact t-CUR decompositions have been detailed in [13, 21]. Let’s first define the tubal-rank and multi-rank of a tensor:

Definition 1 (Tubal-rank and multi-rank) *Suppose that the tensor $\mathcal{T} \in \mathbb{K}^{n_1 \times n_2 \times n_3}$ satisfies $\text{rank}([\widehat{\mathcal{T}}]_{:, :, k}) = r_k$ for $k \in [n_3]$, where $\widehat{\mathcal{T}} = \text{fft}(\mathcal{T}, [], 3)$. Then $\vec{r} = (r_1, r_2, \dots, r_{n_3})$ is called the multi-rank of \mathcal{T} , denoted by $\text{rank}_m(\mathcal{T})$. In addition, $\max\{r_i : i \in [n_3]\}$ is called the tubal-rank of \mathcal{T} , denoted by $\text{rank}(\mathcal{T})$. We denote tubal-rank as r or $\|\vec{r}\|_\infty$, and $\|\vec{r}\|_1$ for the sum of the multi-rank.*

For convenience, we present a result about the exact t-CUR decomposition below.

Theorem 1 ([13]) Let $\mathcal{T} \in \mathbb{K}^{n_1 \times n_2 \times n_3}$ with multi-rank $\text{rank}_m(\mathcal{T}) = \vec{r}$. Let $I \subseteq [n_1]$ and $J \subseteq [n_2]$ be two index sets. Denote $\mathcal{C} = [\mathcal{T}]_{:, J, :}$, $\mathcal{R} = [\mathcal{T}]_{I, :, :}$, and $\mathcal{U} = [\mathcal{T}]_{I, J, :}$. Then $\mathcal{T} = \mathcal{C} * \mathcal{U}^\dagger * \mathcal{R}$ if and only if $\text{rank}_m(\mathcal{C}) = \text{rank}_m(\mathcal{R}) = \vec{r}$.

As demonstrated in Theorem 1, the success of the exact t-CUR decomposition depends on the careful selection of the indices I and J . Our work provides theoretical insights into the required number of horizontal and lateral slices for exact t-CUR decomposition, further detailed in Theorem 3.

Drawing from the findings presented in Theorem 1, it is clear that an underlying low tubal-rank tensor can be reconstructed using t-CUR decomposition by selecting appropriate horizontal and lateral slices. This makes t-CUR a potential solver for tensor completion when entries within the selected slices are fully observable. However, the scope of the t-CUR sampling model is limited in large-scale scenarios, such as in extensive collaborative filtering, where it is assumed that certain users evaluate all items and certain items are rated by all users over all periods—an assumption that is practically untenable. While both the Bernoulli sampling model and t-CUR sampling have their limitations in real applications, the space between them presents an opportunity to develop a more adaptable and practical sampling strategy.

In this study, we introduce the sampling model termed tensor Cross-Concentrated Sampling (t-CCS), which combines the principles of the Bernoulli and t-CUR sampling. This innovative approach facilitates partial observations across selected horizontal and lateral slices, enhancing its practicality for a variety of applications. The t-CCS model specifically addresses the limitations inherent in traditional sampling techniques by allowing for more flexible and application-specific data collection strategies, thereby broadening the scope of its utility in complex data environments. Consider the well-known Netflix challenge, where data about users, movies, and times form a 3D tensor. The t-CCS model may effectively leverage user background information to select a more diverse user group. Unlike t-CUR sampling, t-CCS focuses on efficiently collecting data over time, accounting for evolving preferences and trends in movie watching. This flexible approach allows for tailored sample concentration, streamlining the data collection process and meeting specific research and analytical needs more effectively.

2. Notation and preliminaries

We begin by introducing the notation used throughout the paper. We use \mathbb{K} to denote an algebraically closed field, either \mathbb{R} or \mathbb{C} . We represent a matrix as a capital italic letter (e.g., A) and a tensor by a cursive italic letter (e.g., \mathcal{T}). The notation $[n]$ denotes the set of the first n positive integers, i.e., $\{1, \dots, n\}$, for any $n \in \mathbb{Z}^+$. Submatrices and subtensors are denoted as $[A]_{I,J}$ and $[\mathcal{T}]_{I,J,K}$, respectively, with I, J, K as subsets of appropriate index sets. In particular, if I is the full index set, we denote $[\mathcal{T}]_{:,J,K}$ as $[\mathcal{T}]_{I,J,K}$, and similar rules apply to J and K . Additionally, $|S|$ denotes the cardinality of the set S . If I is a subset of the set $[n]$, then I^c denotes the set of elements in $[n]$ that are not in I . For a given matrix A , we use A^\dagger to denote its Moore-Penrose inverse and A^\top for its conjugate transpose. The spectral norm of A , represented by $\|A\|$, is its largest singular value. Additionally, the Frobenius norm of A is denoted by $\|A\|_F$, where $\|A\|_F = \sqrt{\sum_{i,j} |A_{i,j}|^2}$, and its nuclear norm, represented by $\|A\|_*$, is the sum of all its singular values.

The Kronecker product is denoted by \otimes . The column vector \mathbf{e}_i has a 1 in the i -th position, with other elements as 0, and its dimension is specified when used. For a tensor $\mathcal{T} \in \mathbb{K}^{n_1 \times n_2 \times n_3}$, $\widehat{\mathcal{T}}$ represents the tensor after applying a discrete Fourier transform along its third dimension.

Now, we will review the key tensor terminologies in the tubal-rank setting that will be integral to our subsequent discussion. For a more comprehensive understanding, see [31, 32] and references therein.

Given $\mathcal{T} \in \mathbb{K}^{n_1 \times n_2 \times n_3}$, one can define the associated block circulant matrix as

$$\text{bcirc}(\mathcal{T}) := \begin{bmatrix} \mathcal{T}_1 & \mathcal{T}_{n_3} & \cdots & \mathcal{T}_2 \\ \mathcal{T}_2 & \mathcal{T}_1 & \cdots & \mathcal{T}_3 \\ \vdots & \vdots & \ddots & \vdots \\ \mathcal{T}_{n_3} & \mathcal{T}_{n_3-1} & \cdots & \mathcal{T}_1 \end{bmatrix} \in \mathbb{K}^{n_1 n_3 \times n_2 n_3} \text{ with } \mathcal{T}_i := [\mathcal{T}]_{:,i,i}.$$

We define $\text{unfold}(\mathcal{T}) := [\mathcal{T}_1^\top \quad \mathcal{T}_2^\top \quad \cdots \quad \mathcal{T}_{n_3}^\top]^\top \in \mathbb{K}^{n_1 n_3 \times n_2}$ and $\text{fold}(\text{unfold}(\mathcal{T})) = \mathcal{T}$. The t-product of tensors $\mathcal{T} \in \mathbb{K}^{n_1 \times n_2 \times n_3}$ and $\mathcal{S} \in \mathbb{K}^{n_2 \times n_4 \times n_3}$ is denoted by $\mathcal{T} * \mathcal{S} \in \mathbb{K}^{n_1 \times n_4 \times n_3}$ and is defined as $\mathcal{T} * \mathcal{S} = \text{fold}(\text{bcirc}(\mathcal{T})\text{unfold}(\mathcal{S}))$. In fact, the t product is equivalent to matrix multiplication in the Fourier domain with circulant convolution instead of multiplication between elements [31].

For convenience, we set $\overline{\mathcal{T}}$ as $\overline{\mathcal{T}} = (F_{n_3} \otimes I_{n_1}) \cdot \text{bcirc}(\mathcal{T}) \cdot (F_{n_3}^\top \otimes I_{n_2})$, where F_n represents the $n \times n$ Discrete Fourier Transform (DFT) matrix and F_n^\top is its conjugate transpose. By the property that a circulant matrix can be block-diagonalized by DFT, one can see that $\overline{\mathcal{T}}$ is a block diagonal matrix. Building upon these foundations, we are ready to introduce the definitions of t-SVD and its related concepts.

Definition 2 (f -diagonal tensor) A tensor is called f -diagonal if each of its frontal slices is a diagonal matrix.

Definition 3 (Tensor transpose) The conjugate transpose of a tensor $\mathcal{T} \in \mathbb{K}^{n_1 \times n_2 \times n_3}$ is denoted as \mathcal{T}^\top which is a tensor in $\mathbb{K}^{n_2 \times n_1 \times n_3}$ and is obtained by conjugate transposing each of the frontal slice and then reversing the order of the second to last frontal slices.

Definition 4 (Identity tensor) The identity tensor $\mathcal{I} \in \mathbb{K}^{n \times n \times n_3}$ is a tensor where the first frontal slice is the $n \times n$ identity matrix and all other frontal slices are zeros.

Definition 5 (Orthogonal tensor) A tensor $\mathcal{T} \in \mathbb{K}^{n \times n \times n_3}$ is orthogonal if

$$\mathcal{T}^\top * \mathcal{T} = \mathcal{T} * \mathcal{T}^\top = \mathcal{I} \in \mathbb{K}^{n \times n \times n_3}.$$

Definition 6 (t-SVD) Given $\mathcal{T} \in \mathbb{K}^{n_1 \times n_2 \times n_3}$, the t-SVD of \mathcal{T} is defined by

$$\mathcal{T} = \mathcal{W} * \mathcal{S} * \mathcal{V}^\top,$$

where $\mathcal{W} \in \mathbb{K}^{n_1 \times n_1 \times n_3}$, $\mathcal{V} \in \mathbb{K}^{n_2 \times n_2 \times n_3}$ are orthogonal tensors and $\mathcal{S} \in \mathbb{K}^{n_1 \times n_2 \times n_3}$ is a f-diagonal tensor. Additionally, if the tubal-rank of \mathcal{T} is r , the compact t-SVD of \mathcal{T} is $\mathcal{T} = \mathcal{W}_r * \mathcal{S}_r * \mathcal{V}_r^\top$, where $\mathcal{W}_r = [\mathcal{W}]_{:,1:r,:}$, $\mathcal{V}_r = [\mathcal{V}]_{:,1:r,:}$ and $\mathcal{S}_r = [\mathcal{S}]_{1:r,1:r,:}$. For simplicity, we omit the subscript 'r' in \mathcal{W}_r , \mathcal{V}_r and \mathcal{S}_r and write $\mathcal{T} = \mathcal{W} * \mathcal{S} * \mathcal{V}^\top$ as the compact t-SVD of \mathcal{T} .

Next, let us introduce several other key definitions relevant to our work.

Definition 7 (Moore-Penrose inverse) $\mathcal{T}^\dagger \in \mathbb{K}^{n_2 \times n_1 \times n_3}$ is the Moore-Penrose inverse of $\mathcal{T} \in \mathbb{K}^{n_1 \times n_2 \times n_3}$, if \mathcal{T}^\dagger satisfies

$$\begin{aligned} \mathcal{T} * \mathcal{T}^\dagger * \mathcal{T} &= \mathcal{T}, & \mathcal{T}^\dagger * \mathcal{T} * \mathcal{T}^\dagger &= \mathcal{T}^\dagger, \\ (\mathcal{T} * \mathcal{T}^\dagger)^\top &= \mathcal{T} * \mathcal{T}^\dagger, & (\mathcal{T}^\dagger * \mathcal{T})^\top &= \mathcal{T}^\dagger * \mathcal{T}. \end{aligned}$$

Definition 8 (Tensor Frobenius norm) The Frobenius norm $\|\mathcal{T}\|_F$ of tensor $\mathcal{T} \in \mathbb{K}^{n_1 \times n_2 \times n_3}$ is defined as $\|\mathcal{T}\|_F := \sqrt{\sum_{i,j,k} |[\mathcal{T}]_{i,j,k}|^2} = \frac{1}{\sqrt{n_3}} \|\text{bcirc}(\mathcal{T})\|_F$.

Definition 9 (Standard tensor lateral basis) The lateral basis $\mathring{\mathbf{e}}_i \in \mathbb{K}^{n_1 \times 1 \times n_3}$, is the tensor with only $[\mathring{\mathbf{e}}_i]_{i,1,1}$ equal to 1 and the remaining being zero.

Definition 10 (Tensor μ_0 -incoherence condition) Let $\mathcal{T} \in \mathbb{K}^{n_1 \times n_2 \times n_3}$ be a tubal-rank r tensor with a compact t-SVD $\mathcal{T} = \mathcal{W} * \mathcal{S} * \mathcal{V}^\top$. Then \mathcal{T} has μ_0 -incoherence if for all $k \in \{1 \cdots, n_3\}$, the following hold:

$$\max_{i=1,2,\dots,n_1} \left\| \left[\widehat{\mathcal{W}} \right]_{:, :, k}^\top \cdot \mathbf{e}_i \right\|_F \leq \sqrt{\frac{\mu_0 r}{n_1}} \quad \text{and} \quad \max_{j=1,2,\dots,n_2} \left\| \left[\widehat{\mathcal{V}} \right]_{:, :, k}^\top \cdot \mathbf{e}_j \right\|_F \leq \sqrt{\frac{\mu_0 r}{n_2}}.$$

In some cases, to highlight the incoherence parameter of a specific tensor \mathcal{T} , we will denote this parameter as $\mu_{\mathcal{T}}$.

As our work focuses on the subtensors of an underlying tensor with low tubal-rank, we will introduce the concept of the sampling tensor for the completeness of this work.

Definition 11 (Sampling tensor) Given a tensor $\mathcal{T} \in \mathbb{K}^{n_1 \times n_2 \times n_3}$ and $I \subseteq [n_1]$, the horizontal subtensor \mathcal{R} of \mathcal{T} with indices I can be obtained via $\mathcal{R} := [\mathcal{T}]_{I, :, :} = [\mathcal{I}]_{I, :, :} * \mathcal{T}$, where \mathcal{I} is the identity tensor (see Definition 4). For convenience, $[\mathcal{I}]_{I, :, :}$ will be called the horizontal sampling tensor and denoted as \mathcal{S}_I .

Similarly, the lateral sub-tensor \mathcal{C} with indices $J \subseteq [n_2]$ can be obtained as $\mathcal{C} := [\mathcal{T}]_{:, J, :} = \mathcal{T} * [\mathcal{I}]_{:, J, :}$. $[\mathcal{I}]_{:, J, :}$ will be called the lateral sampling tensor and denoted by \mathcal{S}_J with index J . The subtensor \mathcal{U} of \mathcal{T} with horizontal indices I and lateral indices J can be represented as $\mathcal{U} := [\mathcal{T}]_{I, J, :} = \mathcal{S}_I * \mathcal{T} * \mathcal{S}_J$.

Definition 12 (Tensor nuclear norm [51]) The tensor nuclear norm (TNN) of \mathcal{T} is defined as $\|\mathcal{T}\|_{\text{TNN}} = \frac{1}{n_3} \|\text{bcirc}(\mathcal{T})\|_* = \frac{1}{n_3} \|\overline{\mathcal{T}}\|_*$, where $\|\cdot\|_*$ is the matrix nuclear norm.

Definition 13 (Tensor spectral norm and condition number) The tensor spectral norm $\|\mathcal{T}\|$ of a third-order tensor \mathcal{T} is defined as $\|\mathcal{T}\| = \|\text{bcirc}(\mathcal{T})\|$. The condition number of \mathcal{T} is defined as: $\kappa(\mathcal{T}) = \|\mathcal{T}^\dagger\| \cdot \|\mathcal{T}\|$.

3. Proposed sampling model

We aim to develop a sampling strategy that is both efficient and effective for a range of real-world scenarios. Inspired by the cross-concentrated sampling model for matrix completion [10] and t-CUR decomposition [51], we introduce a novel sampling model tailored for tensor data, named Tensor Cross-Concentrated Sampling (t-CCS). The t-CCS model extracts samples from both horizontal and lateral subtensors of the original tensor. Formally, let $\mathcal{R} = [\mathcal{T}]_{I, :, :}$ and $\mathcal{C} = [\mathcal{T}]_{:, J, :}$ represent the selected horizontal and lateral subtensors of \mathcal{T} , determined by index sets I and J respectively. We then sample entries on \mathcal{R} and \mathcal{C} based on the Bernoulli sampling model. The t-CCS procedure is detailed in Procedure 1. Moreover, we illustrate t-CCS against Bernoulli and t-CUR sampling in Figure 1. Notably, t-CCS transitions to t-CUR sampling when the samples are dense enough to fully capture the subtensors, and it reverts to Bernoulli sampling when all horizontal and lateral slices are selected. The indices of the cross-concentrated samples are denoted by $\Omega_{\mathcal{R}}$ and $\Omega_{\mathcal{C}}$, corresponding to the notation used for the subtensors. Our task is to recover an underlying tensor \mathcal{T} with tubal-rank r from the observations on $\Omega_{\mathcal{R}} \cup \Omega_{\mathcal{C}}$. We approach this recovery through the following optimization problem:

$$\min_{\tilde{\mathcal{T}}} \left\langle \mathcal{P}_{\Omega_{\mathcal{R}} \cup \Omega_{\mathcal{C}}}(\mathcal{T} - \tilde{\mathcal{T}}), \mathcal{T} - \tilde{\mathcal{T}} \right\rangle, \quad \text{subject to} \quad \text{tubal-rank}(\tilde{\mathcal{T}}) = r, \quad (3)$$

where $\langle \cdot, \cdot \rangle$ is the Frobenius inner product and $\mathcal{P}_{\Omega_{\mathcal{R}} \cup \Omega_{\mathcal{C}}}$ is defined in (2).

Procedure 1 Tensor Cross-Concentrated Sampling (t-CCS)

- 1: **Input:** $\mathcal{T} \in \mathbb{K}^{n_1 \times n_2 \times n_3}$.
 - 2: Uniformly select the horizontal and lateral indices, denoted as I and J , respectively.
 - 3: Set $\mathcal{R} := [\mathcal{T}]_{I, :, :}$ and $\mathcal{C} := [\mathcal{T}]_{:, J, :}$.
 - 4: Sample entries from \mathcal{R} and \mathcal{C} based on Bernoulli sampling models. Record the locations of these samples as $\Omega_{\mathcal{R}}$ and $\Omega_{\mathcal{C}}$ for \mathcal{R} and \mathcal{C} , respectively.
 - 5: **Output:** $[\mathcal{T}]_{\Omega_{\mathcal{R}} \cup \Omega_{\mathcal{C}}}$, $\Omega_{\mathcal{R}}$, $\Omega_{\mathcal{C}}$, I , J .
-

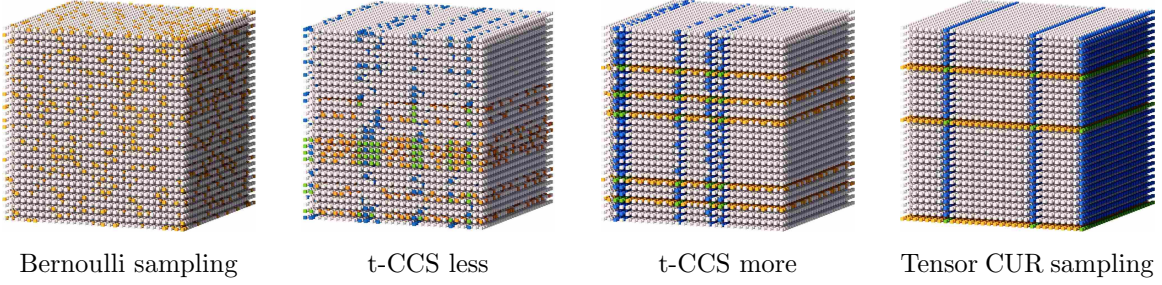


Figure 1: Visual comparison of four sampling strategies at the same total observation rate: Bernoulli, less concentrated t-CCS, more concentrated t-CCS, and tensor CUR. The blue, yellow and green grids mark the observed entries in the lateral, horizontal and intersected subtensors, respectively.

3.1 Theoretical results

In this section, we present our main theoretical result, i.e., Theorem 2, which supports the effectiveness of the proposed t-CCS model.

Theorem 2 *Let $\mathcal{T} \in \mathbb{K}^{n_1 \times n_2 \times n_3}$ satisfy the tensor μ_0 -incoherence condition and have a multi-rank \vec{r} with condition number κ . Let $I \subseteq [n_1]$ and $J \subseteq [n_2]$ be chosen uniformly with replacement to yield $\mathcal{R} = [\mathcal{T}]_{I, :, :}$ and $\mathcal{C} = [\mathcal{T}]_{:, J, :}$. And suppose that $\Omega_{\mathcal{R}}$ and $\Omega_{\mathcal{C}}$ are generated from \mathcal{R} and \mathcal{C} according to the Bernoulli distributions with probability $p_{\mathcal{R}}$ and $p_{\mathcal{C}}$, respectively. If*

$$\begin{aligned}
 & |I| \geq 3200\beta\mu_0r\kappa^2 \log^2(n_1n_3 + n_2n_3), \quad |J| \geq 3200\beta\mu_0r\kappa^2 \log^2(n_1n_3 + n_2n_3), \\
 p_{\mathcal{R}} \geq & \frac{1600(|I| + n_2)\mu_0r\kappa^2 \log^2((n_1 + n_2)n_3)}{|I|n_2}, \quad p_{\mathcal{C}} \geq \frac{1600(|J| + n_1)\mu_0r\kappa^2 \log^2((n_1 + n_2)n_3)}{|J|n_1}
 \end{aligned}$$

for some absolute constant $\beta > 1$, then \mathcal{T} can be uniquely determined from the entries on $\Omega_{\mathcal{R}} \cup \Omega_{\mathcal{C}}$ with probability at least

$$\begin{aligned}
 & 1 - \frac{1}{(n_1n_3 + n_2n_3)^{800\beta\kappa^2 \log(n_2)}} - \frac{1}{(n_1n_3 + n_2n_3)^{800\beta\kappa^2 \log(n_1)}} \\
 & - \frac{3 \log(n_1n_3 + |J|n_3)}{(n_1n_3 + |J|n_3)^{4\beta-2}} - \frac{3 \log(n_2n_3 + |I|n_3)}{(n_2n_3 + |I|n_3)^{4\beta-2}}.
 \end{aligned}$$

Remark 1 (i) When $n_1 = n_2 = n$, the results in the above theorem can be simplified to that \mathcal{T} can be uniquely determined from the entries on $\Omega_{\mathcal{R}} \cup \Omega_{\mathcal{C}}$ with probability at least $1 - \frac{6 \log(2nn_3)}{(nn_3)^{4\beta-2}}$.

(ii) Supposed \mathcal{T} with multi-rank \vec{r} of low tubal-rank r is the underlying tensor we aim to recover. Notice that such \mathcal{T} is one of feasible solutions to the optimization problem (1) since $\text{tubal-rank}(\mathcal{T}) = r$. Additionally, it is evident that for any $\tilde{\mathcal{T}}$ with tubal-rank r , $\langle \mathcal{P}_{\Omega}(\tilde{\mathcal{T}} - \mathcal{T}), \tilde{\mathcal{T}} - \mathcal{T} \rangle \geq 0$ and $\langle \mathcal{P}_{\Omega}(\mathcal{T} - \mathcal{T}), \mathcal{T} - \mathcal{T} \rangle = 0$. Thus, \mathcal{T} is a global minimizer to the optimization problem (1). According to Theorem 2, \mathcal{T} with low tubal-rank r can be reliably recovered using the t -CCS model with high probability. Consequently, we can obtain a minimizer for (1) through samples that are partially observed from the t -CCS model.

Theorem 2 elucidates that a sampling complexity of

$$\mathcal{O}(r\kappa^2 \max\{n_1, n_2\}n_3 \log^2(n_1n_3 + n_2n_3))$$

is sufficient for TC on t -CCS model. This complexity is a κ^2 factor worse than that of the benchmark provided by the state-of-the-art Bernoulli-sampling-based TC methods, such as TNN method detailed in [64], which demands

$$\mathcal{O}(r \max\{n_1, n_2\}n_3 \log^2(n_1n_3 + n_2n_3))$$

samples. This observation suggests the potential for identifying a more optimal lower bound, which will leave as a future direction.

To support the proof of Theorem 2, we rely on two critical theorems. The first theorem, Theorem 3, establishes the necessary lower bounds for the number of lateral and horizontal slices required when uniformly sampling these slices to ensure an exact t -CUR decomposition. Theorem 3 is an adaptation of [51, Corollary 3.10], which introduces a unique proof method tailored for uniform sampling and exact t -CUR, offering a more detailed analysis for this specific context.

Before presenting Theorem 3, let's briefly review the sampling schemes for matrix CUR decomposition [22]. Various sampling schemes have been designed to ensure the selected rows and columns validate the CUR decomposition. For example, deterministic methods are explored in works such as [4, 5, 34]. Randomized sampling algorithms for CUR decompositions and the column subset selection problem have been extensively studied, as seen in [14, 15, 39, 53, 57]. For a comprehensive overview of both approaches, refer to [23]. Hybrid methods that combine both approaches are discussed in [6, 9].

Specifically, for a rank r matrix in $\mathbb{K}^{n_1 \times n_2}$ with μ -incoherence, sampling $\mathcal{O}(\mu r \log(n_1))$ rows and $\mathcal{O}(\mu r \log(n_2))$ columns is sufficient to ensure the exact matrix CUR decomposition [7]. In this work, we extend the uniform sampling results from the matrix setting to the tensor setting.

Theorem 3 Consider a tensor $\mathcal{T} \in \mathbb{K}^{n_1 \times n_2 \times n_3}$ that satisfies the tensor μ_0 -incoherence condition and has a multi-rank \vec{r} . The indices I and J are selected uniformly randomly without replacement from $[n_1]$ and $[n_2]$, respectively. Set $\mathcal{C} = [\mathcal{T}]_{:,J,:}$, $\mathcal{R} = [\mathcal{T}]_{I,,:}$ and $\mathcal{U} = [\mathcal{T}]_{I,J,:}$. Then $\mathcal{T} = \mathcal{C} * \mathcal{U}^\dagger * \mathcal{R}$ holds with probability at least $1 - \frac{1}{n_1^\beta} - \frac{1}{n_2^\beta}$, provided that $|I| \geq 2\beta\mu_0\|\vec{r}\|_\infty \log(n_1\|\vec{r}\|_1)$ and $|J| \geq 2\beta\mu_0\|\vec{r}\|_\infty \log(n_2\|\vec{r}\|_1)$.

Another important supporting theorem is Theorem 4, which adapts [64, Theorem 3.1] for tensor recovery with tubal-rank r under Bernoulli sampling, essential for Theorem 2. Our contribution refines the theorem by explicitly detailing the numerical constants in the original sampling probability. The proof of Theorem 4 is under the same framework as in [64].

Theorem 4 Let $\mathcal{Z} \in \mathbb{K}^{n_1 \times n_2 \times n_3}$ of tubal-rank r satisfy the tensor μ_0 -incoherence condition. And its compact t-SVD is $\mathcal{Z} = \mathcal{W} * \mathcal{S} * \mathcal{V}^\top$ where $\mathcal{W} \in \mathbb{K}^{n_1 \times r \times n_3}$, $\mathcal{S} \in \mathbb{K}^{r \times r \times n_3}$ and $\mathcal{V} \in \mathbb{K}^{n_2 \times r \times n_3}$. Suppose the entries in Ω are sampled according to the Bernoulli model with probability p . If

$$p \geq \frac{256\beta(n_1 + n_2)\mu_0 r \log^2(n_1 n_3 + n_2 n_3)}{n_1 n_2} \text{ with } \beta \geq 1, \quad (4)$$

then \mathcal{Z} is the unique minimizer to

$$\min_{\mathcal{X}} \|\mathcal{X}\|_{\text{TNN}}, \text{ subject to } \mathcal{P}_\Omega(\mathcal{X}) = \mathcal{P}_\Omega(\mathcal{Z}),$$

with probability at least $1 - \frac{3 \log(n_1 n_3 + n_2 n_3)}{(n_1 n_3 + n_2 n_3)^{4\beta - 2}}$.

4. An efficient solver for t-CCS

In this section, we explore how to solve the t-CCS-based TC problem efficiently. Initially, we apply existing TC algorithms, including BCPF [66], TMac [59], TNN [64], and F-TNN [29], to a t-CCS-based image recovery problem. BCPF is CP-based, TMac is Tucker-based, while TNN and F-TNN are tubal-rank-based. However, these methods prove unsuitable for the t-CCS model, as shown in Figure 2, where they fail to produce reliable visualization. This highlights the need for new algorithm(s) tailored to the t-CCS model.

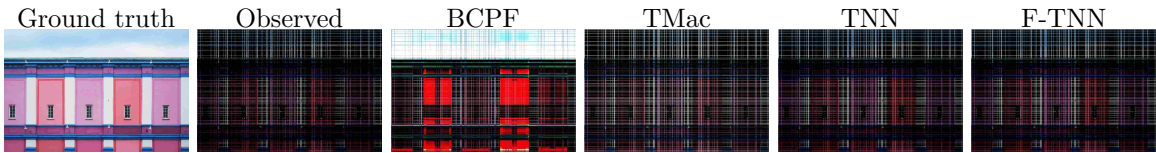


Figure 2: Visual results of color image inpainting using t-CCS samples at an overall sampling rate of 20% with BCPF, TMac, TNN, and F-TNN algorithms.

4.1 Iterative t-CUR tensor completion algorithm

To efficiently use the t-CCS structure, we develop the Iterative t-CUR Tensor Completion (ITCURTC) algorithm, a non-convex method inspired by projected gradient descent. ITCURTC updates \mathcal{R} , \mathcal{C} , and \mathcal{U} at each iteration to preserve the tubal-rank r of \mathcal{T} . The update formulas are:

$$[\mathcal{R}_{k+1}]_{:,j^c,:} := [\mathcal{T}_k]_{I,j^c,:} + \eta_R [\mathcal{P}_{\Omega_{\mathcal{R}}} (\mathcal{T} - \mathcal{T}_k)]_{I,j^c,:}, \quad (5)$$

$$[\mathcal{C}_{k+1}]_{I^c,,:} := [\mathcal{T}_k]_{I^c,J} + \eta_C [\mathcal{P}_{\Omega_{\mathcal{C}}} (\mathcal{T} - \mathcal{T}_k)]_{I^c,J}, \quad (6)$$

$$\mathcal{U}_{k+1} := \mathcal{H}_r \left([\mathcal{T}_k]_{I,J,:} + \eta_U [\mathcal{P}_{\Omega_{\mathcal{R}} \cup \Omega_{\mathcal{C}}} (\mathcal{T} - \mathcal{T}_k)]_{I,J,:} \right), \quad (7)$$

where η_R, η_C, η_U are step sizes, and \mathcal{H}_r is the truncated t-SVD operator. $[\mathcal{R}_{k+1}]_{:,j^c,:}$ and $[\mathcal{C}_{k+1}]_{I^c,,:}$ are updated to \mathcal{U}_{k+1} . The algorithm, starting from $\mathcal{T}_0 = \mathbf{0}$, iterates until $e_k \leq \varepsilon$, where ε is a preset tolerance and

$$e_k = \frac{\langle \mathcal{P}_{\Omega_{\mathcal{R}} \cup \Omega_{\mathcal{C}}} (\mathcal{T} - \mathcal{T}_k), \mathcal{T} - \mathcal{T}_k \rangle}{\langle \mathcal{P}_{\Omega_{\mathcal{R}} \cup \Omega_{\mathcal{C}}} (\mathcal{T}), \mathcal{T} \rangle}. \quad (8)$$

The algorithm is summarized in Algorithm 2.

Algorithm 2 Iterative t-CUR Tensor Completion (ITCURTC) for t-CCS

- 1: **Input:** $[\mathcal{T}]_{\Omega_{\mathcal{R}} \cup \Omega_{\mathcal{C}}}$: observed data; $\Omega_{\mathcal{R}}, \Omega_{\mathcal{C}}$: observed locations; I, J : horizontal and lateral indexes that define \mathcal{R} and \mathcal{C} respectively; η_R, η_C, η_U : step sizes; r : target tubal-rank; ε : tolerance level.
 - 2: Set $\mathcal{T}_0 = \mathbf{0} \in \mathbb{K}^{n_1 \times n_2 \times n_3}$
 - 3: **while** $e_k > \varepsilon$ **do** ▷ e_k is defined in (8)
 - 4: $[\mathcal{R}_{k+1}]_{:,j^c,:} = [\mathcal{T}_k]_{I,j^c,:} + \eta_R [\mathcal{P}_{\Omega_{\mathcal{R}}} ([\mathcal{T}]_{\Omega_{\mathcal{R}} \cup \Omega_{\mathcal{C}}} - \mathcal{T}_k)]_{I,j^c,:}$
 - 5: $[\mathcal{C}_{k+1}]_{I^c,,:} = [\mathcal{T}_k]_{I^c,J} + \eta_C [\mathcal{P}_{\Omega_{\mathcal{C}}} ([\mathcal{T}]_{\Omega_{\mathcal{R}} \cup \Omega_{\mathcal{C}}} - \mathcal{T}_k)]_{I^c,J}$
 - 6: $\mathcal{U}_{k+1} = \mathcal{H}_r ([\mathcal{T}_k]_{I,J,:} + \eta_U [\mathcal{P}_{\Omega_{\mathcal{R}} \cup \Omega_{\mathcal{C}}} ([\mathcal{T}]_{\Omega_{\mathcal{R}} \cup \Omega_{\mathcal{C}}} - \mathcal{T}_k)]_{I,J,:})$
 - 7: $[\mathcal{R}_{k+1}]_{:,j^c,:} = \mathcal{U}_{k+1}$ and $[\mathcal{C}_{k+1}]_{I^c,,:} = \mathcal{U}_{k+1}$
 - 8: Update \mathcal{T}_{k+1} ▷ More details see (9), (10), (11)
 - 9: $k = k + 1$
 - 10: **end while**
 - 11: **Output:** $\mathcal{C}_{k+1}, \mathcal{U}_{k+1}$ and \mathcal{R}_{k+1}
-

4.2 Computational complexity analysis

This section outlines the implementation and computational costs of Algorithm 2. Updating $[\mathcal{R}_{k+1}]_{:,j^c,:}$ and $[\mathcal{C}_{k+1}]_{I^c,,:}$ incurs $\mathcal{O}(|\Omega_{\mathcal{R}}| + |\Omega_{\mathcal{C}}| - |\Omega_{\mathcal{U}}|)$ flops, focusing only on observed locations (refer to (5) and (6)). The update of $\mathcal{U}_{k+1} \in \mathbb{K}^{I \times |J| \times n_3}$ involves (i) computing $\tilde{\mathcal{U}}_{k+1} := [\mathcal{T}_k]_{I,J,:} + \eta_U [\mathcal{P}_{\Omega_{\mathcal{R}} \cup \Omega_{\mathcal{C}}} ([\mathcal{T}]_{\Omega_{\mathcal{R}} \cup \Omega_{\mathcal{C}}} - \mathcal{T}_k)]_{I,J,:}$ and (ii) finding its tubal-rank r approximation via t-SVD. The cost for (i) is $\mathcal{O}(|\Omega_{\mathcal{U}}|)$, while (ii) requires $\max\{\mathcal{O}(|I||J|rn_3), \mathcal{O}(|I||J|n_3 \log(n_3))\}$, making the total update cost for \mathcal{U}_k to be $\max\{\mathcal{O}(|I||J|rn_3), \mathcal{O}(|I||J|n_3 \log(n_3))\}$.

Considering the cost of updating \mathcal{T}_{k+1} in Algorithm 2, we focus on $[\mathcal{T}_{k+1}]_{I^c, J, :}$, $[\mathcal{T}_{k+1}]_{I, J^c, :}$, and $[\mathcal{T}_{k+1}]_{I, J, :}$ each iteration. The update for $[\mathcal{T}_{k+1}]_{I^c, J, :}$ is:

$$[\mathcal{T}_{k+1}]_{I^c, J, :} = [\mathcal{C}_k]_{I^c, :, :} * \mathcal{U}_k^\dagger * \mathcal{U}_k = [\mathcal{C}_k]_{I^c, :, :} * [\mathcal{V}_k]_{:, 1:r, :} * [\mathcal{V}_k]_{:, 1:r, :}^\top \quad (9)$$

where $\mathcal{U}_k = \mathcal{W}_k * \mathcal{S}_k * \mathcal{V}_k^\top$ is \mathcal{U}_k 's t-SVD. Given $[\mathcal{V}_k]_{:, 1:r, :}$'s size as $|J| \times r \times n_3$, the computational cost is $\mathcal{O}(n_1 |J| r n_3)$ flops for (9), making the total complexity for updating $[\mathcal{T}_{k+1}]_{I^c, J, :}$ also $\mathcal{O}(n_1 |J| r n_3)$ flops. We update $[\mathcal{T}_{k+1}]_{I, J^c, :}$ by

$$[\mathcal{T}_{k+1}]_{I, J^c, :} := [\mathcal{W}_k]_{:, 1:r, :} * [\mathcal{W}_k]_{:, 1:r, :}^\top * [\mathcal{R}_k]_{:, J^c, :} \quad (10)$$

Similar analysis for updating $[\mathcal{T}_{k+1}]_{I, J^c, :}$, the computational complexity of updating $[\mathcal{T}_{k+1}]_{I, J^c, :}$ is $\mathcal{O}(n_2 |I| r n_3)$. And we update $[\mathcal{T}_{k+1}]_{I, J, :}$ by setting

$$[\mathcal{T}_{k+1}]_{I, J, :} := \mathcal{U}_k. \quad (11)$$

Thus, the total computational complexity of updating \mathcal{T}_{k+1} is $\mathcal{O}(|I| r n_2 n_3 + |J| r n_1 n_3)$.

Computing the stopping criterion e_k costs $\mathcal{O}(|\Omega_R| + |\Omega_C| - |\Omega_U|)$ flops as we only make computations on the observed locations.

The computational costs per iteration are summarized in Table 1, showing a complexity of $\mathcal{O}(r |I| n_2 n_3 + r |J| n_1 n_3)$ when $|I| \ll n_1$ and $|J| \ll n_2$.

Table 1: Computational costs per iteration for ITCURTC.

STEP	COMPUTATIONAL COMPLEXITY
Line 3: Computing the stopping criterion e_k	$\mathcal{O}(\Omega_R + \Omega_C - \Omega_U)$
Line 4: $[\mathcal{R}_{k+1}]_{:, J^c, :} = [\mathcal{T}_k]_{I, J^c, :} + \eta_R [\mathcal{P}_{\Omega_R}([\mathcal{T}]_{\Omega_R \cup \Omega_C} - \mathcal{T}_k)]_{I, J^c, :}$	$\mathcal{O}(\Omega_R - \Omega_U)$
Line 5: $[\mathcal{C}_{k+1}]_{I^c, :, :} = [\mathcal{T}_k]_{I^c, J, :} + \eta_C [\mathcal{P}_{\Omega_C}([\mathcal{T}]_{\Omega_R \cup \Omega_C} - \mathcal{T}_k)]_{I^c, J, :}$	$\mathcal{O}(\Omega_C - \Omega_U)$
Line 6: $\mathcal{U}_{k+1} = \mathcal{H}_r([\mathcal{T}_k]_{I, J, :} + \eta_U [\mathcal{P}_{\Omega_R \cup \Omega_C}([\mathcal{T}]_{\Omega_R \cup \Omega_C} - \mathcal{T}_k)]_{I, J, :})$	$\mathcal{O}(\max\{ I J r n_3, J I n_3 \log(n_3)\})$
Line 8: Updating \mathcal{T}_{k+1}	$\mathcal{O}(r I n_2 n_3 + r J n_1 n_3)$

5. Numerical experiments

This section presents the performance of our t-CCS based ITCURTC through numerical experiments on both synthetic and real-world data. The computations are performed on one of the shared nodes of the Computing Cluster with a 64-bit Linux system (GLNXA64), featuring an Intel(R) Xeon(R) Gold 6148 CPU (2.40 GHz). All experiments are carried out using MATLAB 2022a.

5.1 Synthetic data examples

This section evaluates ITCURTC for t-CCS-based TC, exploring the needed sample sizes and the impact of Bernoulli sampling probability and fiber sampling rates on low-tubal-rank tensor recovery. We assess ITCURTC's tensor recovery capability under different combinations of horizontal and lateral slice numbers $|I| = \delta n_1, |J| = \delta n_2$ and Bernoulli sampling rates p on selected subtensors. The study uses tensors of size $768 \times 768 \times 256$ with tubal-ranks $r \in \{2, 5, 7\}$. We conduct 25 tests for each (δ, p, r) tuple, a test is considered successful if $\varepsilon_k := \|\mathcal{T} - \mathcal{C}_k * \mathcal{W}_k^\dagger * \mathcal{R}_k\|_F / \|\mathcal{T}\|_F \leq 10^{-3}$.

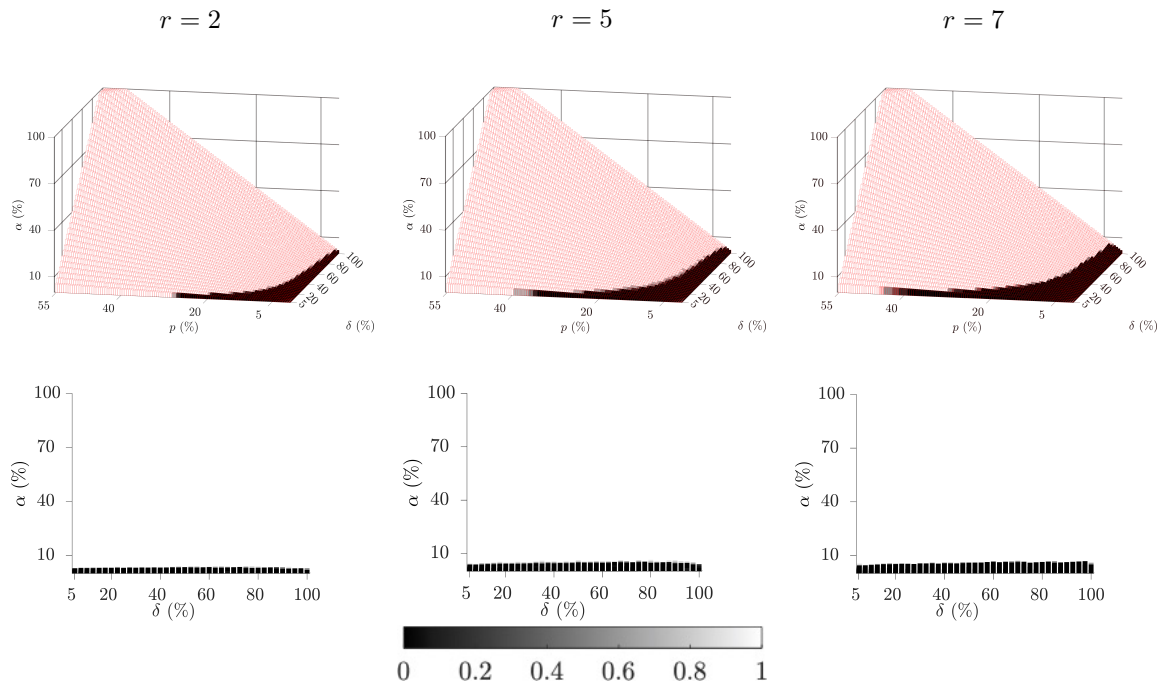


Figure 3: **(Row 1)** 3D and **(Row 2)** 2D views illustrate ITCURTC’s empirical phase transition for the t-CCS model. $\delta = |I|/768 = |J|/768$ shows sampled indices ratios, p is the Bernoulli sampling probability over subtensors, and α is the overall tensor sampling rate. White and black in the $768 \times 768 \times 256$ tensor results represent success and failure, respectively, across 25 tests for tubal ranks 2, 5, and 7 (Columns 1-3). The α needed for success remains consistent across different combinations δ and p .

Our empirical phase transition results are presented in Figure 3, with the first row showing a 3D view of the phase transition results and the second row the corresponding 2D view. White and black pixels in these visuals represent the success and failure of all the 25 tests, respectively. The results highlight that higher overall sampling rates are needed for successful completion with larger tubal-ranks r . Importantly, tensor completion is achievable with sufficiently large overall sampling rates, regardless of the specific combinations of the horizontal, lateral slice sizes, and subtensor sampling rates, as demonstrated by the results in the 2D view. This demonstrates ITCURTC’s flexibility in sampling low-tubal-rank tensors for successful reconstruction. Additionally, we include our numerical results for the convergence of ITCURTC in Appendix D.

5.2 Real-world applications

This section compares the t-CCS model with the Bernoulli sampling model in TC tasks across various data types to evaluate the t-CCS model’s practical feasibility and applicability. We compare ITCURTC, based on the t-CCS model, with established TC methods based on the Bernoulli sampling model, including BCPF, TMac, TNN,

and F-TNN. The performance is measured by reconstruction quality and execution time. The quality is measured by the Peak Signal-to-Noise Ratio (PSNR) and the Structural Similarity Index (SSIM), where

$$\text{PSNR} = 10 \log_{10} \left(\frac{n_1 n_2 n_3 \|\mathcal{T}\|_{\infty}^2}{\|\mathcal{T} - \tilde{\mathcal{T}}\|_{\text{F}}^2} \right). \quad (12)$$

and SSIM evaluates the structural similarity between two images, as detailed in [58]. Higher PSNR and SSIM scores indicate better reconstruction quality, and SSIM values are reported as the average across all frontal slices.

Our experimental process is as follows. We first generate random observations via the t-CCS model: uniformly randomly selecting concentrated horizontal (\mathcal{R}) and lateral (\mathcal{C}) subtensors, defined as $\mathcal{R} = [\mathcal{T}]_{I, :, :}$ and $\mathcal{C} = [\mathcal{T}]_{:, J, :}$, with $|I| = \delta n_1$ and $|J| = \delta n_2$; entries in \mathcal{R} and \mathcal{C} are sampled based on the Bernoulli sampling model with the locations of the observed entries denoted by $\Omega_{\mathcal{R}}$ and $\Omega_{\mathcal{C}}$. The procedure of the t-CCS model results in a tensor that is only partially observed in \mathcal{R} and \mathcal{C} . ITCURTC is then applied to estimate the missing entries and thus recover the original tensor. For comparison, we also generate observations of the entire original tensor \mathcal{T} using the Bernoulli sampling model with a probability $p_{\mathcal{T}} := \frac{|\Omega_{\mathcal{R}} \cup \Omega_{\mathcal{C}}|}{n_1 n_2 n_3}$. Additionally, we estimate the missing data using several TC methods: BCPF¹, which is based on the CP decomposition framework; TMac², which utilizes the Tucker decomposition framework; and TNN³ and F-TNN⁴, which are both grounded in the t-SVD framework. To ensure reliable results, we repeat this entire procedure 30 times, averaging the PSNR and SSIM scores and the runtime to minimize the effects of randomness.

5.2.1 Color image completion

Color images, viewed as 3D tensors with dimensions for height, width, and color channels, are effectively modeled as low-tubal-rank tensors [35, 38]. In our tests, we focus on two images: ‘Building’⁵ (of size $2579 \times 3887 \times 3$) and ‘Window’⁶ (of size $3009 \times 4513 \times 3$). We present averaged test results over various overall observation rates (α) in Table 2, and visual comparisons at $\alpha = 20\%$ in Figure 4.

Figure 4 presents a clear visual comparison of results from different methods at a 20% overall sampling rate, where the algorithms BCPF, TMac, TNN, and F-TNN are applied on the Bernoulli sampling model and ITCURTC are applied on t-CCS model. The ground truth is the original image of the building and the window. BCPF underperforms in visual effects compared to other methods. TNN shows slight variations from the ground truth, maintaining colors and details with minor discrepancies.

1. <https://github.com/qbzhao/BCPF>
2. <https://xu-yangyang.github.io/TMac/>
3. <https://github.com/jamiezeminzhang/>
4. <https://github.com/TaiXiangJiang/Framelet-TNN>
5. <https://pxhere.com/en/photo/57707>
6. <https://pxhere.com/en/photo/1421981>

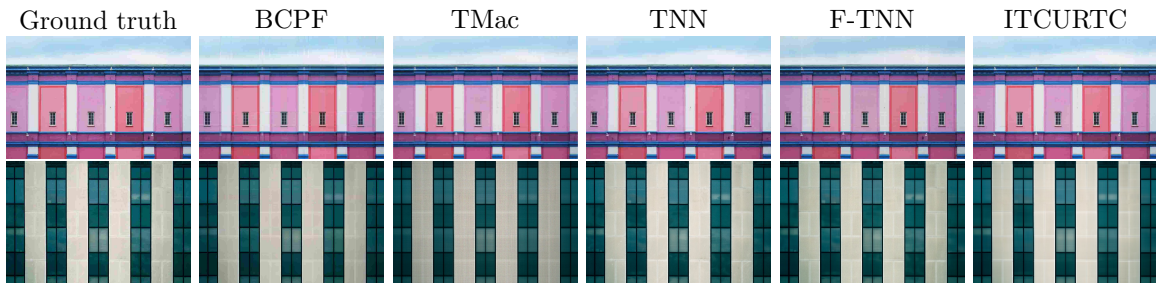


Figure 4: The visualization of color image inpainting for Building and Window datasets by setting tubal-rank $r = 35$ with the percentage of selected horizontal and lateral slices $\delta = 13\%$ and overall sampling rate 20% for ITCURTC. Other algorithms are applied based on Bernoulli sampling model with the same overall sampling rate 20%. Additionally, t-CCS samples on the Building for ITCURTC are the same as those in Figure 2.

TMac reveals some notable differences. F-TNN improves reflection fidelity and color saturation, closely resembling the ground truth. ITCURTC also achieves the high similarity to the ground truth, accurately reproducing colors and details. Moreover, ITCURTC significantly outperforms BCPF, TMac, TNN, and F-TNN in the t-CCS-based color image inpainting task, as evidenced by the unsatisfactory results of BCPF, TMac, TNN, and F-TNN under the t-CCS model (see Figure 2).

Table 2 shows that ITCURTC for t-CCS typically offers quality comparable to that of Bernoulli sampling-based TC algorithms. In runtime efficiency, ITCURTC leveraging the t-CCS model significantly surpasses BCPF, TMac, TNN, and F-TNN, all of which are based on the Bernoulli sampling model. This efficiency enhancement highlights the t-CCS model’s superior performance in practical applications. Additionally, ITCURTC’s consistent performance in delivering similar quality results across different δ , provided the same overall sampling rates. These highlight the flexibility and feasibility of the t-CCS model.

5.2.2 MRI reconstruction

In this study, we evaluate our model on an MRI heart dataset⁷ (of size $320 \times 320 \times 110$), where compact t-SVD with tubal-rank 35 yields less than 10% relative error, suggesting a low-tubal-rank property of the dataset. The visualization results of the reconstruction of the MRI using different methods at a 30% overall sampling rate are presented in Figure 5, and reconstruction quality and runtime are detailed in Table 3.

Figure 5 shows recovery results for four frontal MRI slices using BCPF, TMac, TNN, and F-TNN, all under Bernoulli sampling model, and ITCURTC under the t-CCS model. The ground truth serves as the actual dataset, from which missing values are to be predicted by different algorithms. BCPF shows notable artifacts and lacks the sharp edges of the heart’s interior structures. TMac improves over BCPF but still presents a softer representation of cardiac anatomy. TNN enhances

7. <http://medicaldecathlon.com/dataaws>

Table 2: Image inpainting results on the Building and Window datasets. The **best results** are emphasized in bold, while the second-best results are underlined. ITCURTC- δ refers to the ITCURTC method with the percentages of selected horizontal and lateral slices set at a fixed rate of $\delta\%$. The t-CCS-based algorithm ITCURTC- δ s are performed on t-CCS scheme while other Bernoulli-based algorithms are performed on Bernoulli sampling scheme.

DATASET		Building			Window		
OVERALL OBSERVATION RATE		12%	16%	20%	12%	16%	20%
PSNR	ITCURTC-11	28.9249	31.0050	32.1645	<u>35.2830</u>	36.1611	37.0236
	ITCURTC-12	<u>28.5518</u>	<u>30.8055</u>	31.9489	35.1195	36.1145	37.0174
	ITCURTC-13	28.1893	30.7260	31.6825	35.0196	36.1215	36.8885
	BCPF	26.7939	28.2949	29.4298	30.1611	33.9990	35.4780
	TMac	27.0425	30.1755	<u>32.3632</u>	33.2673	<u>36.6370</u>	37.5877
	TNN	26.3466	30.3844	31.7512	31.8747	34.6443	36.7893
	F-TNN	28.2529	30.1521	33.1660	35.6747	36.9233	<u>37.2618</u>
SSIM	ITCURTC-11	0.8310	0.8880	0.9118	<u>0.8571</u>	0.8738	0.8848
	ITCURTC-12	0.8172	<u>0.8818</u>	0.9033	0.8535	0.8733	0.8850
	ITCURTC-13	0.8016	0.8774	0.8954	0.8504	0.8731	0.8837
	BCPF	0.8639	0.8761	0.8873	0.8269	0.8554	0.8727
	TMac	<u>0.8402</u>	0.8586	<u>0.9111</u>	0.8200	0.8928	<u>0.9035</u>
	TNN	0.6458	0.8257	0.8382	0.8333	0.8564	0.8804
	F-TNN	0.7583	0.8354	0.8626	0.8745	<u>0.8899</u>	0.9066
RUNTIME (sec)	ITCURTC-11	<u>10.9354</u>	17.3187	18.1098	23.8990	24.1286	25.1853
	ITCURTC-12	10.7715	<u>19.3517</u>	<u>19.7731</u>	<u>25.5856</u>	<u>26.3275</u>	<u>28.0392</u>
	ITCURTC-13	12.2208	21.2458	22.0287	28.8653	29.4986	30.8361
	BCPF	213.6800	360.2903	613.3072	345.3425	500.3060	1629.8061
	TMac	92.9568	104.8518	108.6827	233.8853	242.7499	259.6068
	TNN	3651.4556	3289.5535	3004.6557	5801.1631	6572.9697	6690.7945
	F-TNN	2642.9409	2692.6197	2267.5622	4739.2703	4134.5206	4105.0327

the detail prediction, resulting in a more accurate completion of the tensor that begins to resemble the reference more closely. F-TNN maintains improvements in detail prediction, and edges within the cardiac structure suggest a refined approach to tensor completion. ITCURTC shows a reconstruction where the cardiac structures are clearly defined, reflecting the structure present in the ground truth without implying superiority, but rather indicating effectiveness in predicting the missing values. The highlighted regions of interest (ROIs), marked in blue, allow for a detailed comparison across the methods. In these ROIs, though ITCURTC's reconstructions may not provide the most visually appealing results, they demonstrate efficiency in preserving structural integrity and texture, which are crucial aspects for clinical applications.

Table 3 effectively demonstrates the flexibility and feasibility of the t-CCS model, showing that the reconstruction performance of the t-CCS-based method ITCURTC generally aligns with or matches the reconstruction quality of Bernoulli-sampling-based TC methods. Furthermore, in terms of runtime, ITCURTC, implemented under the t-CCS model, demonstrates marked superiority by significantly outperforming alternatives such as BCPF, TMac, TNN, and F-TNN, all of which are applied under

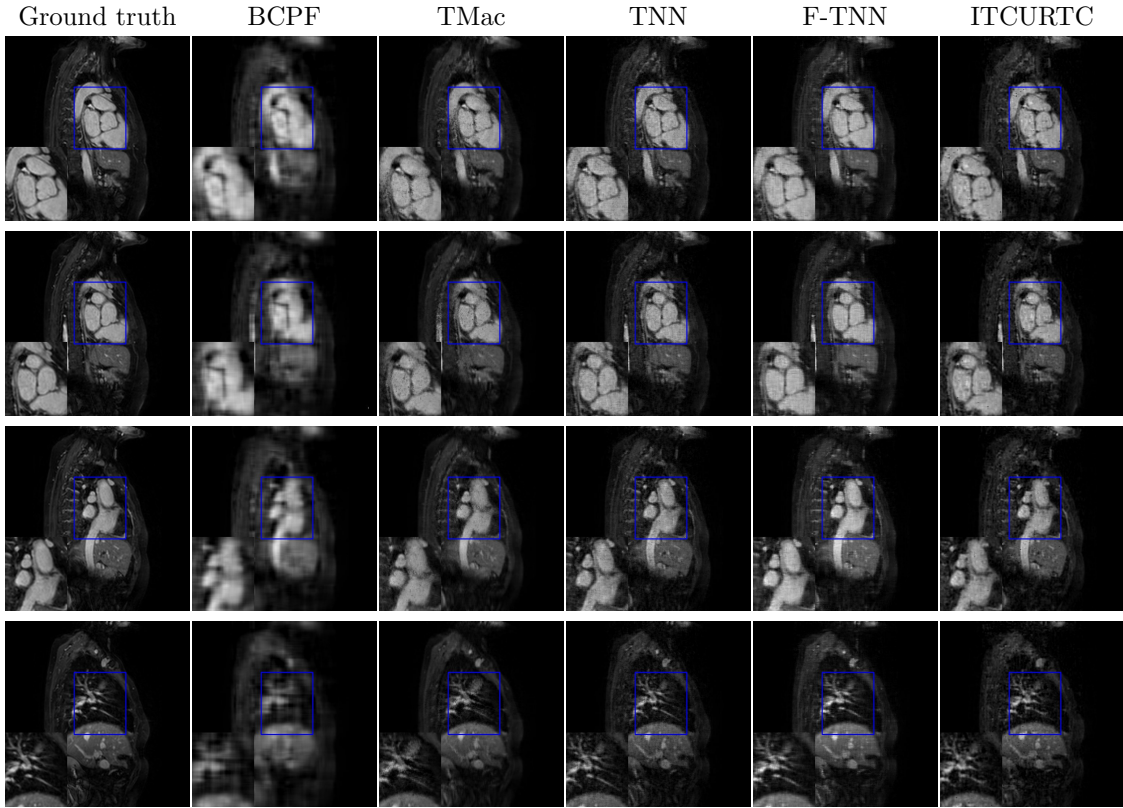


Figure 5: The visualizations of MRI data recovery are obtained by setting a tubal rank of $r = 35$ for ITCURTC with the percentage of selected lateral and horizontal slices $\delta = 27\%$ at an overall sampling rate of 30%. Other algorithms are applied under Bernoulli sampling models with the same overall sampling rate. Results for slices 51, 66, 86, and 106 are shown in rows 1 to 4. Each set includes a $1.3\times$ magnified area for clearer comparison, positioned at the bottom left of each result.

the Bernoulli sampling scheme. This notable advantage distinctly underscores the enhanced effectiveness of the t-CCS model in practical applications.

5.2.3 Seismic data reconstruction

Geophysical 3D seismic data is often modeled as a tensor with inline, crossline, and depth dimensions. In our analysis, we focus on a seismic dataset⁸ of size $51 \times 191 \times 146$, where compact t-SVD with tubal-rank 3 yields less than 5% error, suggesting a low-tubal-rank property of the dataset. The corresponding results are detailed in Figure 6 and Table 4.

Figure 6 presents the comparative analysis of seismic completion algorithms: BCPF, TMac, TNN, and F-TNN, applied based on the Bernoulli sampling model, in contrast to ITCURTC, which is applied based on the t-CCS model. The ground truth serves as the definitive reference, with its stark textural definition. BCPF falls

8. <https://terranubis.com/datainfo/F3-Demo-2020>

Table 3: The quantitative results for MRI data completion are presented, with **the best results** in bold and the second-best underlined. ITCURTC- δ represents the ITCURTC method specifying that the selected proportion of horizontal and lateral slices is exactly $\delta\%$. The t-CCS-based algorithm ITCURTC- δ is performed using the t-CCS scheme, while other Bernoulli-based algorithms are performed using the Bernoulli sampling scheme.

OVERALL OBSERVATION RATE		10%	15%	20%	25%	30%
PSNR	ITCURTC-23	22.4004	24.3553	26.9104	<u>29.1861</u>	30.3911
	ITCURTC-25	22.2548	24.0435	26.9940	29.0219	31.1752
	ITCURTC-27	22.1617	23.9311	27.0871	29.0699	<u>31.2539</u>
	BCPF	22.6581	24.5373	25.1663	25.8111	26.2042
	TMac	22.8690	<u>25.4225</u>	27.7802	29.1526	31.1648
	TNN	23.4779	25.3480	27.9423	28.4522	30.5580
	F-TNN	21.8172	25.7453	27.1969	29.3630	31.3651
SSIM	ITCURTC-23	0.6020	0.6821	0.7584	0.8160	0.8451
	ITCURTC-25	0.5990	0.6769	0.7571	0.8084	0.8619
	ITCURTC-27	0.5990	0.6751	0.7567	0.8086	0.8600
	BCPF	0.6817	0.7151	0.7192	0.7301	0.7367
	TMac	<u>0.6804</u>	0.7323	<u>0.7873</u>	<u>0.8227</u>	0.8924
	TNN	0.6304	<u>0.7494</u>	0.7677	0.7984	0.8793
	F-TNN	0.6442	0.7507	0.8181	0.8562	<u>0.8871</u>
Runtime	ITCURTC-23	<u>5.7908</u>	7.0230	4.8030	5.3058	5.9484
	ITCURTC-25	5.4241	<u>8.3488</u>	<u>5.5303</u>	<u>5.9375</u>	<u>6.7111</u>
	ITCURTC-27	5.8075	8.8408	6.0685	6.4371	7.4916
	BCPF	53.1651	88.2777	111.1949	180.6596	279.2789
	TMac	30.4813	28.0944	28.6216	28.9400	30.0219
	TNN	87.7591	84.0952	56.9761	57.9823	58.2098
	F-TNN	91.2048	86.3112	84.0228	82.2064	81.2119

short of delivering optimal fidelity, with finer details lost in translation. TMac is commendable for preserving the texture’s integrity, providing a cohesive image. TNN improves upon this, sharpening textural nuances and closing in on the ground truth’s visual quality. F-TNN excels visually, capturing essential texture information effectively, a significant advantage when the emphasis is on recognizing general features. ITCURTC demonstrates comparable visual results, though less effective than other methods in terms of PSNR and SSIM.

Table 4 shows that the t-CCS-based method, ITCURTC, achieves the fastest processing speeds while preserving satisfactory levels of PSNR and SSIM. This underscores the suitability of the t-CCS model for applications where rapid processing is essential without significant loss in visual accuracy. Furthermore, the consistent performance of ITCURTC across various subtensor sizes and sampling rates further emphasizes the flexibility and feasibility of the t-CCS model in diverse operational environments.

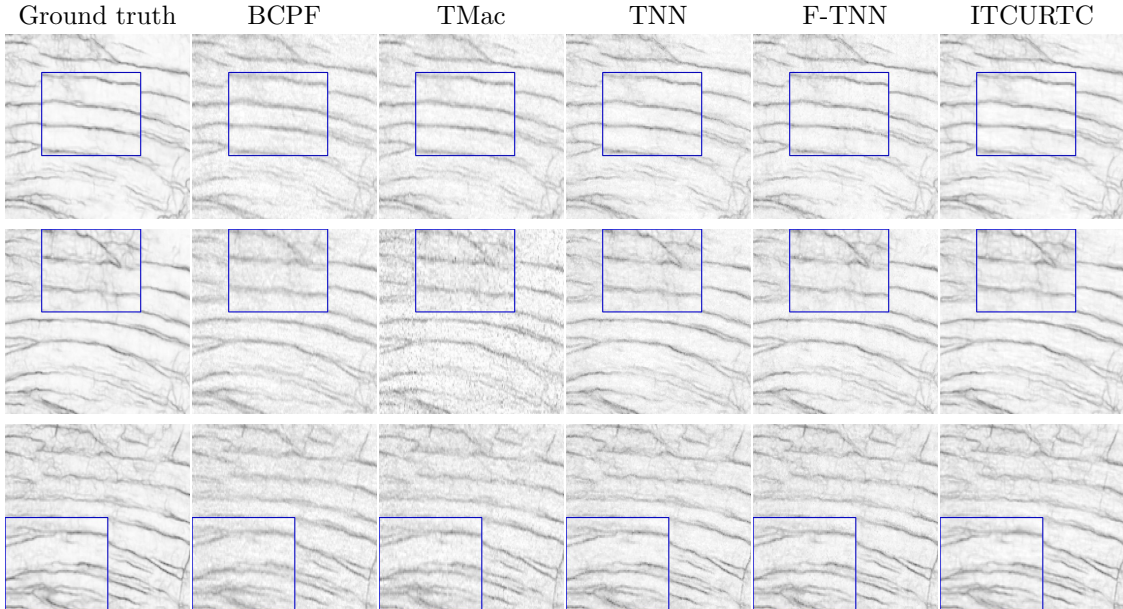


Figure 6: Visualization of seismic data recovery results by setting tubal-rank $r = 3$ for ITCURTC with a percentage of the selected horizontal and lateral slices $\delta = 17\%$ and an overall sampling rate $\alpha = 28\%$, while other methods are applied based on Bernoulli sampling models with the same overall sampling rate 28%. Displayed are slices 15, 25, and 35 from top to bottom, with a $1.2\times$ magnified area in each set for a clearer comparison.

5.3 Discussions on the results of real-world datasets

From the above results, it is evident that our method surpasses others in runtime with significantly lower computational costs. Consider a tensor of size $n_1 \times n_2 \times n_3$. When a framelet transform matrix is constructed using n filters and l levels, the computational cost per iteration for framelet-based Tensor Nuclear Norm (F-TNN) is $\mathcal{O}((nl - l + 1)n_1n_2n_3(n_3 + \min(n_1, n_2)))$. This formulation incorporates the processes involved in generating a framelet transform matrix, as elaborated in seminal works such as [11] and [27]. While enhancing the number of levels and filters in F-TNN can improve the quality of results, it also escalates the computational burden, particularly for tensors of substantial size. In our experiments, we set both the framelet level and the number of filters to 1 for the F-TNN implementation. For comparison, the computational cost per iteration for TNN is $\mathcal{O}(\min(n_1, n_2)n_1n_2n_3 + n_1n_2n_3 \log(n_3))$, and for the TMac, it is $\mathcal{O}((r_1 + r_2 + r_3)n_1n_2n_3)$ where (r_1, r_2, r_3) denotes the Tucker rank. For BCPF, it is $\mathcal{O}(R^3(n_1n_2n_3) + R^2(n_1n_2 + n_2n_3 + n_3n_1))$, where R is the CP rank. In contrast, the computational expense per iteration of our proposed method is significantly reduced to $\mathcal{O}(r|I|n_2n_3 + r|J|n_1n_3)$, assuming $|I| \ll n_1$ and $|J| \ll n_2$, indicating a substantial efficiency improvement over traditional methods.

Note that for F-TNN, [29] formulated the tensor nuclear norm utilizing the M -product [33], a generalization of the t-product for 3-order tensors. In [29], they incorporated a tight wavelet frame (framelet) as the transformation matrix M . This

Table 4: Quantitative results for seismic data completion: TMac, TNN, F-TNN with Bernoulli sampling, and our method with t-CCS. **Best results** are in bold, and second-best are underlined. ITCURTC- δ refers to the ITCURTC method with the percentages of selected horizontal and lateral slices set at a fixed rate of $\delta\%$. The t-CCS based algorithm ITCURTC- $\delta\%$ s are performed on t-CCS scheme while other Bernoulli based algorithms are performed on Bernoulli Sampling scheme.

OVERALL OBSERVATION RATE		12 %	16 %	20 %	24 %	28 %
PSNR	ITCURTC-15	24.8020	26.4092	27.4143	29.3053	30.6585
	ITCURTC-16	24.7386	26.1054	27.4737	29.3542	30.6905
	ITCURTC-17	<u>24.8381</u>	26.1176	27.4768	28.8953	30.5312
	BCPF	24.0733	24.1905	24.2084	24.2454	24.3015
	TMac	24.8859	26.5349	26.9970	28.4662	30.7237
	TNN	23.7395	26.3806	<u>27.7428</u>	29.5430	30.9172
	F-TNN	24.0688	27.5890	28.6408	29.7987	31.2791
SSIM	ITCURTC-15	<u>0.5732</u>	0.6691	0.7338	<u>0.8143</u>	0.8596
	ITCURTC-16	0.5691	0.6507	0.7349	0.8129	<u>0.8610</u>
	ITCURTC-17	0.5724	0.6491	0.7321	0.7939	0.8523
	BCPF	0.5304	0.5407	0.5420	0.5494	0.5532
	TMac	0.5566	<u>0.6738</u>	0.6962	0.7612	0.8504
	TNN	0.5165	0.6442	<u>0.7577</u>	0.8080	0.8486
	F-TNN	0.6607	0.7551	0.8142	0.8479	0.8814
Runtime	ITCURTC-15	<u>6.4327</u>	6.7701	6.2598	6.8633	6.8212
	ITCURTC-16	6.3825	6.3579	<u>6.7522</u>	<u>7.0789</u>	<u>7.0215</u>
	ITCURTC-17	7.0379	<u>6.6306</u>	6.8325	7.1480	7.3253
	BCPF	33.5759	33.1832	32.1258	31.7875	31.2663
	TMac	16.6135	14.3412	16.8581	13.7124	13.1142
	TNN	34.5718	31.3138	29.2464	26.1727	23.9876
	F-TNN	22.1019	21.4482	22.1420	17.8848	18.0547

meticulous design of the M transformation contributes to the superior reconstruction quality of F-TNN. However, the absence of a rapid implementation for multiplying the tensor with matrix M along the third mode leads to F-TNN requiring significantly more computational time compared to other evaluated methods.

It is worth noting that our current approach provides an effective balance between runtime efficiency and reconstruction quality, making it well-suited for potential real-world applications. This balanced approach is particularly relevant in practical settings where it is essential to consider both runtime and quality in big data applications.

6. Conclusion

In this work, we present the t-CCS model, an extension of the matrix CCS model to a tensor framework. We provide both theoretical and experimental evidence demonstrating the model’s flexibility and feasibility. The ITCURTC algorithm, designed for the t-CCS model, provides a balanced trade-off between runtime efficiency and reconstruction quality. While it is not as effective as the state-of-the-art Bernoulli-based TC algorithm, it is still comparable in terms of PSNR and SSIM. Thus, one

of the directions of our future research will focus on enhancing reconstruction quality through the integration of the M -product.

From the theoretical perspective, our current theoretical result shows that the t-CUR sampling scheme, as a special case of t-CCS model, requires a complexity of $\mathcal{O}(\mu_0 r n_3 (n_2 \log(n_1 n_3) + n_1 \log(n_2 n_3)))$ which is more sampling-efficient than that of a general t-CCS scheme. This finding suggests potential to further improve the theoretical sampling complexity for the t-CCS model, an aspect we plan to explore in future work. Additionally, there is a need for a comprehensive theoretical analysis of the convergence behavior of the ITCURTC within the t-CCS framework. Evaluating the algorithm's robustness against additive noise will also be a critical focus for future research. Furthermore, while our current work is limited to third-order tensors, we aim to extend our approach to higher-order tensor configurations in future studies.

Acknowledgement

This work is partially supported by NSF DMS 2304489 and the computational resources provided by the Institute for Cyber-Enabled Research at Michigan State University. We are indebted to Xuanhao Huang Design for making our sketches of Figure 1 a reality.

Appendix A. Proof of Theorem 3

In this section, we provide a detailed proof of Theorem 3, which is one of the two important supporting theorems to our main result Theorem 2.

A.1 Supporting lemmas for Theorem 3

Before proceeding to prove Theorem 3, we will first introduce and discuss several supporting lemmas. These lemmas are crucial to establishing the foundation for the proof of Theorem 3.

Lemma 1 *Let $\mathcal{T} \in \mathbb{K}^{n_1 \times n_2 \times n_3}$, $I \subseteq [n_1]$, and $J \subseteq [n_2]$. \mathcal{S}_I and \mathcal{S}_J are the horizontal and lateral sampling tensors associated with indices I and J , respectively (see Definition 11). Then the following results hold*

$$\overline{\mathcal{S}_I * \mathcal{T}} = \begin{bmatrix} [\mathcal{S}_I]_{:, :, 1} \cdot [\widehat{\mathcal{T}}]_{:, :, 1} & & & & \\ & [\mathcal{S}_I]_{:, :, 1} \cdot [\widehat{\mathcal{T}}]_{:, :, 2} & & & \\ & & \ddots & & \\ & & & [\mathcal{S}_I]_{:, :, 1} \cdot [\widehat{\mathcal{T}}]_{:, :, n_3} & \\ & & & & \end{bmatrix}, \quad (13)$$

$$\overline{\mathcal{T} * \mathcal{S}_J} = \begin{bmatrix} [\widehat{\mathcal{T}}]_{:, :, 1} \cdot [\mathcal{S}_J]_{:, :, 1} & & & & \\ & [\widehat{\mathcal{T}}]_{:, :, 2} \cdot [\mathcal{S}_J]_{:, :, 1} & & & \\ & & \ddots & & \\ & & & [\widehat{\mathcal{T}}]_{:, :, n_3} \cdot [\mathcal{S}_J]_{:, :, 1} & \\ & & & & \end{bmatrix}. \quad (14)$$

Proof Here, we will only focus on the proof of (13). First, it is easy to see that $\overline{\mathcal{S}_I} * \overline{\mathcal{T}} = \overline{\mathcal{S}_I} \cdot \overline{\mathcal{T}}$. In addition,

$$\overline{\mathcal{S}_I} = \begin{bmatrix} [\mathcal{S}_I]_{:,:,1} & & & \\ & [\mathcal{S}_I]_{:,:,1} & & \\ & & \ddots & \\ & & & [\mathcal{S}_I]_{:,:,1} \end{bmatrix} \text{ and } \overline{\mathcal{T}} = \begin{bmatrix} [\widehat{\mathcal{T}}]_{:,:,1} & & & \\ & [\widehat{\mathcal{T}}]_{:,:,2} & & \\ & & \ddots & \\ & & & [\widehat{\mathcal{T}}]_{:,:,n_3} \end{bmatrix}.$$

The result can thus be derived. \blacksquare

Theorem 5 (Matrix Chernoff inequality [54]) Consider a finite sequence $\{X_k\}$ of independent, random, Hermitian matrices with common dimension d . Assume that

$$0 \leq \lambda_{\min}(X_k) \text{ and } \lambda_{\max}(X_k) \leq L \text{ for each index } k.$$

Set $Y = \sum_k X_k$. Let μ_{\min} and μ_{\max} be the minimum and maximum eigenvalues of $\mathbb{E}(Y)$, respectively, where \mathbb{E} is the expectation operator. Then,

$$\begin{aligned} \mathbb{P}\{\lambda_{\min}(Y) \leq (1 - \varepsilon)\mu_{\min}\} &\leq d \left[\frac{e^{-\varepsilon}}{(1-\varepsilon)^{1-\varepsilon}} \right]^{\mu_{\min}/L} \text{ for } \varepsilon \in [0, 1), \text{ and} \\ \mathbb{P}\{\lambda_{\max}(Y) \geq (1 + \varepsilon)\mu_{\max}\} &\leq d \left[\frac{e^{\varepsilon}}{(1+\varepsilon)^{1+\varepsilon}} \right]^{\mu_{\max}/L} \text{ for } \varepsilon \geq 0. \end{aligned}$$

Lemma 2 Suppose A is a block diagonal matrix, i.e., $A = \begin{bmatrix} A_1 & & & \\ & A_2 & & \\ & & \ddots & \\ & & & A_{n_3} \end{bmatrix}$,

where $A_i \in \mathbb{K}^{n_1 \times r_i}$ and $A_i^\top A_i = \mathbb{I}_{r_i}$ ($r_i \times r_i$ identity matrix). Set $\vec{r} = (r_1, \dots, r_{n_3})$. Let I be a random subset of $[n_1]$. Then for any $\delta \in [0, 1)$, the $\|\vec{r}\|_1$ -th singular value of the matrix

$$N =: \begin{bmatrix} [\mathcal{S}_I]_{:,:,1} & & & \\ & [\mathcal{S}_I]_{:,:,1} & & \\ & & \ddots & \\ & & & [\mathcal{S}_I]_{:,:,1} \end{bmatrix} \begin{bmatrix} A_1 & & & \\ & A_2 & & \\ & & \ddots & \\ & & & A_{n_3} \end{bmatrix}$$

will be no less than $\sqrt{\frac{(1-\delta)|I|}{n_1}}$ with probability at least

$$1 - \|\vec{r}\|_1 e^{-(\delta+(1-\delta)\log(1-\delta)) \frac{|I|}{n_1 \max_{i \in [n_1, n_3]} \|A_i\|_{\mathbb{F}}^2}}.$$

Proof Firstly, it is easy to check that

$$N = [\mathbb{I}_{n_3} \otimes [\mathcal{S}_I]_{:,:,1}] \cdot A = \sum_{i \in I} \sum_{j=1}^{n_3} \mathbf{e}_{(j-1)n_1+i} \cdot [A]_{(j-1)n_1+i,:},$$

where $\mathbf{e}_{(j-1)n_1+i} \in \mathbb{K}^{n_1 n_3}$ is the standard column basis vector. Consider $\|\vec{r}\|_1 \times \|\vec{r}\|_1$ Gram matrix

$$Y := N^\top \cdot N = \sum_{i \in I} \sum_{j=1}^{n_3} (\mathbf{e}_{(j-1)n_1+i} \cdot [A]_{(j-1)n_1+i,:})^\top \cdot \mathbf{e}_{(j-1)n_1+i} \cdot [A]_{(j-1)n_1+i,:}$$

$$= \sum_{i \in I} \sum_{j=1}^{n_3} [A]_{(j-1)n_1+i,:}^\top [A]_{(j-1)n_1+i,:} =: \sum_{i \in I} X_i,$$

where $X_i = \sum_{j=1}^{n_3} [A]_{(j-1)n_1+i,:}^\top [A]_{(j-1)n_1+i,:}$. It is easy to see that Y is a random matrix due to randomness inherited from the random set I . It is easy to see that each X_i is a positive semidefinite matrix of size $\|\vec{r}\|_1 \times \|\vec{r}\|_1$. Thus, the random matrix Y in fact is a sum of $|I|$ random matrices sampled without replacement from the set $\{X_1, X_2, \dots, X_{n_1}\}$ of positive semi-definite matrices. Notice that

$$\begin{aligned} \lambda_{\max}(X_i) &= \lambda_{\max} \left(\sum_{j=1}^{n_3} (\mathbf{e}_{(j-1)n_1+i} \cdot [A]_{(j-1)n_1+i,:})^\top \cdot \mathbf{e}_{(j-1)n_1+i} \cdot [A]_{(j-1)n_1+i,:} \right) \\ &= \left| \sigma_{\max} \left(\sum_{j=1}^{n_3} \mathbf{e}_{(j-1)n_1+i} \cdot [A]_{(j-1)n_1+i,:} \right) \right|^2 \leq \max_i \| [A]_{i,:} \|_{\mathbb{F}}^2. \end{aligned}$$

By the orthogonal property of matrix A , it is easy to see that $\mathbb{E}(X_i) = \frac{1}{n_1} \mathbb{I}_{\|\vec{r}\|_1}$ and thus $\mathbb{E}(Y) = \frac{|I|}{n_1}$. Thus, by the fact that $\lambda_{\min}(Y) = \sigma_{\min}^2(N)$ and by the matrix Chernoff inequality, we have

$$\mathbb{P} \left(\sigma_{\min}(N) \leq \sqrt{\frac{(1-\delta)|I|}{n_1}} \right) \leq \|\vec{r}\|_1 e^{-(\delta+(1-\delta)\log(1-\delta)) \frac{|I|}{n_1 \max_{i \in [n_1, n_3]} \| [A]_{i,:} \|_{\mathbb{F}}^2}}, \forall \delta \in [0, 1].$$

■

In the following section, we mainly delve into the proof of Theorem 3 to explain the likelihood of the t-CUR decomposition holding.

A.2 The proof of Theorem 3

Proof According to Theorem 1, $\mathcal{T} = \mathcal{C} * \mathcal{U}^\dagger * \mathcal{R}$ is equivalent to $\text{rank}_m(\mathcal{T}) = \text{rank}_m(\mathcal{C}) = \text{rank}_m(\mathcal{R})$. Therefore, it suffices to prove that $\text{rank}_m(\mathcal{T}) = \text{rank}_m(\mathcal{C}) = \text{rank}_m(\mathcal{R})$ holds with probability at least $1 - \frac{1}{n_1^{\beta_1}} - \frac{1}{n_2^{\beta_2}}$ under the given conditions.

Notice that

$$\begin{aligned} \bar{\mathcal{T}} &= \begin{bmatrix} [\hat{\mathcal{T}}]_{::,1} & & & \\ & [\hat{\mathcal{T}}]_{::,2} & & \\ & & \ddots & \\ & & & [\hat{\mathcal{T}}]_{::,n_3} \end{bmatrix} \\ &= \begin{bmatrix} W_1 \Sigma_1 V_1^\top & & & \\ & W_2 \Sigma_2 V_2^\top & & \\ & & \ddots & \\ & & & W_{n_3} \Sigma_{n_3} V_{n_3}^\top \end{bmatrix} \end{aligned} \tag{15}$$

$$\begin{aligned}
&= \begin{bmatrix} W_1 & & & \\ & W_2 & & \\ & & \ddots & \\ & & & W_{n_3} \end{bmatrix} \cdot \begin{bmatrix} \Sigma_1 & & & \\ & \Sigma_2 & & \\ & & \ddots & \\ & & & \Sigma_{n_3} \end{bmatrix} \cdot \begin{bmatrix} V_1^\top & & & \\ & V_2^\top & & \\ & & \ddots & \\ & & & V_{n_3}^\top \end{bmatrix} \\
&=: W \cdot \Sigma \cdot V^\top,
\end{aligned}$$

where $W_i \Sigma_i V_i^\top$ in (15) is the compact SVD of $[\overline{\mathcal{T}}]_{\dots, i}$ for $i \in [n_3]$. And $\overline{\mathcal{R}} = \overline{\mathcal{S}}_I W \Sigma V^\top$. By the definition of tensor multi-rank, we have $W_i \in \mathbb{K}^{n_1 \times r_i}$, $\Sigma_i \in \mathbb{K}^{r_i \times r_i}$, $V_i \in \mathbb{K}^{n_2 \times r_i}$, $W \in \mathbb{K}^{n_1 n_3 \times \|\overline{r}\|_1}$, $\Sigma \in \mathbb{K}^{\|\overline{r}\|_1 \times \|\overline{r}\|_1}$, and $V \in \mathbb{K}^{n_2 n_3 \times \|\overline{r}\|_1}$.

Consequently, demonstrating that $\text{rank}(\overline{\mathcal{R}}) = \|\overline{r}\|_1$ suffices to ensure the condition that $\text{rank}_m(\mathcal{T}) = \text{rank}_m(\mathcal{R})$. Observe that Σ is a square matrix with full rank and V has full column rank. By the Sylvester rank inequality, $\text{rank}(\overline{\mathcal{R}}) = \|\overline{r}\|_1$ can be guaranteed by showing $\text{rank}(\overline{\mathcal{S}}_I \cdot W) = \|\overline{r}\|_1$. By applying Lemma 2, we have that for all $\delta \in [0, 1)$,

$$\begin{aligned}
&\mathbb{P} \left(\sigma_{\|\overline{r}\|_1}(\overline{\mathcal{S}}_I \cdot W) \leq \sqrt{(1-\delta)|I|/n_1} \right) \leq \|\overline{r}\|_1 e^{-(\delta+(1-\delta)\log(1-\delta))\frac{|I|}{\mu_0 \|\overline{r}\|_\infty}}. \\
|I| \geq \frac{\beta_1 \mu_0 \|r\|_\infty \log(n_1 \|\overline{r}\|_1)}{\delta+(1-\delta)\log(1-\delta)} &\text{ implies } \mathbb{P} \left(\sigma_{\|\overline{r}\|_1}(\overline{\mathcal{S}}_I \cdot W) \leq \sqrt{(1-\delta)|I|/n_1} \right) \leq \frac{1}{n_1^{\beta_1}}. \text{ Note} \\
\text{that } \mathbb{P}(\text{rank}(\overline{\mathcal{S}}_I \cdot W) < \|\overline{r}\|_1) &\leq \mathbb{P} \left(\sigma_{\|\overline{r}\|_1}(\overline{\mathcal{S}}_I \cdot W) \leq \sqrt{\frac{(1-\delta)|I|}{n_1}} \right). \text{ We thus have when} \\
|I| \geq \frac{\beta_1 \mu_0 \|r\|_\infty \log(n_1 \|\overline{r}\|_1)}{\delta+(1-\delta)\log(1-\delta)}, & \\
\mathbb{P}(\text{rank}(\overline{\mathcal{S}}_I \cdot W) = \|\overline{r}\|_1) &= 1 - \mathbb{P}(\text{rank}(\overline{\mathcal{S}}_I \cdot W) < \|\overline{r}\|_1) \\
&\geq 1 - \mathbb{P} \left(\sigma_{\|\overline{r}\|_1}(\overline{\mathcal{S}}_I \cdot W) \leq \sqrt{\frac{(1-\delta)|I|}{n_1}} \right) \geq 1 - \frac{1}{n_1^{\beta_1}}.
\end{aligned}$$

Similarly, one can show that $\text{rank}(\overline{\mathcal{S}}_J \cdot \overline{\mathcal{V}}) = \|\overline{r}\|_1$ holds with probability at least $1 - \frac{1}{n_2^{\beta_2}}$ provided that $|J| \geq \frac{\beta_2 \mu_0 \|r\|_\infty \log(n_2 \|\overline{r}\|_1)}{\delta+(1-\delta)\log(1-\delta)}$.

Combining all the statements and setting $\delta = 0.815$ and $\beta_1 = \beta_2 = \beta$, we conclude that $\mathcal{T} = \mathcal{C} * U^\dagger * \mathcal{R}$ holds with probability at least $1 - \frac{1}{n_1^\beta} - \frac{1}{n_2^\beta}$, provided that $|I| \geq 2\beta\mu_0 \|\overline{r}\|_\infty \log(n_1 \|\overline{r}\|_1)$ and $|J| \geq 2\beta\mu_0 \|\overline{r}\|_\infty \log(n_2 \|\overline{r}\|_1)$. \blacksquare

Next we will present the proof to our another theoretical foundation, Theorem 4, which also plays a vital role in our main theoretical result, Theorem 2.

Appendix B. Proof of Theorem 4

In this section, we provide a detailed proof of Theorem 4, another important supporting theorem for our main theoretical result, Theorem 2. To the best of our knowledge, there is no existing tensor version of the result found in [45, Theorem 1.1], which provides an explicit expression of numerical constants within the theorem's statement. Existing results related to tensor versions, such as [64, Theorem 3.1] in the context of tensor completion, typically imply numerical constants implicitly. One can see that

[64, Theorem 3.1] does not give an explicit expression of the numerical constants of c_0, c_1 and c_2 .

Theorem 6 [64, Theorem 3.1] *Suppose that the reduced t-SVD of $\mathcal{Z} \in \mathbb{K}^{n_1 \times n_2 \times n_3}$ is given by $\mathcal{Z} = \mathcal{W} * \mathcal{S} * \mathcal{V}^\top$ where $\mathcal{W} \in \mathbb{R}^{n_1 \times r \times n_3}$, $\mathcal{S} \in \mathbb{R}^{r \times r \times n_3}$, $\mathcal{V} \in \mathbb{R}^{n_2 \times r \times n_3}$, and \mathcal{Z} also satisfies the standard tensor μ_0 -incoherence condition. Suppose the entries in Ω are sampled according to the Bernoulli model with probability p . Then there exist constants $c_0, c_1, c_2 > 0$ such that if*

$$p \geq c_0 \frac{\mu_0 r \log(n_3(n_1 + n_2))}{\min\{n_1, n_2\}},$$

then \mathcal{Z} is the unique minimizer to the follow optimization

$$\min_{\mathcal{X}} \|\mathcal{X}\|_{\text{TNN}}, \text{ subject to } \mathcal{P}_\Omega(\mathcal{X}) = \mathcal{P}_\Omega(\mathcal{Z}),$$

with probability at least

$$1 - c_1((n_1 + n_2)n_3)^{-c_2}.$$

Our work makes a substantial contribution by meticulously analyzing these numerical constants and providing explicit formulations for their expressions. These theoretical advancements are comprehensively elaborated in our theoretical section.

B.1 Notation

Before moving forward, let us introduce several notations and definitions used throughout the rest of the supplemental material but not covered in earlier sections. We introduce two specific tensors: $\mathring{\mathbf{e}}_i \in \mathbb{K}^{n \times 1 \times n_3}$, which contains a 1 in the $(i, 1, 1)$ -th position and zeros in all other positions; and $\mathring{\mathbf{e}}_k \in \mathbb{K}^{1 \times 1 \times n_3}$, which includes a 1 in the $(1, 1, k)$ -th position with zeros elsewhere. Additionally, for a specified set Ω , we use $\delta_{i,j,k}$ to denote the indicator function $\mathbf{1}_{(i,j,k) \in \Omega}$.

Definition 14 *Suppose \mathcal{Z} is an $n_1 \times n_2 \times n_3$ tensor and its compact t-SVD is given by $\mathcal{Z} = \mathcal{W} * \mathcal{S} * \mathcal{V}^\top$ where $\mathcal{W} \in \mathbb{K}^{n_1 \times r \times n_3}$, $\mathcal{S} \in \mathbb{K}^{r \times r \times n_3}$ and $\mathcal{V} \in \mathbb{K}^{n_2 \times r \times n_3}$. Define projection space \mathbb{T} as*

$$\left\{ \sum_{k=1}^r ([\mathcal{W}]_{:,k,:} * [\mathcal{X}]_{:,k,:}^\top + [\mathcal{Y}]_{:,k,:} * [\mathcal{V}]_{:,k,:}^\top) : \mathcal{X} \in \mathbb{K}^{n_2 \times r \times n_3}, \mathcal{Y} \in \mathbb{K}^{n_1 \times r \times n_3} \right\}$$

and the orthogonal projection space \mathbb{T}^\perp is the orthogonal complement \mathbb{T} in $\mathbb{K}^{n_1 \times n_2 \times n_3}$.

Define $\mathcal{P}_{\mathbb{T}}(\mathcal{X})$ and $\mathcal{P}_{\mathbb{T}^\perp}(\mathcal{X})$ as

$$\mathcal{P}_{\mathbb{T}}(\mathcal{X}) = \mathcal{W} * \mathcal{W}^\top * \mathcal{X} + \mathcal{X} * \mathcal{V} * \mathcal{V}^\top - \mathcal{W} * \mathcal{W}^\top * \mathcal{X} * \mathcal{V} * \mathcal{V}^\top,$$

$$\text{and } \mathcal{P}_{\mathbb{T}^\perp}(\mathcal{X}) = (\mathcal{I}_{n_1} - \mathcal{W} * \mathcal{W}^\top) * \mathcal{X} * (\mathcal{I}_{n_2} - \mathcal{V} * \mathcal{V}^\top),$$

where $\mathcal{I}_{n_1} \in \mathbb{K}^{n_1 \times n_1 \times n_3}$ and $\mathcal{I}_{n_2} \in \mathbb{K}^{n_2 \times n_2 \times n_3}$ are the identity tensors.

Definition 15 *Define the operator $\mathcal{R}_\Omega : \mathbb{K}^{n_1 \times n_2 \times n_3} \rightarrow \mathbb{K}^{n_1 \times n_2 \times n_3}$ as:*

$$\mathcal{R}_\Omega(\mathcal{X}) = \sum_{i,j,k} \frac{1}{p} \delta_{i,j,k} [\mathcal{X}]_{i,j,k} \mathring{\mathbf{e}}_i * \mathring{\mathbf{e}}_k * \mathring{\mathbf{e}}_j^\top.$$

Definition 16 Given two tensors $\mathcal{A} \in \mathbb{K}^{n_1 \times n_2 \times n_3}$ and $\mathcal{B} \in \mathbb{K}^{n_1 \times n_2 \times n_3}$, the inner product of these two tensors is defined as:

$$\langle \mathcal{A}, \mathcal{B} \rangle = \frac{1}{n_3} \text{trace} \left(\overline{\mathcal{B}}^\top \cdot \overline{\mathcal{A}} \right).$$

Before introducing the tensor operator norm, we need to define a transformed version of a tensor operator. Given a tensor operator $\mathcal{F} : \mathbb{K}^{n_1 \times n_2 \times n_3} \rightarrow \mathbb{K}^{n_1 \times n_2 \times n_3}$, the associated transformed operator $\overline{\mathcal{F}} : \mathbb{B} \rightarrow \mathbb{B}$ is defined as $\overline{\mathcal{F}}(\overline{\mathcal{X}}) = \overline{\mathcal{F}(\mathcal{X})}$, where $\mathbb{B} = \{\overline{\mathcal{B}} : \mathcal{B} \in \mathbb{K}^{n_1 \times n_2 \times n_3}\}$.

Definition 17 (Tensor operator norm) Given an operator $\mathcal{F} : \mathbb{K}^{n_1 \times n_2 \times n_3} \rightarrow \mathbb{K}^{n_1 \times n_2 \times n_3}$, the operator norm $\|\mathcal{F}\|$ is defined as $\|\mathcal{F}\| = \|\overline{\mathcal{F}}\| = \max_{\|\overline{\mathcal{X}}\|_{\text{F}}=1} \|\overline{\mathcal{F}}(\overline{\mathcal{X}})\|_{\text{F}} = \max_{\|\overline{\mathcal{X}}\|_{\text{F}}=1} \left\| \overline{\mathcal{F}(\mathcal{X})} \right\|_{\text{F}}$.

Definition 18 ($\ell_{\infty,2}$ norm [64]) Given a tensor $\mathcal{X} \in \mathbb{K}^{n_1 \times n_2 \times n_3}$, its $\ell_{\infty,2}$ norm is defined as

$$\|\mathcal{X}\|_{\infty,2} := \max \left\{ \max_i \sqrt{\sum_{b,k} [\mathcal{X}]_{i,b,k}^2}, \max_j \sqrt{\sum_{a,k} [\mathcal{X}]_{a,j,k}^2} \right\}.$$

Definition 19 (Tensor infinity norm) Given a tensor $\mathcal{X} \in \mathbb{K}^{n_1 \times n_2 \times n_3}$, its infinity norm is defined as $\|\mathcal{X}\|_{\infty} := \max_{i,j,k} |[\mathcal{X}]_{i,j,k}|$.

B.2 Problem statement

In this section, we present a formal definition of the tensor completion problem based on the Bernoulli sampling model. Consider a third-order tensor $\mathcal{Z} \in \mathbb{K}^{n_1 \times n_2 \times n_3}$ with tubal-rank r . We denote Ω as the set of indices of the observed entries, generated according to the Bernoulli sampling model with probability p . We define the sampling operator \mathcal{P}_{Ω} such that for a given tensor \mathcal{X} in $\mathbb{K}^{n_1 \times n_2 \times n_3}$,

$$\mathcal{P}_{\Omega}(\mathcal{X}) = \sum_{(i,j,k) \in \Omega} [\mathcal{X}]_{i,j,k} \mathcal{E}_{i,j,k},$$

where $\mathcal{E}_{i,j,k}$ is a tensor in $\{0, 1\}^{n_1 \times n_2 \times n_3}$ with all elements zero except for the one at the position indexed by (i, j, k) . The primary goal of the tensor completion problem is to reconstruct the tensor \mathcal{Z} from the entries in Ω .

We utilize the approach proposed by [64], which addresses the TC issue through a specific convex optimization problem formulated as follows:

$$\min_{\mathcal{X}} \|\mathcal{X}\|_{\text{TNN}}, \text{ subject to } \mathcal{P}_{\Omega}(\mathcal{X}) = \mathcal{P}_{\Omega}(\mathcal{Z}). \quad (16)$$

Notice that TNN is convex but not strictly convex. Thus, there might be more than one local minimizer to (16). Therefore, we need to establish conditions to ensure that our optimization problem has a unique minimizer, which is exactly the tensor we seek to recover. The question of under what conditions \mathcal{Z} is the unique minimizer of (16) naturally arises. In response, Proposition 1 gives an affirmative answer.

Before proceeding, it is important to highlight that in the following context, for convenience, we will interchangeably use $\|\cdot\|$ to denote the tensor spectral norm, tensor operator norm or the matrix spectral norm, depending on the specific situation.

Proposition 1 ([37]) *Assume that $\mathcal{Z} \in \mathbb{K}^{n_1 \times n_2 \times n_3}$ of tubal-rank r satisfies the tensor μ_0 -incoherence condition and its compact t -SVD is given by $\mathcal{Z} = \mathcal{W} * \mathcal{S} * \mathcal{V}^\top$, where $\mathcal{W} \in \mathbb{K}^{n_1 \times r \times n_3}$, $\mathcal{S} \in \mathbb{K}^{r \times r \times n_3}$, and $\mathcal{V} \in \mathbb{K}^{n_2 \times r \times n_3}$. Suppose that Ω is generated according to the Bernoulli sampling model with probability p . Then tensor \mathcal{Z} is the unique minimizer of (16) if the following two conditions hold:*

Condition 1 $\|\mathcal{P}_\mathbb{T} \mathcal{R}_\Omega \mathcal{P}_\mathbb{T} - \mathcal{P}_\mathbb{T}\| \leq \frac{1}{2}$.

Condition 2 *There exists a tensor \mathcal{Y} such that $\mathcal{P}_\Omega(\mathcal{Y}) = \mathcal{Y}$ and*

$$(a) \quad \|\mathcal{P}_\mathbb{T}(\mathcal{Y}) - \mathcal{W} * \mathcal{V}^\top\|_{\text{F}} \leq \frac{1}{4} \sqrt{\frac{p}{n_3}};$$

$$(b) \quad \|\mathcal{P}_{\mathbb{T}^\perp}(\mathcal{Y})\| \leq \frac{1}{2}.$$

Based on Proposition 1, our main result is derived through probabilistic estimation of the Condition 1 and Condition 2. Throughout this computation, we explicitly determine both the lower bound of the sampling probability p and the probability of the exact recovery of \mathcal{Z} . The architecture of the entire proof is described in B.3.

B.3 Architecture of the proof of Theorem 4

The proof of Theorem 4 follows the pipeline developed in [37, 64]. We first state a sufficient condition for \mathcal{Z} to be the unique solution to (16) by constructing a dual certificate \mathcal{Y} obeying two conditions. This result is summarized in Proposition 1. To obtain our result Theorem 4, we just need to show that the conditions in Proposition 1 hold with high probability. Theorem 4 is built on the basis of Lemma 6, Lemma 7, Lemma 8, and Corollary 1. A detailed roadmap of the proof towards Theorem 4 is outlined in Figure 7.

B.4 Proof of Theorem 4

In this section, we present a comprehensive proof of Theorem 4. Our primary objective is to demonstrate that, under the stipulated condition on p as specified in (4) of the main text, Conditions 1 and 2 in Proposition 1 are satisfied with high probability. Before delving into the proof of Theorem 4, we will introduce several supporting lemmas to establish the necessary theoretical foundation.

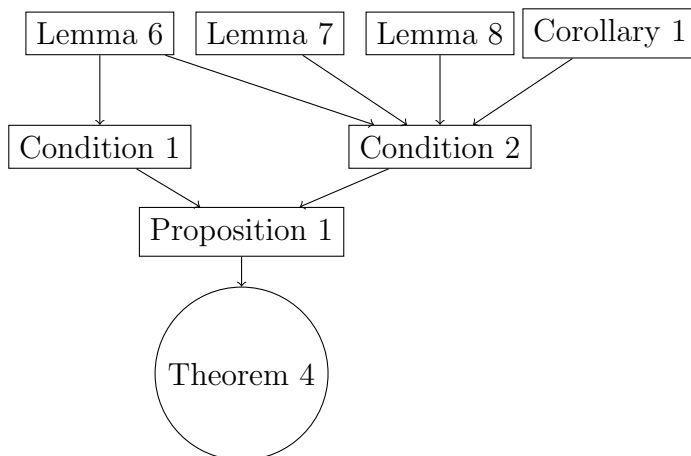


Figure 7: The structure of the proof of Theorem 4: The core of the proof for Theorem 4 relies on assessing the probability that certain conditions, specified in Proposition 1, are met. Condition 1 and Condition 2 serve as sufficient criteria to ensure the applicability of Proposition 1. Thus, the proof of Theorem 4 primarily involves determining the likelihood that Condition 1 and Condition 2 are satisfied. The probabilistic assessment of Condition 1 utilizes Lemma 6 as a fundamental instrument. Similarly, the evaluation of Condition 2 employs Lemmas 6 to 8, and Corollary 1 as essential tools.

B.4.1 Supporting lemmas for the proof of Theorem 4

Lemma 3 (Non-commutative Bernstein inequality [54]) *Let $X_1, \dots, X_L \in \mathbb{K}^{n_1 \times n_2}$ be independent zero-mean random matrices. Suppose*

$$\sigma^2 = \max \left\{ \left\| \mathbb{E} \left[\sum_{k=1}^L X_k X_k^\top \right] \right\|, \left\| \mathbb{E} \left[\sum_{k=1}^L X_k^\top X_k \right] \right\| \right\}$$

and $\|X_k\| \leq M$. Then for any $\tau \geq 0$,

$$\mathbb{P} \left(\left\| \sum_{k=1}^L X_k \right\| \geq \tau \right) \leq (n_1 + n_2) \exp \left(\frac{-\tau^2/2}{\sigma^2 + \frac{M\tau}{3}} \right).$$

The following lemma is a variant of Non-commutative Bernstein inequality by choosing $\tau = \sqrt{2c\sigma^2 \log(n_1 + n_2)} + cM \log(n_1 + n_2)$.

Lemma 4 Let $X_1, \dots, X_L \in \mathbb{K}^{n_1 \times n_2}$ be independent zero-mean random matrices. Suppose

$$\sigma^2 = \max \left\{ \left\| \mathbb{E} \left[\sum_{k=1}^L X_k X_k^\top \right] \right\|, \left\| \mathbb{E} \left[\sum_{k=1}^L X_k^\top X_k \right] \right\| \right\}$$

and $\|X_k\| \leq M$. Then

$$\mathbb{P} \left(\left\| \sum_{k=1}^L X_k \right\| \geq \sqrt{2c\sigma^2 \log(n_1 + n_2)} + cM \log(n_1 + n_2) \right) \leq (n_1 + n_2)^{1-c},$$

where c is any positive number greater than 1.

The following fact is very useful, and we will frequently use the result for the proofs of Theorem 4 and Proposition 1.

Lemma 5 Suppose that \mathcal{Z} is an $n_1 \times n_2 \times n_3$ tensor with its compact t -SVD given by $\mathcal{Z} = \mathcal{W} * \mathcal{S} * \mathcal{V}^\top$ and satisfies the tensor μ_0 -incoherence condition. Then,

$$\|\mathcal{P}_\mathbb{T}(\mathring{\mathbf{e}}_i * \mathring{\mathbf{e}}_k * \mathring{\mathbf{e}}_j^\top)\|_{\mathbb{F}}^2 \leq \frac{(n_1 + n_2)\mu_0 r}{n_1 n_2}.$$

The next lemma determines the likelihood that $\|\mathcal{P}_\mathbb{T}\mathcal{R}_\Omega\mathcal{P}_\mathbb{T} - \mathcal{P}_\mathbb{T}\| \leq \frac{1}{2}$, which is essential for verifying Condition 1 in Proposition 1.

Lemma 6 Assume that Ω is generated according to the Bernoulli distribution with probability p , then

$$\|\mathcal{P}_\mathbb{T}\mathcal{R}_\Omega\mathcal{P}_\mathbb{T} - \mathcal{P}_\mathbb{T}\| \leq \frac{1}{2}$$

holds with probability at least $1 - 2n_1 n_2 n_3 \exp\left(-\frac{3pn_1 n_2}{28(n_1 + n_2)\mu_0 r}\right)$.

The following lemma establishes that for an arbitrary tensor $\mathcal{X} \in \mathbb{K}^{n_1 \times n_2 \times n_3}$, $\|\mathcal{R}_\Omega(\mathcal{X}) - \mathcal{X}\|$ can be bounded by a combination of the tensor infinity norm and the $\ell_{\infty,2}$ norm with high probability.

Lemma 7 Let $\mathcal{X} \in \mathbb{K}^{n_1 \times n_2 \times n_3}$. Assume that Ω is generated according to the Bernoulli distribution with probability p . Then, for any constant $c_2 > 1$,

$$\|\mathcal{R}_\Omega(\mathcal{X}) - \mathcal{X}\| \leq \sqrt{\frac{2c_2}{p} \log((n_1 + n_2)n_3)} \|\mathcal{X}\|_{\infty,2} + \frac{c_2 \log((n_1 + n_2)n_3)}{p} \|\mathcal{X}\|_\infty \quad (17)$$

holds with probability at least $1 - ((n_1 + n_2)n_3)^{1-c_2}$.

The following lemma states that for $\mathcal{X} \in \mathbb{K}^{n_1 \times n_2 \times n_3}$, $\|(\mathcal{P}_\mathbb{T}\mathcal{R}_\Omega(\mathcal{X}) - \mathcal{P}_\mathbb{T}(\mathcal{X}))\|_{\infty,2}$ can be controlled by a combination of the $\ell_{\infty,2}$ norm and the tensor infinity norm of \mathcal{X} with high probability.

Lemma 8 Assume that Ω is generated according to the Bernoulli distribution with probability p . For any positive number $c_1 \geq 2$ and $\mathcal{X} \in \mathbb{K}^{n_1 \times n_2 \times n_3}$, then

$$\begin{aligned} \mathbb{P} \left(\left\| (\mathcal{P}_\mathbb{T}\mathcal{R}_\Omega(\mathcal{X}) - \mathcal{P}_\mathbb{T}(\mathcal{X})) \right\|_{\infty,2} \leq \sqrt{\frac{4c_1(n_1 + n_2)\mu_0 r \log((n_1 + n_2)n_3)}{pn_1 n_2}} \cdot \|\mathcal{X}\|_{\infty,2} \right. \\ \left. + \frac{c_1 \log((n_1 + n_2)n_3)}{p} \sqrt{\frac{(n_1 + n_2)\mu_0 r}{n_1 n_2}} \|\mathcal{X}\|_\infty \right) \geq 1 - ((n_1 + n_2)n_3)^{2-c_1}. \end{aligned}$$

The following lemma states that, for $\mathcal{X} \in \mathbb{R}^{n_1 \times n_2 \times n_3}$, $\|\mathcal{P}_\mathbb{T}\mathcal{R}_\Omega\mathcal{P}_\mathbb{T}(\mathcal{X}) - \mathcal{P}_\mathbb{T}(\mathcal{X})\|_\infty$ can be bounded by the tensor infinity norm of $\mathcal{P}_\mathbb{T}(\mathcal{X})$ with high probability.

Lemma 9 Assume that Ω is generated according to the Bernoulli distribution with probability p . For any $\mathcal{X} \in \mathbb{K}^{n_1 \times n_2 \times n_3}$, then

$$\|(\mathcal{P}_{\mathbb{T}}\mathcal{R}_{\Omega}\mathcal{P}_{\mathbb{T}} - \mathcal{P}_{\mathbb{T}})(\mathcal{X})\|_{\infty} \leq \frac{1}{2}\|\mathcal{P}_{\mathbb{T}}(\mathcal{X})\|_{\infty}$$

holds with probability at least $1 - 2n_1n_2n_3 \exp\left(\frac{-3pn_1n_2}{16(n_1+n_2)\mu_0r}\right)$.

When $\mathcal{P}_{\mathbb{T}}(\mathcal{X}) = \mathcal{X}$, we can easily achieve the following corollary.

Corollary 1 Assume that Ω is generated according to the Bernoulli distribution with probability q . For any $\mathcal{X} \in \mathbb{K}^{n_1 \times n_2 \times n_3}$, if $\mathcal{P}_{\mathbb{T}}(\mathcal{X}) = \mathcal{X}$, then

$$\|(\mathcal{P}_{\mathbb{T}}\mathcal{R}_{\Omega_t}\mathcal{P}_{\mathbb{T}} - \mathcal{P}_{\mathbb{T}})(\mathcal{X})\|_{\infty} \leq \frac{1}{2}\|\mathcal{X}\|_{\infty}$$

holds with probability at least $1 - 2n_1n_2n_3 \exp\left(\frac{-3qn_1n_2}{28(n_1+n_2)\mu_0r}\right)$.

Corollary 1 is used to provide a probabilistic estimate for the lower bound of $\|\mathcal{D}_t\|_{\infty}$, where \mathcal{D}_t is defined in (20) later. With this groundwork, we are now prepared to present the proof of Theorem 4.

B.4.2 Proof of Theorem 4

First of all, one can get that Condition 1 holds with probability at least

$$1 - 2n_1n_2n_3 \exp\left(-\frac{3pn_1n_2}{28(n_1+n_2)\mu_0r}\right) \quad (18)$$

according to Lemma 6.

Next, our main goal is to construct a dual certificate \mathcal{Y} that satisfies Condition 2. We do this using the Golfing Scheme [12]. Choose t_0 as

$$t_0 \geq \left\lceil \log_2 \left(4\sqrt{\frac{n_3r}{p}} \right) \right\rceil, \quad (19)$$

where $\lceil \cdot \rceil$ is the ceiling function. Suppose that the set Ω is generated from $\Omega = \cup_{t=1}^{t_0} \Omega_t$. For each t , we assume that $\mathbb{P}[(i, j, k) \in \Omega_t] = q := 1 - (1 - p)^{\frac{1}{t_0}}$. It is easy to see that for any $(i, j, k) \in [n_1] \times [n_2] \times [n_3]$,

$$\begin{aligned} \mathbb{P}[(i, j, k) \in \Omega] &= 1 - \mathbb{P}[(i, j, k) \notin \cup_{t=1}^{t_0} \Omega_t] \\ &= 1 - \prod_{t=1}^{t_0} \mathbb{P}[(i, j, k) \in \Omega_t^c] = 1 - \prod_{t=0}^{t_0} (1 - p)^{\frac{1}{t_0}} = p. \end{aligned}$$

Therefore, the construction of $\Omega = \cup_{t=1}^{t_0} \Omega_t$ shares the same distribution as that of the original Ω . Let $\{\mathcal{A}_t \in \mathbb{K}^{n_1 \times n_2 \times n_3} : t \in \{0\} \cup [t_0]\}$ be a sequence of tensors with

$$\mathcal{A}_0 = \mathbf{0} \text{ and } \mathcal{A}_t = \mathcal{A}_{t-1} + \mathcal{R}_{\Omega_t}\mathcal{P}_{\mathbb{T}}(\mathcal{W} * \mathcal{V}^{\top} - \mathcal{P}_{\mathbb{T}}(\mathcal{A}_{t-1})), \text{ for } t \geq 1,$$

where $\mathcal{R}_{\Omega_t}(\mathcal{Z}) := \sum_{i \in [n_1], j \in [n_2], k \in [n_3]} \frac{1}{q} \mathbf{1}_{\Omega_t}(i, j, k) [\mathcal{Z}]_{i,j,k} \hat{\mathbf{e}}_i * \hat{\mathbf{e}}_k * \hat{\mathbf{e}}_j^{\top}$. Set $\mathcal{Y} := \mathcal{A}_{t_0}$.

Next, we aim to prove that $\mathcal{P}_{\Omega}(\mathcal{Y}) = \mathcal{Y}$ using mathematical induction. For $t = 0$, $\mathcal{P}_{\Omega}(\mathcal{A}_0) = \mathcal{P}_{\Omega}(\mathbf{0}) = \mathbf{0} = \mathcal{A}_0$. Notice that

$$\begin{aligned} \mathcal{A}_1 &= \mathcal{A}_0 + \mathcal{R}_{\Omega_1}\mathcal{P}_{\mathbb{T}}(\mathcal{W} * \mathcal{V}^{\top} - \mathcal{P}_{\mathbb{T}}(\mathcal{A}_0)) \\ &= \mathcal{A}_0 + \mathcal{R}_{\Omega_1}\mathcal{P}_{\mathbb{T}}(\mathcal{W} * \mathcal{V}^{\top}) \end{aligned}$$

$$\begin{aligned}
&= \mathcal{R}_{\Omega_1}(\mathcal{W} * \mathcal{W}^\top * (\mathcal{W} * \mathcal{V}^\top) + (\mathcal{W} * \mathcal{V}^\top) * \mathcal{V} * \mathcal{V}^\top - \mathcal{W} * \mathcal{W}^\top * (\mathcal{W} * \mathcal{V}^\top) * \mathcal{V} * \mathcal{V}^\top) \\
&= \mathcal{R}_{\Omega_1}(\mathcal{W} * \mathcal{V}^\top).
\end{aligned}$$

Since $\Omega_1 \subseteq \Omega$, it is evident that $\mathcal{P}_\Omega(\mathcal{A}_1) = \mathcal{P}_\Omega(\mathcal{R}_{\Omega_1}(\mathcal{W} * \mathcal{V}^\top)) = \mathcal{R}_{\Omega_1}(\mathcal{W} * \mathcal{V}^\top) = \mathcal{A}_1$. Assume that for $k \leq t_0 - 1$, it holds that $\mathcal{P}_\Omega(\mathcal{A}_k) = \mathcal{A}_k$. Given the linearity of the operator \mathcal{P}_Ω and the inclusion $\Omega_{t_0} \subseteq \Omega$, it follows that

$$\begin{aligned}
\mathcal{P}_\Omega(\mathcal{Y}) &= \mathcal{P}_\Omega(\mathcal{A}_{t_0}) = \mathcal{P}_\Omega(\mathcal{A}_{t_0-1} + \mathcal{R}_{\Omega_{t_0}} \mathcal{P}_\mathbb{T}(\mathcal{W} * \mathcal{V}^\top - \mathcal{P}_\mathbb{T}(\mathcal{A}_{t_0-1}))) \\
&= \mathcal{P}_\Omega(\mathcal{A}_{t_0-1}) + \mathcal{P}_\Omega(\mathcal{R}_{\Omega_{t_0}} \mathcal{P}_\mathbb{T}(\mathcal{W} * \mathcal{V}^\top - \mathcal{P}_\mathbb{T}(\mathcal{A}_{t_0-1}))) \\
&= \mathcal{A}_{t_0-1} + \mathcal{R}_{\Omega_{t_0}} \mathcal{P}_\mathbb{T}(\mathcal{W} * \mathcal{V}^\top - \mathcal{P}_\mathbb{T}(\mathcal{A}_{t_0-1})) = \mathcal{A}_{t_0} = \mathcal{Y}.
\end{aligned}$$

Therefore $\mathcal{Y} = \mathcal{A}_{t_0}$ is the dual certificate.

Now let's prove that $\|\mathcal{P}_\mathbb{T}(\mathcal{Y}) - \mathcal{W} * \mathcal{V}^\top\|_F \leq \frac{1}{4} \sqrt{\frac{p}{n_3}}$. For $t \in \{0\} \cup [t_0]$, set

$$\mathcal{D}_t = \mathcal{W} * \mathcal{V}^\top - \mathcal{P}_\mathbb{T}(\mathcal{A}_t). \quad (20)$$

Notice that

$$q = 1 - (1 - p)^{\frac{1}{t_0}} \geq 1 - (1 - \frac{p}{t_0}) = \frac{p}{t_0}. \quad (21)$$

Thus, one can derive the following results by Lemma 6: for each t ,

$$\|\mathcal{D}_t\|_F \leq \|\mathcal{P}_\mathbb{T} - \mathcal{P}_\mathbb{T} \mathcal{R}_{\Omega_t} \mathcal{P}_\mathbb{T}\| \|\mathcal{D}_{t-1}\|_F \leq \frac{1}{2} \|\mathcal{D}_{t-1}\|_F \quad (22)$$

holds with probability at least

$$1 - 2n_1 n_2 n_3 \exp\left(-\frac{3qn_1 n_2}{28(n_1 + n_2)\mu_0 r}\right).$$

Applying (22) from $t = t_0$ to $t = 1$, we will have that

$$\|\mathcal{P}_\mathbb{T}(\mathcal{Y} - \mathcal{W} * \mathcal{V}^\top)\|_F = \|\mathcal{D}_{t_0}\|_F \leq \frac{1}{2} \|\mathcal{D}_{t_0-1}\|_F \leq \dots \leq \frac{1}{2^{t_0}} \|\mathcal{W} * \mathcal{V}^\top\|_F \leq \frac{\sqrt{r}}{2^{t_0}} \quad (23)$$

holds with probability at least

$$1 - 2t_0 n_1 n_2 n_3 \exp\left(-\frac{3qn_1 n_2}{28(n_1 + n_2)\mu_0 r}\right).$$

Since $t_0 \geq \left\lceil \log_2 \left(4 \sqrt{\frac{n_3 r}{p}}\right) \right\rceil$, we have

$$\mathbb{P} \left(\|\mathcal{P}_\mathbb{T}(\mathcal{Y} - \mathcal{W} * \mathcal{V}^\top)\|_F \leq \frac{1}{4} \sqrt{\frac{p}{n_3}} \right) \geq 1 - 2t_0 n_1 n_2 n_3 \exp\left(-\frac{3qn_1 n_2}{28(n_1 + n_2)\mu_0 r}\right). \quad (24)$$

Next, we proceed to prove that $\|\mathcal{P}_{\mathbb{T}^\perp}(\mathcal{Y})\| \leq \frac{1}{2}$. Recall that $\mathcal{Y} = \sum_{t=1}^{t_0} \mathcal{R}_{\Omega_t} \mathcal{P}_\mathbb{T} \mathcal{D}_{t-1}$. By applying Lemma 7 for t_0 times, we can get

$$\begin{aligned}
\|\mathcal{P}_{\mathbb{T}^\perp}(\mathcal{Y})\| &\leq \sum_{t=1}^{t_0} \|\mathcal{P}_{\mathbb{T}^\perp}(\mathcal{R}_{\Omega_t} \mathcal{P}_\mathbb{T} - \mathcal{P}_\mathbb{T})(\mathcal{D}_{t-1})\| \leq \sum_{t=1}^{t_0} \|(\mathcal{R}_{\Omega_t} - \mathcal{I})(\mathcal{P}_\mathbb{T}(\mathcal{D}_{t-1}))\| \\
&\leq \sum_{t=1}^{t_0} \left(\frac{c_2 \log((n_1 + n_2)n_3)}{q} \|\mathcal{P}_\mathbb{T}(\mathcal{D}_{t-1})\|_\infty + \sqrt{\frac{2c_2 \log((n_1 + n_2)n_3)}{q}} \|\mathcal{P}_\mathbb{T}(\mathcal{D}_{t-1})\|_{\infty,2} \right)
\end{aligned} \quad (25)$$

$$= \sum_{t=1}^{t_0} \left(\frac{c_2 \log((n_1 + n_2)n_3)}{q} \|\mathcal{D}_{t-1}\|_\infty + \sqrt{\frac{2c_2 \log((n_1 + n_2)n_3)}{q}} \|\mathcal{D}_{t-1}\|_{\infty,2} \right) \quad (26)$$

holds with probability at least

$$1 - \frac{t_0}{((n_1 + n_2)n_3)^{c_2-1}}, \quad (27)$$

where (25) holds due to (21), and (26) holds because $\mathcal{P}_\mathbb{T}(\mathcal{D}_t) = \mathcal{D}_t$.

Next, we will bound (26) by bounding these two terms:

- (i) $\sum_{t=1}^{t_0} \frac{c_2 \log((n_1+n_2)n_3)}{q} \|\mathcal{D}_{t-1}\|_\infty$
- (ii) $\sum_{t=1}^{t_0} \sqrt{\frac{2c_2 \log((n_1+n_2)n_3)}{q}} \|\mathcal{D}_{t-1}\|_{\infty,2}$

via estimating the upper bounds of $\|\mathcal{D}_{t-1}\|_\infty$ and $\|\mathcal{D}_{t-1}\|_{\infty,2}$.

By applying Corollary 1 for $t-1$ times, where $2 \leq t \leq t_0$, we have

$$\|\mathcal{D}_{t-1}\|_\infty = \|(\mathcal{P}_\mathbb{T} - \mathcal{P}_\mathbb{T}\mathcal{R}_{\Omega_{t-1}}\mathcal{P}_\mathbb{T}) \cdots (\mathcal{P}_\mathbb{T} - \mathcal{P}_\mathbb{T}\mathcal{R}_{\Omega_1}\mathcal{P}_\mathbb{T}) \mathcal{D}_0\|_\infty \leq \frac{\|\mathcal{D}_0\|_\infty}{2^{t-1}}$$

holds with probability at least $1 - 2n_1n_2n_3(t-1) \exp\left(\frac{-3qn_1n_2}{28(n_1+n_2)\mu_0r}\right)$. Therefore,

$$\sum_{t=1}^{t_0} \frac{c_2 \log((n_1 + n_2)n_3)}{q} \|\mathcal{D}_{t-1}\|_\infty \leq \frac{2c_2 \log((n_1 + n_2)n_3)}{q} \cdot \|\mathcal{D}_0\|_\infty$$

holds with probability at least

$$1 - 2n_1n_2n_3(t_0 - 1) \exp\left(\frac{-3qn_1n_2}{28(n_1 + n_2)\mu_0r}\right). \quad (28)$$

Now we are going to estimate the upper bound for $\sum_{t=1}^{t_0} \sqrt{\frac{2c_2 \log((n_1+n_2)n_3)}{q}} \|\mathcal{D}_{t-1}\|_{\infty,2}$ by bounding $\|\mathcal{D}_{t-1}\|_{\infty,2}$. For simplicity, we set

$$a = 2 \cdot \sqrt{\frac{c_1 \log((n_1 + n_2)n_3)}{q}} \sqrt{\frac{(n_1 + n_2)\mu_0r}{n_1n_2}} \quad \text{and} \quad b = \frac{c_1(\log((n_1 + n_2)n_3))}{q} \sqrt{\frac{(n_1 + n_2)\mu_0r}{n_1n_2}}.$$

By applying Lemma 8 for $t-1$ times and considering the fact that $\mathcal{P}_\mathbb{T}(\mathcal{D}_s) = \mathcal{D}_s$ for all $0 \leq s \leq t_0$, we obtain that

$$\begin{aligned} \|\mathcal{D}_{t-1}\|_{\infty,2} &= \|(\mathcal{P}_\mathbb{T} - \mathcal{P}_\mathbb{T}\mathcal{R}_{\Omega_{t-1}}\mathcal{P}_\mathbb{T})(\mathcal{D}_{t-2})\|_{\infty,2} \\ &\leq a\|\mathcal{D}_{t-2}\|_{\infty,2} + b\|\mathcal{D}_{t-2}\|_\infty \leq \cdots \leq a^{t-1}\|\mathcal{D}_0\|_{\infty,2} + b \sum_{i=0}^{t-2} a^i \|\mathcal{D}_{t-2-i}\|_\infty \end{aligned}$$

holds with probability at least $1 - \frac{t-1}{(n_1n_3+n_2n_3)^{c_1-2}}$ for $2 \leq t \leq t_0$. Therefore,

$$\begin{aligned} &\sum_{t=1}^{t_0} \sqrt{\frac{2c_2 \log((n_1 + n_2)n_3)}{q}} \|\mathcal{D}_{t-1}\|_{\infty,2} \\ &\leq \sqrt{\frac{2c_2 \log((n_1 + n_2)n_3)}{q}} \left(\left(\sum_{t=1}^{t_0} a^{t-1} \|\mathcal{D}_0\|_{\infty,2} \right) + \sum_{t=2}^{t_0} b \sum_{i=0}^{t-2} a^i \|\mathcal{D}_{t-2-i}\|_\infty \right) \end{aligned}$$

$$= \sqrt{\frac{2c_2 \log((n_1 + n_2)n_3)}{q}} \cdot \left(\|\mathcal{D}_0\|_{\infty,2} \frac{1 - a^{t_0}}{1 - a} + b \cdot \sum_{t=2}^{t_0} \sum_{i=0}^{t-2} a^i \|\mathcal{D}_{t-2-i}\|_{\infty} \right)$$

holds with probability at least

$$1 - \frac{t_0 - 1}{(n_1 n_3 + n_2 n_3)^{c_1 - 2}}. \quad (29)$$

Considering the process of estimating the upper bound for $\|\mathcal{D}_t\|_{\infty}$, we have

$$\begin{aligned} (26) &\leq \frac{2c_2 \log((n_1 + n_2)n_3)}{q} \cdot \|\mathcal{D}_0\|_{\infty} + \sqrt{\frac{2c_2 \log((n_1 + n_2)n_3)}{q}} \cdot \frac{\|\mathcal{D}_0\|_{\infty,2}}{1 - a} \\ &\quad + \sqrt{\frac{2c_2 \log((n_1 + n_2)n_3)}{q}} \cdot b \cdot \sum_{t=2}^{t_0} \sum_{i=0}^{t-2} a^i \left(\frac{1}{2}\right)^{t-2-i} \|\mathcal{D}_0\|_{\infty} \\ &\leq \frac{2c_2 \log((n_1 + n_2)n_3)}{q} \cdot \|\mathcal{D}_0\|_{\infty} + \sqrt{\frac{2c_2 \log((n_1 + n_2)n_3)}{q}} \cdot \frac{\|\mathcal{D}_0\|_{\infty,2}}{1 - a} \\ &\quad + \sqrt{\frac{2c_2 \log((n_1 + n_2)n_3)}{q}} \cdot \frac{2b}{1 - 2a} \cdot \|\mathcal{D}_0\|_{\infty} \end{aligned}$$

holds with probability at least $1 - \frac{t_0 - 1}{(n_1 n_3 + n_2 n_3)^{c_1 - 2}} - 2(t_0 - 1)n_1 n_2 n_3 \exp\left(\frac{-3qn_1 n_2}{28(n_1 + n_2)\mu_0 r}\right)$ when $0 < a \leq \frac{1}{4}$. Therefore,

$$\begin{aligned} \|\mathcal{P}_{\mathbb{T}^\perp}(\mathcal{Y})\| &\leq \sum_{t=1}^{t_0} \left(\frac{c_2 \log((n_1 + n_2)n_3)}{q} \|\mathcal{D}_{t-1}\|_{\infty} + \sqrt{\frac{2c_2 \log((n_1 + n_2)n_3)}{q}} \|\mathcal{D}_{t-1}\|_{\infty,2} \right) \\ &\leq \frac{2c_2 \log((n_1 + n_2)n_3)}{q} \cdot \|\mathcal{D}_0\|_{\infty} + \sqrt{\frac{2c_2 \log((n_1 + n_2)n_3)}{q}} \cdot \frac{\|\mathcal{D}_0\|_{\infty,2}}{1 - a} \\ &\quad + \sqrt{\frac{2c_2 \log((n_1 + n_2)n_3)}{q}} \cdot \frac{2b}{1 - 2a} \cdot \|\mathcal{D}_0\|_{\infty} \end{aligned}$$

holds with probability at least

$$1 - \frac{t_0 - 1}{(n_1 n_3 + n_2 n_3)^{c_1 - 2}} - 2(t_0 - 1)n_1 n_2 n_3 \exp\left(\frac{-3qn_1 n_2}{28(n_1 + n_2)\mu_0 r}\right) - \frac{t_0}{(n_1 n_3 + n_2 n_3)^{c_2 - 1}}$$

provided that $0 < a \leq \frac{1}{4}$. Note that $\|\mathcal{D}_0\|_{\infty} = \|\mathcal{W} * \mathcal{V}^\top\|_{\infty} \leq \frac{(n_1 + n_2)\mu_0 r}{2n_1 n_2}$ and $\|\mathcal{D}_0\|_{\infty,2} = \|\mathcal{W} * \mathcal{V}^\top\|_{\infty,2} \leq \sqrt{\frac{(n_1 + n_2)\mu_0 r}{n_1 n_2}}$. Combining (27), (28), and (29), we thus have

$$\begin{aligned} \|\mathcal{P}_{\mathbb{T}^\perp}(\mathcal{Y})\| &\leq \frac{c_2 \log((n_1 + n_2)n_3)}{q} \cdot \frac{(n_1 + n_2)\mu_0 r}{n_1 n_2} + \sqrt{\frac{2c_2 \log((n_1 + n_2)n_3)}{q}} \cdot \frac{\sqrt{(n_1 + n_2)\mu_0 r}}{(1 - a)\sqrt{n_1 n_2}} \\ &\quad + \sqrt{\frac{2c_2 \log((n_1 + n_2)n_3)}{q}} \cdot \frac{b}{1 - 2a} \cdot \frac{(n_1 + n_2)\mu_0 r}{n_1 n_2} \end{aligned}$$

$$\begin{aligned} &\leq \frac{c_2 \log((n_1 + n_2)n_3)}{q} \cdot \frac{(n_1 + n_2)\mu_0 r}{n_1 n_2} + \frac{4\sqrt{2c_2}}{3} \cdot \sqrt{\frac{\log((n_1 + n_2)n_3)}{q} \cdot \frac{(n_1 + n_2)\mu_0 r}{n_1 n_2}} \\ &\quad + 2c_1 \sqrt{2c_2} \left(\frac{\log((n_1 + n_2)n_3)}{q} \cdot \frac{(n_1 + n_2)\mu_0 r}{n_1 n_2} \right)^{3/2} \end{aligned}$$

holds with probability at least

$$1 - \frac{t_0 - 1}{(n_1 n_3 + n_2 n_3)^{c_1 - 2}} - 2(t_0 - 1)n_1 n_2 n_3 \exp\left(\frac{-3qn_1 n_2}{28(n_1 + n_2)\mu_0 r}\right) - \frac{t_0}{(n_1 n_3 + n_2 n_3)^{c_2 - 1}}$$

provided that $0 < a \leq \frac{1}{4}$.

Since $a = 2 \cdot \sqrt{\frac{c_1 \log((n_1 + n_2)n_3)}{q}} \sqrt{\frac{(n_1 + n_2)\mu_0 r}{n_1 n_2}}$, the restriction $0 < a \leq \frac{1}{4}$ is equivalent to

$$q \geq 64c_1 \log((n_1 + n_2)n_3) \cdot \frac{(n_1 + n_2)\mu_0 r}{n_1 n_2}.$$

Notice that

$$p \geq \frac{256(n_1 + n_2)\mu_0 \beta r \log^2((n_1 + n_2)n_3)}{n_1 n_2}.$$

We thus have

$$\begin{aligned} t_0 &= \lceil \log_2 \left(4\sqrt{\frac{n_3 r}{p}} \right) \rceil \\ &\leq \left\lceil \log_2 \left(4\sqrt{\frac{n_1 n_2 n_3}{256(n_1 + n_2)\mu_0 \beta \log^2((n_1 + n_2)n_3)}} \right) \right\rceil \\ &\leq \left\lceil \frac{1}{2} \log_2 \left(\frac{n_1 n_2 n_3}{(n_1 + n_2)\mu_0 \beta} \right) - 2 \right\rceil \leq \log((n_1 + n_2)n_3) \end{aligned}$$

In addition $q \geq \frac{p}{t_0}$, we have

$$\begin{aligned} q &\geq \frac{256(n_1 + n_2)\mu_0 \beta r \log^2((n_1 + n_2)n_3)}{n_1 n_2} \cdot \frac{1}{\log((n_1 + n_2)n_3)} \\ &= \frac{256(n_1 + n_2)\mu_0 \beta r \log((n_1 + n_2)n_3)}{n_1 n_2}, \end{aligned}$$

i.e., $\frac{(n_1 + n_2)\mu_0 r \log((n_1 + n_2)n_3)}{qn_1 n_2} \leq \frac{1}{256\beta}$.

Therefore the condition that $q \geq 64c_1 \log((n_1 + n_2)n_3) \frac{(n_1 + n_2)\mu_0 r}{n_1 n_2}$ holds when $c_1 = 4\beta$.

Hence, the condition $a \leq \frac{1}{4}$ holds. In addition, by setting $c_2 = 12\beta$, we have

$$\begin{aligned} \|\mathcal{P}_{\mathbb{T}^\perp}(\mathcal{Y})\| &\leq \frac{c_2 \log((n_1 + n_2)n_3)}{q} \cdot \frac{(n_1 + n_2)\mu_0 r}{n_1 n_2} + \frac{4\sqrt{2c_2}}{3} \cdot \sqrt{\frac{\log((n_1 + n_2)n_3)}{q} \cdot \frac{(n_1 + n_2)\mu_0 r}{n_1 n_2}} \\ &\quad + 2c_1 \sqrt{2c_2} \left(\frac{\log((n_1 + n_2)n_3)}{q} \cdot \frac{(n_1 + n_2)\mu_0 r}{n_1 n_2} \right)^{3/2} \\ &\leq \frac{c_2}{256\beta} + \frac{4\sqrt{2c_2}}{3} \sqrt{\frac{1}{256\beta}} + 2c_1 \sqrt{2c_2} \left(\frac{1}{256\beta} \right)^{3/2} < \frac{1}{2}. \end{aligned}$$

with probability at least

$$1 - \frac{\log(n_1 n_3 + n_2 n_3)}{(n_1 n_3 + n_2 n_3)^{4\beta-2}} - \frac{\log(n_1 n_3 + n_2 n_3)}{(n_1 n_3 + n_2 n_3)^{27\beta-2}} - \frac{\log(n_1 n_3 + n_2 n_3)}{(n_1 n_3 + n_2 n_3)^{12\beta-1}} \geq 1 - \frac{3 \log(n_1 n_3 + n_2 n_3)}{(n_1 n_3 + n_2 n_3)^{4\beta-2}}. \quad (30)$$

Notice that the probabilistic estimation for the validity of Condition 2 is based on the assumption that Condition 1 holds, where we show $\|\mathcal{D}\|_\infty \leq (\frac{1}{2})^{t-1} \|\mathcal{D}_0\|_\infty$ based on Condition 1. Thus, \mathcal{Z} is the unique minimizer with probability at least

$$1 - \frac{3 \log(n_1 n_3 + n_2 n_3)}{(n_1 n_3 + n_2 n_3)^{4\beta-2}}.$$

B.4.3 Proof of supporting lemmas

Proof of Lemma 4 Substitute $\tau = \sqrt{2c\sigma^2 \log(n_1 + n_2)} + cM \log(n_1 + n_2)$ into $\frac{-\tau^2/2}{\sigma^2 + \frac{M\tau}{3}}$ in Lemma 3. We get

$$\begin{aligned} \frac{-\tau^2/2}{\sigma^2 + \frac{M\tau}{3}} &= -\frac{2c\sigma^2 \log(n_1 + n_2) + 2\sqrt{2}c^{\frac{3}{2}}\sigma M \log^{\frac{3}{2}}(n_1 + n_2) + c^2 M^2 \log^2(n_1 + n_2)}{2\sigma^2 + \frac{2\sqrt{2}}{3}c^{\frac{1}{2}}\sigma M \log^{\frac{1}{2}}(n_1 + n_2) + \frac{2cM^2}{3} \log(n_1 + n_2)} \\ &\leq -c \log(n_1 + n_2). \end{aligned}$$

■

Proof of Lemma 5

$$\begin{aligned} \|\mathcal{P}_\mathbb{T}(\mathring{\mathbf{e}}_i * \mathring{\mathbf{e}}_k * \mathring{\mathbf{e}}_j^\top)\|_{\mathbb{F}}^2 &= \langle \mathcal{P}_\mathbb{T}(\mathring{\mathbf{e}}_i * \mathring{\mathbf{e}}_k * \mathring{\mathbf{e}}_j^\top), \mathcal{P}_\mathbb{T}(\mathring{\mathbf{e}}_i * \mathring{\mathbf{e}}_k * \mathring{\mathbf{e}}_j^\top) \rangle \\ &= \langle \mathcal{P}_\mathbb{T}(\mathring{\mathbf{e}}_i * \mathring{\mathbf{e}}_k * \mathring{\mathbf{e}}_j^\top), \mathring{\mathbf{e}}_i * \mathring{\mathbf{e}}_k * \mathring{\mathbf{e}}_j^\top \rangle \\ &= \|\mathcal{W}^\top * \mathring{\mathbf{e}}_i\|_{\mathbb{F}}^2 + \|\mathcal{V}^\top * \mathring{\mathbf{e}}_j\|_{\mathbb{F}}^2 - \left\| \mathcal{W}^\top * \mathring{\mathbf{e}}_i * \mathring{\mathbf{e}}_k * \mathring{\mathbf{e}}_j^\top * \mathcal{V} \right\|_{\mathbb{F}}^2, \\ &\leq \|\mathcal{W}^\top * \mathring{\mathbf{e}}_i\|_{\mathbb{F}}^2 + \|\mathcal{V}^\top * \mathring{\mathbf{e}}_j\|_{\mathbb{F}}^2 = \frac{(n_1 + n_2)\mu_0 r}{n_1 n_2} \end{aligned}$$

■

Proof of Lemma 6 By the fact that $\mathcal{P}_\mathbb{T}$ is a self-adjoint and idempotent operator, we can get that $\mathbb{E}[\mathcal{P}_\mathbb{T} \mathcal{R}_\Omega \mathcal{P}_\mathbb{T}] = \mathcal{P}_\mathbb{T}(\mathbb{E} \mathcal{R}_\Omega) \mathcal{P}_\mathbb{T} = \mathcal{P}_\mathbb{T}$. It is easy to check that

$$\mathcal{P}_\mathbb{T} \mathcal{R}_\Omega \mathcal{P}_\mathbb{T}(\mathcal{X}) = \sum_{i,j,k} \frac{1}{p} \delta_{i,j,k} \left\langle \mathcal{X}, \mathcal{P}_\mathbb{T}(\mathring{\mathbf{e}}_i * \mathring{\mathbf{e}}_k * \mathring{\mathbf{e}}_j^\top) \right\rangle \mathcal{P}_\mathbb{T}(\mathring{\mathbf{e}}_i * \mathring{\mathbf{e}}_k * \mathring{\mathbf{e}}_j^\top).$$

Fix a tensor $\mathcal{X} \in \mathbb{K}^{n_1 \times n_2 \times n_3}$, we can write

$$\begin{aligned} (\mathcal{P}_\mathbb{T} \mathcal{R}_\Omega \mathcal{P}_\mathbb{T} - \mathcal{P}_\mathbb{T})(\mathcal{X}) &= \sum_{i,j,k} \left(\frac{1}{p} \delta_{i,j,k} - 1 \right) \left\langle \mathring{\mathbf{e}}_i * \mathring{\mathbf{e}}_k * \mathring{\mathbf{e}}_j^\top, \mathcal{P}_\mathbb{T}(\mathcal{X}) \right\rangle \mathcal{P}_\mathbb{T}(\mathring{\mathbf{e}}_i * \mathring{\mathbf{e}}_k * \mathring{\mathbf{e}}_j^\top) \\ &=: \sum_{i,j,k} \mathcal{H}_{ijk}(\mathcal{X}) \end{aligned}$$

where $\mathcal{H}_{ijk} : \mathbb{K}^{n_1 \times n_2 \times n_3} \rightarrow \mathbb{K}^{n_1 \times n_2 \times n_3}$ is a self-adjoint random operator and $\delta_{i,j,k}$ is the indicator function. One can see that $\mathbb{E}[\mathcal{H}_{ijk}] = 0$ as $\mathbb{E}(\frac{1}{p} \delta_{i,j,k} - 1) = \frac{1}{p} \mathbb{E}(\delta_{i,j,k}) - 1 = 0$.

Define the operator $\overline{\mathcal{H}}_{ijk} : \mathbb{B} \rightarrow \mathbb{B}$ with $\mathbb{B} = \{\overline{\mathcal{B}} : \mathcal{B} \in \mathbb{K}^{n_1 \times n_2 \times n_3}\}$. As

$$\overline{\mathcal{H}}_{ijk}(\overline{\mathcal{X}}) := \overline{\mathcal{H}_{ijk}(\mathcal{X})} = \left(\frac{1}{p}\delta_{ijk} - 1\right) \langle \dot{\mathbf{e}}_i * \dot{\mathbf{e}}_k * \dot{\mathbf{e}}_j^\top, \mathcal{P}_{\mathbb{T}}(\mathcal{X}) \rangle \overline{\mathcal{P}_{\mathbb{T}}(\dot{\mathbf{e}}_i * \dot{\mathbf{e}}_k * \dot{\mathbf{e}}_j^\top)}.$$

It is easy to check that $\overline{\mathcal{H}}_{ijk}$ is also self-adjoint by using the fact that the operator $\mathcal{P}_{\mathbb{T}}(\cdot)$ is self-adjoint. Using the fact that $\mathbb{E}\left(\frac{1}{p}\delta_{i,j,k} - 1\right) = 0$ again, we have $\mathbb{E}[\overline{\mathcal{H}}_{ijk}] = 0$. To prove the result using the non-commutative Bernstein inequality, we need to bound

$\|\overline{\mathcal{H}}_{ijk}\|$ and $\left\| \sum_{i,j,k} \mathbb{E}[\overline{\mathcal{H}}_{i,j,k}^2] \right\|$. Firstly, we have

$$\begin{aligned} \|\overline{\mathcal{H}}_{ijk}\| &= \sup_{\|\overline{\mathcal{X}}\|_{\mathbb{F}}=1} \|\overline{\mathcal{H}}_{i,j,k}(\overline{\mathcal{X}})\|_{\mathbb{F}} \\ &= \sup_{\|\overline{\mathcal{X}}\|_{\mathbb{F}}=1} \left\| \left(\frac{1}{p}\delta_{ijk} - 1\right) \langle \dot{\mathbf{e}}_i * \dot{\mathbf{e}}_k * \dot{\mathbf{e}}_j^\top, \mathcal{P}_{\mathbb{T}}(\mathcal{X}) \rangle \overline{\mathcal{P}_{\mathbb{T}}(\dot{\mathbf{e}}_i * \dot{\mathbf{e}}_k * \dot{\mathbf{e}}_j^\top)} \right\|_{\mathbb{F}} \\ &= \sup_{\|\overline{\mathcal{X}}\|_{\mathbb{F}}=1} \left\| \left(\frac{1}{p}\delta_{ijk} - 1\right) \langle \mathcal{P}_{\mathbb{T}}(\dot{\mathbf{e}}_i * \dot{\mathbf{e}}_k * \dot{\mathbf{e}}_j^\top), \mathcal{X} \rangle \overline{\mathcal{P}_{\mathbb{T}}(\dot{\mathbf{e}}_i * \dot{\mathbf{e}}_k * \dot{\mathbf{e}}_j^\top)} \right\|_{\mathbb{F}} \\ &\leq \sup_{\|\overline{\mathcal{X}}\|_{\mathbb{F}}=1} \frac{1}{p} \|\mathcal{P}_{\mathbb{T}}(\dot{\mathbf{e}}_i * \dot{\mathbf{e}}_k * \dot{\mathbf{e}}_j^\top)\|_{\mathbb{F}} \|\mathcal{X}\|_{\mathbb{F}} \|\overline{\mathcal{P}_{\mathbb{T}}(\dot{\mathbf{e}}_i * \dot{\mathbf{e}}_k * \dot{\mathbf{e}}_j^\top)}\|_{\mathbb{F}} \\ &= \sup_{\|\overline{\mathcal{X}}\|_{\mathbb{F}}=1} \frac{1}{p} \|\mathcal{P}_{\mathbb{T}}(\dot{\mathbf{e}}_i * \dot{\mathbf{e}}_k * \dot{\mathbf{e}}_j^\top)\|_{\mathbb{F}} \|\mathcal{X}\|_{\mathbb{F}} \sqrt{n_3} \|\mathcal{P}_{\mathbb{T}}(\dot{\mathbf{e}}_i * \dot{\mathbf{e}}_k * \dot{\mathbf{e}}_j^\top)\|_{\mathbb{F}} \\ &= \sup_{\|\overline{\mathcal{X}}\|_{\mathbb{F}}=1} \frac{1}{p} \|\mathcal{P}_{\mathbb{T}}(\dot{\mathbf{e}}_i * \dot{\mathbf{e}}_k * \dot{\mathbf{e}}_j^\top)\|_{\mathbb{F}} \|\overline{\mathcal{X}}\|_{\mathbb{F}} \|\mathcal{P}_{\mathbb{T}}(\dot{\mathbf{e}}_i * \dot{\mathbf{e}}_k * \dot{\mathbf{e}}_j^\top)\|_{\mathbb{F}} \\ &= \frac{1}{p} \|\mathcal{P}_{\mathbb{T}}(\dot{\mathbf{e}}_i * \dot{\mathbf{e}}_k * \dot{\mathbf{e}}_j^\top)\|_{\mathbb{F}}^2 \leq \frac{\mu_0(n_1 + n_2)r}{n_1 n_2 p}. \end{aligned}$$

Next, we move on to bound $\left\| \sum_{i,j,k} \mathbb{E}[\overline{\mathcal{H}}_{i,j,k}^2] \right\|$. By using the fact that $\mathcal{P}_{\mathbb{T}}$ is a self-adjoint and an idempotent operator, we can get that

$$\overline{\mathcal{H}}_{i,j,k}^2(\overline{\mathcal{X}}) = \left(\frac{1}{p}\delta_{ijk} - 1\right)^2 \langle \dot{\mathbf{e}}_i * \dot{\mathbf{e}}_k * \dot{\mathbf{e}}_j^\top, \mathcal{P}_{\mathbb{T}}(\mathcal{X}) \rangle \langle \dot{\mathbf{e}}_i * \dot{\mathbf{e}}_k * \dot{\mathbf{e}}_j^\top, \mathcal{P}_{\mathbb{T}}(\dot{\mathbf{e}}_i * \dot{\mathbf{e}}_k * \dot{\mathbf{e}}_j^\top) \rangle \overline{\mathcal{P}_{\mathbb{T}}(\dot{\mathbf{e}}_i * \dot{\mathbf{e}}_k * \dot{\mathbf{e}}_j^\top)}.$$

Note that $\mathbb{E}\left[\left(\frac{1}{p}\delta_{ijk} - 1\right)^2\right] = \frac{1-p}{p} \leq \frac{1}{p}$. Notice that

$$\begin{aligned} &\left\| \sum_{i,j,k} \mathbb{E}[\overline{\mathcal{H}}_{i,j,k}^2(\overline{\mathcal{X}})] \right\|_{\mathbb{F}} \\ &\leq \frac{1}{p} \left\| \sum_{i,j,k} \langle \dot{\mathbf{e}}_i * \dot{\mathbf{e}}_k * \dot{\mathbf{e}}_j^\top, \mathcal{P}_{\mathbb{T}}(\mathcal{X}) \rangle \langle \dot{\mathbf{e}}_i * \dot{\mathbf{e}}_k * \dot{\mathbf{e}}_j^\top, \mathcal{P}_{\mathbb{T}}(\dot{\mathbf{e}}_i * \dot{\mathbf{e}}_k * \dot{\mathbf{e}}_j^\top) \rangle \overline{\mathcal{P}_{\mathbb{T}}(\dot{\mathbf{e}}_i * \dot{\mathbf{e}}_k * \dot{\mathbf{e}}_j^\top)} \right\|_{\mathbb{F}} \\ &= \frac{\sqrt{n_3}}{p} \left\| \sum_{i,j,k} \langle \dot{\mathbf{e}}_i * \dot{\mathbf{e}}_k * \dot{\mathbf{e}}_j^\top, \mathcal{P}_{\mathbb{T}}(\mathcal{X}) \rangle \langle \dot{\mathbf{e}}_i * \dot{\mathbf{e}}_k * \dot{\mathbf{e}}_j^\top, \mathcal{P}_{\mathbb{T}}(\dot{\mathbf{e}}_i * \dot{\mathbf{e}}_k * \dot{\mathbf{e}}_j^\top) \rangle \overline{\mathcal{P}_{\mathbb{T}}(\dot{\mathbf{e}}_i * \dot{\mathbf{e}}_k * \dot{\mathbf{e}}_j^\top)} \right\|_{\mathbb{F}} \end{aligned}$$

$$\begin{aligned}
&\leq \frac{\sqrt{n_3}}{p} \left\| \sum_{i,j,k} \langle \dot{\mathbf{e}}_i * \dot{\mathbf{e}}_k * \dot{\mathbf{e}}_j^\top, \mathcal{P}_\mathbb{T}(\mathcal{X}) \rangle \langle \dot{\mathbf{e}}_i * \dot{\mathbf{e}}_k * \dot{\mathbf{e}}_j^\top, \mathcal{P}_\mathbb{T}(\dot{\mathbf{e}}_i * \dot{\mathbf{e}}_k * \dot{\mathbf{e}}_j^\top) \rangle \cdot (\dot{\mathbf{e}}_i * \dot{\mathbf{e}}_k * \dot{\mathbf{e}}_j^\top) \right\|_{\mathbb{F}} \\
&\leq \frac{\sqrt{n_3}}{p} \cdot \max_{i,j,k} \{ \langle \dot{\mathbf{e}}_i * \dot{\mathbf{e}}_k * \dot{\mathbf{e}}_j^\top, \mathcal{P}_\mathbb{T}(\dot{\mathbf{e}}_i * \dot{\mathbf{e}}_k * \dot{\mathbf{e}}_j^\top) \rangle \} \left\| \sum_{i,j,k} \langle \dot{\mathbf{e}}_i * \dot{\mathbf{e}}_k * \dot{\mathbf{e}}_j^\top, \mathcal{P}_\mathbb{T}(\mathcal{X}) \rangle \cdot (\dot{\mathbf{e}}_i * \dot{\mathbf{e}}_k * \dot{\mathbf{e}}_j^\top) \right\|_{\mathbb{F}} \\
&= \frac{\sqrt{n_3}}{p} \cdot (\max_{i,j,k} \|\mathcal{P}_\mathbb{T}(\dot{\mathbf{e}}_i * \dot{\mathbf{e}}_k * \dot{\mathbf{e}}_j^\top)\|_{\mathbb{F}}^2) \cdot \|\mathcal{P}_\mathbb{T}(\mathcal{X})\|_{\mathbb{F}} \\
&\leq \frac{\sqrt{n_3}(n_1 + n_2)\mu_0 r}{pn_1 n_2} \|\mathcal{P}_\mathbb{T}(\mathcal{X})\|_{\mathbb{F}} \quad (\text{By Lemma 5}) \\
&\leq \frac{\sqrt{n_3}(n_1 + n_2)\mu_0 r}{pn_1 n_2} \|\mathcal{X}\|_{\mathbb{F}} = \frac{(n_1 + n_2)\mu_0 r}{pn_1 n_2} \|\bar{\mathcal{X}}\|_{\mathbb{F}}.
\end{aligned}$$

We thus have $\|\sum_{i,j,k} \mathbb{E}[\bar{\mathcal{H}}_{ijk}^2]\|$ is bounded above by $\frac{(n_1+n_2)\mu_0 r}{pn_1 n_2}$. Thus, we use the non-commutative Bernstein inequality to derive the following result:

$$\begin{aligned}
\mathbb{P}\left[\|\mathcal{P}_\mathbb{T}\mathcal{P}_\Omega\mathcal{P}_\mathbb{T} - \mathcal{P}_\mathbb{T}\| \geq \frac{1}{2}\right] &= \mathbb{P}\left[\left\|\sum_{i,j,k} \mathcal{H}_{ijk}\right\| \geq \frac{1}{2}\right] \\
&= \mathbb{P}\left[\left\|\sum_{i,j,k} \bar{\mathcal{H}}_{ijk}\right\| \geq \frac{1}{2}\right] \\
&\leq 2n_1 n_2 n_3 \exp\left(-\frac{3pn_1 n_2}{28(n_1 + n_2)\mu_0 r}\right).
\end{aligned}$$

■

Proof of Lemma 7 It is easy to check that

$$\mathcal{R}_\Omega(\mathcal{X}) - \mathcal{X} = \sum_{i,j,k} \left(\frac{1}{p}\delta_{i,j,k} - 1\right) [\mathcal{X}]_{i,j,k} \dot{\mathbf{e}}_i * \dot{\mathbf{e}}_k * \dot{\mathbf{e}}_j^\top =: \sum_{i,j,k} \mathcal{E}_{i,j,k}.$$

Notice that $\mathbb{E}[\overline{\mathcal{E}_{i,j,k}}] = 0$ and $\|\overline{\mathcal{E}_{i,j,k}}\| \leq \frac{1}{p}\|\mathcal{X}\|_\infty$. In order to use the non-commutative Bernstein inequality, we just need to check the uniform boundness of $\|\mathbb{E}(\sum_{i,j,k} (\overline{\mathcal{E}_{i,j,k}})^\top \overline{\mathcal{E}_{i,j,k}})\|$ and $\|\mathbb{E}(\sum_{i,j,k} \overline{\mathcal{E}_{i,j,k}} (\overline{\mathcal{E}_{i,j,k}})^\top)\|$. Using the fact that $\dot{\mathbf{e}}_k^\top * \dot{\mathbf{e}}_k = \dot{\mathbf{e}}_k^\top * \dot{\mathbf{e}}_k = \dot{\mathbf{e}}_1, \dot{\mathbf{e}}_1 * \dot{\mathbf{e}}_k = \dot{\mathbf{e}}_k$, and $\dot{\mathbf{e}}_j * \dot{\mathbf{e}}_1 = \dot{\mathbf{e}}_j$, we have the following result:

$$\begin{aligned}
\mathcal{E}_{i,j,k}^\top * \mathcal{E}_{i,j,k} &= \left(\frac{1}{p}\delta_{i,j,k} - 1\right)^2 [\mathcal{X}]_{i,j,k}^2 (\dot{\mathbf{e}}_i * \dot{\mathbf{e}}_k * \dot{\mathbf{e}}_j^\top)^\top * (\dot{\mathbf{e}}_i * \dot{\mathbf{e}}_k * \dot{\mathbf{e}}_j^\top) \\
&= \left(\frac{1}{p}\delta_{i,j,k} - 1\right)^2 [\mathcal{X}]_{i,j,k}^2 (\dot{\mathbf{e}}_j * \dot{\mathbf{e}}_k^\top * \dot{\mathbf{e}}_i^\top) * (\dot{\mathbf{e}}_i * \dot{\mathbf{e}}_k * \dot{\mathbf{e}}_j^\top) \\
&= \left(\frac{1}{p}\delta_{i,j,k} - 1\right)^2 [\mathcal{X}]_{i,j,k}^2 \dot{\mathbf{e}}_j * \dot{\mathbf{e}}_k^\top * (\dot{\mathbf{e}}_i^\top * \dot{\mathbf{e}}_i) * \dot{\mathbf{e}}_k * \dot{\mathbf{e}}_j^\top
\end{aligned}$$

$$\begin{aligned}
&= \left(\frac{1}{p} \delta_{i,j,k} - 1 \right)^2 [\mathcal{X}]_{i,j,k}^2 \mathring{\mathbf{e}}_j * \mathring{\mathbf{e}}_k^\top * (\mathring{\mathbf{e}}_1 * \mathring{\mathbf{e}}_k) * \mathring{\mathbf{e}}_j^\top \\
&= \left(\frac{1}{p} \delta_{i,j,k} - 1 \right)^2 [\mathcal{X}]_{i,j,k}^2 \mathring{\mathbf{e}}_j * (\mathring{\mathbf{e}}_k^\top * \mathring{\mathbf{e}}_k) * \mathring{\mathbf{e}}_j^\top \\
&= \left(\frac{1}{p} \delta_{i,j,k} - 1 \right)^2 [\mathcal{X}]_{i,j,k}^2 \mathring{\mathbf{e}}_j * (\mathring{\mathbf{e}}_1) * \mathring{\mathbf{e}}_j^\top = \left(\frac{1}{p} \delta_{i,j,k} - 1 \right)^2 [\mathcal{X}]_{i,j,k}^2 \mathring{\mathbf{e}}_j * \mathring{\mathbf{e}}_j^\top.
\end{aligned}$$

Notice that $\mathring{\mathbf{e}}_j * \mathring{\mathbf{e}}_j^\top$ returns a zero tensor except for $(j, j, 1)$ -th entry being 1. We have

$$\begin{aligned}
\left\| \sum_{i,j,k} \mathbb{E}[\bar{\mathcal{E}}_{i,j,k}^\top \bar{\mathcal{E}}_{i,j,k}] \right\| &= \left\| \sum_{i,j,k} \mathbb{E}[\mathcal{E}_{i,j,k}^\top * \mathcal{E}_{i,j,k}] \right\| \leq \frac{1}{p} \left\| \sum_{i,j,k} [\mathcal{X}]_{i,j,k}^2 \mathring{\mathbf{e}}_j * \mathring{\mathbf{e}}_j^\top \right\| \\
&= \frac{1}{p} \left\| \sum_{i,j,k} [\mathcal{X}]_{i,j,k}^2 \bar{\mathring{\mathbf{e}}}_j \bar{\mathring{\mathbf{e}}}_j^\top \right\| \quad (\text{by the definition of spectral norm of tensor}) \\
&= \frac{1}{p} \left\| \begin{pmatrix} \sum_{i,k} [\mathcal{X}]_{i,1,k}^2 & & & \\ & \sum_{i,k} [\mathcal{X}]_{i,2,k}^2 & & \\ & & \ddots & \\ & & & \sum_{i,k} [\mathcal{X}]_{i,n_2,k}^2 \\ & & & & O_{n_2(n_3-1) \times n_2(n_3-1)} \end{pmatrix} \right\| \\
&= \frac{1}{p} \max_{j \in [n_3]} \left\{ \sum_{i,k} [\mathcal{X}]_{i,j,k}^2 \right\} = \frac{1}{p} \max_{j \in [n_3]} \|\mathcal{X}_{:,j,:}\|_{\text{F}}^2.
\end{aligned}$$

Similarly, we can get $\left\| \sum_{i,j,k} \mathbb{E}[\bar{\mathcal{E}}_{i,j,k} \bar{\mathcal{E}}_{i,j,k}^\top] \right\| \leq \frac{1}{p} \max_{i \in [n_3]} \|\mathcal{X}_{i,:,\cdot}\|_{\text{F}}^2$. Thus,

$$\max \left\{ \mathbb{E} \left(\sum_{i,j,k} (\bar{\mathcal{E}}_{i,j,k})^\top \bar{\mathcal{E}}_{i,j,k} \right), \mathbb{E} \left(\sum_{i,j,k} \bar{\mathcal{E}}_{i,j,k} (\bar{\mathcal{E}}_{i,j,k})^\top \right) \right\} \leq \frac{1}{p} \|\mathcal{X}\|_{\infty,2}^2.$$

By Lemma 4, for any $c > 1$,

$$\begin{aligned}
\|\mathcal{R}_\Omega(\mathcal{X}) - \mathcal{X}\| &= \|\overline{\mathcal{R}_\Omega(\mathcal{X})} - \bar{\mathcal{X}}\| = \left\| \sum_{i,j,k} \bar{\mathcal{E}}_{i,j,k} \right\| \\
&\leq \sqrt{\frac{2c_2}{p} \|\mathcal{X}\|_{\infty,2}^2 \log((n_1 + n_2)n_3)} + \frac{c_2 \log((n_1 + n_2)n_3)}{p} \|\mathcal{X}\|_\infty
\end{aligned}$$

holds with probability at least $1 - ((n_1 + n_2)n_3)^{1-c_2}$. ■

Proof of Lemma 8 Consider any b -th lateral column of $\mathcal{P}_\top \mathcal{R}_\Omega(\mathcal{X}) - \mathcal{P}_\top(\mathcal{X})$:

$$(\mathcal{P}_\top \mathcal{R}_\Omega(\mathcal{X}) - \mathcal{P}_\top(\mathcal{X})) * \mathring{\mathbf{e}}_b = \sum_{i,j,k} \left(\frac{1}{p} \delta_{i,j,k} - 1 \right) [\mathcal{X}]_{i,j,k} \mathcal{P}_\top(\mathring{\mathbf{e}}_i * \mathring{\mathbf{e}}_k * \mathring{\mathbf{e}}_j^\top) * \mathring{\mathbf{e}}_b =: \sum_{i,j,k} \mathbf{a}_{i,j,k},$$

where $\mathbf{a}_{i,j,k} \in \mathbb{K}^{n_1 \times 1 \times n_3}$ are zero-mean independent lateral tensor columns. Denote $\vec{\mathbf{a}}_{i,j,k} \in \mathbb{K}^{n_1 n_3 \times 1}$ as the vectorized column vector of $\mathbf{a}_{i,j,k}$. Then, we have

$$\|\vec{\mathbf{a}}_{i,j,k}\| = \|\mathbf{a}_{i,j,k}\|_{\text{F}} \leq \frac{1}{p} [\mathcal{X}]_{i,j,k} \|\mathcal{P}_{\mathbb{T}}(\hat{\mathbf{e}}_i * \hat{\mathbf{e}}_k * \hat{\mathbf{e}}_j^{\top}) * \hat{\mathbf{e}}_b\|_{\text{F}} \leq \frac{1}{p} \sqrt{\frac{(n_1 + n_2)\mu_0 r}{n_1 n_2}} \|\mathcal{X}\|_{\infty}.$$

We also have

$$\left| \mathbb{E} \left(\sum_{i,j,k} \vec{\mathbf{a}}_{i,j,k}^{\top} \vec{\mathbf{a}}_{i,j,k} \right) \right| = \mathbb{E} \left(\sum_{i,j,k} \|\mathbf{a}_{i,j,k}\|_{\text{F}}^2 \right) = \frac{1-p}{p} \sum_{i,j,k} [\mathcal{X}]_{i,j,k}^2 \|\mathcal{P}_{\mathbb{T}}(\hat{\mathbf{e}}_i * \hat{\mathbf{e}}_k * \hat{\mathbf{e}}_j^{\top}) * \hat{\mathbf{e}}_b\|_{\text{F}}^2.$$

By the definition of $\mathcal{P}_{\mathbb{T}}$ and the tensor μ_0 -incoherence condition, we have:

$$\begin{aligned} & \|\mathcal{P}_{\mathbb{T}}(\hat{\mathbf{e}}_i * \hat{\mathbf{e}}_k * \hat{\mathbf{e}}_j^{\top}) * \hat{\mathbf{e}}_b\|_{\text{F}} \\ &= \|(\mathcal{W} * \mathcal{W}^{\top} * \hat{\mathbf{e}}_i * \hat{\mathbf{e}}_k) * \hat{\mathbf{e}}_j^{\top} * \hat{\mathbf{e}}_b + (\mathcal{I}_{n_1} - \mathcal{W} * \mathcal{W}^{\top}) * \hat{\mathbf{e}}_i * \hat{\mathbf{e}}_k * \hat{\mathbf{e}}_j^{\top} * \mathcal{V} * \mathcal{V}^{\top} * \hat{\mathbf{e}}_b\|_{\text{F}} \\ &\leq \sqrt{\frac{\mu_0 r}{n_1}} \|\hat{\mathbf{e}}_j^{\top} * \hat{\mathbf{e}}_b\|_{\text{F}} + \|(\mathcal{I}_{n_1} - \mathcal{W} * \mathcal{W}^{\top}) * \hat{\mathbf{e}}_i * \hat{\mathbf{e}}_k\| \|\hat{\mathbf{e}}_j^{\top} * \mathcal{V} * \mathcal{V}^{\top} * \hat{\mathbf{e}}_b\|_{\text{F}} \\ &\leq \sqrt{\frac{\mu_0 r}{n_1}} \|\hat{\mathbf{e}}_j^{\top} * \hat{\mathbf{e}}_b\|_{\text{F}} + \|\hat{\mathbf{e}}_j^{\top} * \mathcal{V} * \mathcal{V}^{\top} * \hat{\mathbf{e}}_b\|_{\text{F}} \end{aligned}$$

By Cauchy-Schwartz inequality, we have $\|\mathcal{P}_{\mathbb{T}}(\hat{\mathbf{e}}_i * \hat{\mathbf{e}}_k * \hat{\mathbf{e}}_j^{\top}) * \hat{\mathbf{e}}_b\|_{\text{F}}^2 \leq \frac{2\mu_0 r}{n_1} \|\hat{\mathbf{e}}_j^{\top} * \hat{\mathbf{e}}_b\|_{\text{F}}^2 + 2 \|\hat{\mathbf{e}}_j^{\top} * \mathcal{V} * \mathcal{V}^{\top} * \hat{\mathbf{e}}_b\|_{\text{F}}^2$. Thus,

$$\begin{aligned} \left| \mathbb{E} \left(\sum_{i,j,k} \vec{\mathbf{a}}_{i,j,k}^{\top} \vec{\mathbf{a}}_{i,j,k} \right) \right| &\leq \frac{2\mu_0 r}{pn_1} \sum_{i,j,k} [\mathcal{X}]_{i,j,k}^2 \|\hat{\mathbf{e}}_j^{\top} * \hat{\mathbf{e}}_b\|_{\text{F}}^2 + \frac{2}{p} \sum_{i,j,k} [\mathcal{X}]_{i,j,k}^2 \|\hat{\mathbf{e}}_j^{\top} * \mathcal{V} * \mathcal{V}^{\top} * \hat{\mathbf{e}}_b\|_{\text{F}}^2 \\ &= \frac{2\mu_0 r}{pn_1} \sum_{i,j,k} [\mathcal{X}]_{i,j,k}^2 \|\hat{\mathbf{e}}_j^{\top} * \hat{\mathbf{e}}_b\|_{\text{F}}^2 + \frac{2}{p} \sum_j \|\hat{\mathbf{e}}_j^{\top} * \mathcal{V} * \mathcal{V}^{\top} * \hat{\mathbf{e}}_b\|_{\text{F}}^2 \sum_{i,k} [\mathcal{X}]_{i,j,k}^2 \\ &\leq \frac{2\mu_0 r}{pn_1} \sum_{i,j,k} [\mathcal{X}]_{i,j,k}^2 \|\hat{\mathbf{e}}_j^{\top} * \hat{\mathbf{e}}_b\|_{\text{F}}^2 + \frac{2}{p} \sum_j \|\hat{\mathbf{e}}_j^{\top} * \mathcal{V} * \mathcal{V}^{\top} * \hat{\mathbf{e}}_b\|_{\text{F}}^2 \|\mathcal{X}\|_{\infty,2}^2 \\ &= \frac{2\mu_0 r}{pn_1} \sum_{i,k} [\mathcal{X}]_{i,b,k}^2 + \frac{2}{p} \|\mathcal{V} * \mathcal{V}^{\top} * \hat{\mathbf{e}}_b\|_{\text{F}}^2 \|\mathcal{X}\|_{\infty,2}^2 \\ &\leq \frac{2\mu_0 r}{pn_1} \|\mathcal{X}\|_{\infty,2}^2 + \frac{2\mu_0 r}{pn_2} \|\mathcal{X}\|_{\infty,2}^2 \leq \frac{2(n_1 + n_2)\mu_0 r}{pn_1 n_2} \|\mathcal{X}\|_{\infty,2}^2 \end{aligned}$$

Similarly, we can bound $\left| \mathbb{E} \left(\sum_{i,j,k} \vec{\mathbf{a}}_{i,j,k} \vec{\mathbf{a}}_{i,j,k}^{\top} \right) \right|$ by the same quantity.

For simplicity, we let $M = \frac{1}{p} \sqrt{\frac{(n_1 + n_2)\mu_0 r}{n_1 n_2}} \|\mathcal{X}\|_{\infty}$ and $\sigma^2 = \frac{2(n_1 + n_2)\mu_0 r}{pn_1 n_2} \|\mathcal{X}\|_{\infty,2}^2$. By Lemma 4, for any $c_1 > 1$, we have

$$\begin{aligned} & \mathbb{P} \left(\left\| \sum_{i,j,k} \vec{\mathbf{a}}_{i,j,k} \right\| \leq \sqrt{2c_1 \sigma^2 \log((n_1 + n_2)n_3)} + c_1 M \log((n_1 + n_2)n_3) \right) \\ &= \mathbb{P} \left(\left\| \sum_{i,j,k} \vec{\mathbf{a}}_{i,j,k} \right\| \leq \sqrt{\frac{4c_1 \log((n_1 + n_2)n_3) (n_1 + n_2)\mu_0 r}{pn_1 n_2}} \cdot \|\mathcal{X}\|_{\infty,2} \right) \end{aligned}$$

$$+ \frac{c_1 \log((n_1 + n_2)n_3) \sqrt{(n_1 + n_2)\mu_0 r}}{p\sqrt{n_1 n_2}} \|\mathcal{X}\|_\infty \Big) \geq 1 - ((n_1 + n_2)n_3)^{1-c_1}.$$

Notice that

$$\|(\mathcal{P}_\mathbb{T}\mathcal{R}_\Omega(\mathcal{X}) - \mathcal{P}_\mathbb{T}(\mathcal{X})) * \mathring{\mathbf{e}}_b\|_F = \left\| \sum_{i,j,k} \mathbf{a}_{i,j,k} \right\|_F = \left\| \sum_{i,j,k} \vec{\mathbf{a}}_{i,j,k} \right\|.$$

Therefore,

$$\mathbb{P} \left(\left\| (\mathcal{P}_\mathbb{T}\mathcal{R}_\Omega(\mathcal{X}) - \mathcal{P}_\mathbb{T}(\mathcal{X})) * \mathring{\mathbf{e}}_b \right\|_F \leq \sqrt{\frac{4c_1(n_1 + n_2) \log((n_1 + n_2)n_3) \mu_0 r}{pn_1 n_2}} \cdot \|\mathcal{X}\|_{\infty,2} + \frac{c_1 \log((n_1 + n_2)n_3) \sqrt{(n_1 + n_2)\mu_0 r}}{p\sqrt{n_1 n_2}} \|\mathcal{X}\|_\infty \right) \geq 1 - ((n_1 + n_2)n_3)^{1-c_1}.$$

Using a union bound over all the tensor lateral slices, we have

$$\mathbb{P} \left(\max_b \left\{ \left\| (\mathcal{P}_\mathbb{T}\mathcal{R}_\Omega(\mathcal{X}) - \mathcal{P}_\mathbb{T}(\mathcal{X})) * \mathring{\mathbf{e}}_b \right\|_F \right\} \leq \sqrt{\frac{4c_1(n_1 + n_2) \log((n_1 + n_2)n_3) \mu_0 r}{pn_1 n_2}} \cdot \|\mathcal{X}\|_{\infty,2} + \frac{c_1 \log((n_1 + n_2)n_3) \sqrt{(n_1 + n_2)\mu_0 r}}{p\sqrt{n_1 n_2}} \|\mathcal{X}\|_\infty \right) \geq 1 - n_2((n_1 + n_2)n_3)^{1-c_1}.$$

Similarly, we can show that

$$\mathbb{P} \left(\max_b \left\{ \left\| \mathring{\mathbf{e}}_b^\top * (\mathcal{P}_\mathbb{T}\mathcal{R}_\Omega(\mathcal{X}) - \mathcal{P}_\mathbb{T}(\mathcal{X})) \right\|_F \right\} \leq \sqrt{\frac{4c_1(n_1 + n_2) \log((n_1 + n_2)n_3) \mu_0 r}{pn_1 n_2}} \cdot \|\mathcal{X}\|_{\infty,2} + \frac{c_1 \log((n_1 + n_2)n_3) \sqrt{(n_1 + n_2)\mu_0 r}}{p\sqrt{n_1 n_2}} \|\mathcal{X}\|_\infty \right) \geq 1 - n_1((n_1 + n_2)n_3)^{1-c_1}.$$

Thus, we can get

$$\mathbb{P} \left(\left\| (\mathcal{P}_\mathbb{T}\mathcal{R}_\Omega(\mathcal{X}) - \mathcal{P}_\mathbb{T}(\mathcal{X})) \right\|_{\infty,2} \leq \sqrt{\frac{4c_1(n_1 + n_2) \log((n_1 + n_2)n_3) \mu_0 r}{pn_1 n_2}} \cdot \|\mathcal{X}\|_{\infty,2} + \frac{c_1 \log((n_1 + n_2)n_3) \sqrt{(n_1 + n_2)\mu_0 r}}{p\sqrt{n_1 n_2}} \|\mathcal{X}\|_\infty \right) \geq 1 - ((n_1 + n_2)n_3)^{2-c_1}.$$

■

Proof of Lemma 9 Notice that

$$\mathcal{P}_\mathbb{T}\mathcal{R}_\Omega\mathcal{P}_\mathbb{T}(\mathcal{X}) = \mathcal{P}_\mathbb{T}\mathcal{R}_\Omega \left(\sum_{i,j,k} \langle \mathcal{P}_\mathbb{T}(\mathcal{X}), \mathring{\mathbf{e}}_i * \mathring{\mathbf{e}}_k * \mathring{\mathbf{e}}_j^\top \rangle \mathring{\mathbf{e}}_i * \mathring{\mathbf{e}}_k * \mathring{\mathbf{e}}_j^\top \right) \quad (31)$$

$$\begin{aligned} &= \mathcal{P}_\mathbb{T} \left(\sum_{i,j,k} \frac{1}{p} \delta_{i,j,k} \langle \mathcal{P}_\mathbb{T}(\mathcal{X}), \mathring{\mathbf{e}}_i * \mathring{\mathbf{e}}_k * \mathring{\mathbf{e}}_j^\top \rangle \mathring{\mathbf{e}}_i * \mathring{\mathbf{e}}_k * \mathring{\mathbf{e}}_j^\top \right) \\ &= \sum_{i,j,k} \frac{1}{p} \delta_{i,j,k} \langle \mathcal{P}_\mathbb{T}(\mathcal{X}), \mathring{\mathbf{e}}_i * \mathring{\mathbf{e}}_k * \mathring{\mathbf{e}}_j^\top \rangle \mathcal{P}_\mathbb{T}(\mathring{\mathbf{e}}_i * \mathring{\mathbf{e}}_k * \mathring{\mathbf{e}}_j^\top), \end{aligned} \quad (32)$$

where (31) holds because $\mathcal{P}_{\mathbb{T}}(\mathcal{X}) = \sum_{i,j,k} \langle \mathcal{P}_{\mathbb{T}}(\mathcal{X}), \mathring{\mathbf{e}}_i * \mathring{\mathbf{e}}_k * \mathring{\mathbf{e}}_j^{\top} \rangle \mathring{\mathbf{e}}_i * \mathring{\mathbf{e}}_k * \mathring{\mathbf{e}}_j^{\top}$, and (32) follows from the linearity of the operator $\mathcal{P}_{\mathbb{T}}$. Notice that

$$\begin{aligned} \mathcal{P}_{\mathbb{T}}(\mathcal{X}) &= \mathcal{P}_{\mathbb{T}}(\mathcal{P}_{\mathbb{T}}(\mathcal{X})) = \mathcal{P}_{\mathbb{T}} \left(\sum_{i,j,k} \langle \mathcal{P}_{\mathbb{T}}(\mathcal{X}), \mathring{\mathbf{e}}_i * \mathring{\mathbf{e}}_k * \mathring{\mathbf{e}}_j^{\top} \rangle \mathring{\mathbf{e}}_i * \mathring{\mathbf{e}}_k * \mathring{\mathbf{e}}_j^{\top} \right) \\ &= \sum_{i,j,k} \langle \mathcal{P}_{\mathbb{T}}(\mathcal{X}), \mathring{\mathbf{e}}_i * \mathring{\mathbf{e}}_k * \mathring{\mathbf{e}}_j^{\top} \rangle \mathcal{P}_{\mathbb{T}}(\mathring{\mathbf{e}}_i * \mathring{\mathbf{e}}_k * \mathring{\mathbf{e}}_j^{\top}) \end{aligned}$$

Thus, we have that any (a, b, c) -th entry of $\mathcal{P}_{\mathbb{T}}\mathcal{R}_{\Omega}\mathcal{P}_{\mathbb{T}}(\mathcal{X}) - \mathcal{P}_{\mathbb{T}}(\mathcal{X})$ can be given by

$$\begin{aligned} &\langle \mathcal{P}_{\mathbb{T}}\mathcal{R}_{\Omega}\mathcal{P}_{\mathbb{T}}(\mathcal{X}) - \mathcal{P}_{\mathbb{T}}(\mathcal{X}), \mathring{\mathbf{e}}_a * \mathring{\mathbf{e}}_c * \mathring{\mathbf{e}}_b^{\top} \rangle \\ &= \left\langle \sum_{i,j,k} \left(\frac{1}{p} \delta_{i,j,k} - 1 \right) \langle \mathcal{P}_{\mathbb{T}}(\mathcal{X}), \mathring{\mathbf{e}}_i * \mathring{\mathbf{e}}_k * \mathring{\mathbf{e}}_j^{\top} \rangle \mathcal{P}_{\mathbb{T}}(\mathring{\mathbf{e}}_i * \mathring{\mathbf{e}}_k * \mathring{\mathbf{e}}_j^{\top}), \mathring{\mathbf{e}}_a * \mathring{\mathbf{e}}_c * \mathring{\mathbf{e}}_b^{\top} \right\rangle \\ &= \sum_{i,j,k} \left(\frac{1}{p} \delta_{i,j,k} - 1 \right) \langle \mathcal{P}_{\mathbb{T}}(\mathcal{X}), \mathring{\mathbf{e}}_i * \mathring{\mathbf{e}}_k * \mathring{\mathbf{e}}_j^{\top} \rangle \langle \mathcal{P}_{\mathbb{T}}(\mathring{\mathbf{e}}_i * \mathring{\mathbf{e}}_k * \mathring{\mathbf{e}}_j^{\top}), \mathring{\mathbf{e}}_a * \mathring{\mathbf{e}}_c * \mathring{\mathbf{e}}_b^{\top} \rangle =: \sum_{i,j,k} h_{i,j,k} \end{aligned}$$

It is easy to see that $\mathbb{E}(h_{i,j,k}) = 0$. Notice that

$$\begin{aligned} |h_{i,j,k}| &= \left| \left(\frac{1}{p} \delta_{i,j,k} - 1 \right) \langle \mathcal{P}_{\mathbb{T}}(\mathcal{X}), \mathring{\mathbf{e}}_i * \mathring{\mathbf{e}}_k * \mathring{\mathbf{e}}_j^{\top} \rangle \langle \mathcal{P}_{\mathbb{T}}(\mathring{\mathbf{e}}_i * \mathring{\mathbf{e}}_k * \mathring{\mathbf{e}}_j^{\top}), \mathring{\mathbf{e}}_a * \mathring{\mathbf{e}}_c * \mathring{\mathbf{e}}_b^{\top} \rangle \right| \\ &= \left| \left(\frac{1}{p} \delta_{i,j,k} - 1 \right) \langle \mathcal{P}_{\mathbb{T}}(\mathcal{X}), \mathring{\mathbf{e}}_i * \mathring{\mathbf{e}}_k * \mathring{\mathbf{e}}_j^{\top} \rangle \langle \mathcal{P}_{\mathbb{T}}(\mathring{\mathbf{e}}_i * \mathring{\mathbf{e}}_k * \mathring{\mathbf{e}}_j^{\top}), \mathcal{P}_{\mathbb{T}}(\mathring{\mathbf{e}}_a * \mathring{\mathbf{e}}_c * \mathring{\mathbf{e}}_b^{\top}) \rangle \right| \\ &\leq \frac{1}{p} \|\mathcal{P}_{\mathbb{T}}(\mathcal{X})\|_{\infty} \|\mathcal{P}_{\mathbb{T}}(\mathring{\mathbf{e}}_i * \mathring{\mathbf{e}}_k * \mathring{\mathbf{e}}_j^{\top})\|_{\text{F}} \|\mathcal{P}_{\mathbb{T}}(\mathring{\mathbf{e}}_a * \mathring{\mathbf{e}}_c * \mathring{\mathbf{e}}_b^{\top})\|_{\text{F}} \leq \frac{(n_1 + n_2)\mu_0 r}{pn_1 n_2} \|\mathcal{P}_{\mathbb{T}}(\mathcal{X})\|_{\infty} \end{aligned}$$

It is easy to check that

$$\begin{aligned} \left| \sum_{i,j,k} \mathbb{E}[h_{i,j,k}^2] \right| &= \mathbb{E} \left(\left| \left(\frac{1}{p} \delta_{i,j,k} - 1 \right) \langle \mathcal{P}_{\mathbb{T}}(\mathcal{X}), \mathring{\mathbf{e}}_i * \mathring{\mathbf{e}}_k * \mathring{\mathbf{e}}_j^{\top} \rangle \langle \mathcal{P}_{\mathbb{T}}(\mathring{\mathbf{e}}_i * \mathring{\mathbf{e}}_k * \mathring{\mathbf{e}}_j^{\top}), \mathring{\mathbf{e}}_a * \mathring{\mathbf{e}}_c * \mathring{\mathbf{e}}_b^{\top} \rangle \right|^2 \right) \\ &= \mathbb{E} \left(\left(\frac{1}{p} \delta_{i,j,k} - 1 \right)^2 \left| \langle \mathcal{P}_{\mathbb{T}}(\mathcal{X}), \mathring{\mathbf{e}}_i * \mathring{\mathbf{e}}_k * \mathring{\mathbf{e}}_j^{\top} \rangle \langle \mathcal{P}_{\mathbb{T}}(\mathring{\mathbf{e}}_i * \mathring{\mathbf{e}}_k * \mathring{\mathbf{e}}_j^{\top}), \mathring{\mathbf{e}}_a * \mathring{\mathbf{e}}_c * \mathring{\mathbf{e}}_b^{\top} \rangle \right|^2 \right) \\ &\leq \frac{1}{p} \|\mathcal{P}_{\mathbb{T}}(\mathcal{X})\|_{\infty}^2 \|\mathcal{P}_{\mathbb{T}}(\mathring{\mathbf{e}}_i * \mathring{\mathbf{e}}_k * \mathring{\mathbf{e}}_j^{\top})\|_{\text{F}}^2 \leq \frac{(n_1 + n_2)\mu_0 r}{pn_1 n_2} \|\mathcal{P}_{\mathbb{T}}(\mathcal{X})\|_{\infty}^2. \end{aligned}$$

Thus, by the non-commutative Bernstein inequality, we have

$$\begin{aligned} &\mathbb{P} \left[(\mathcal{P}_{\mathbb{T}}\mathcal{R}_{\Omega}\mathcal{P}_{\mathbb{T}}(\mathcal{X}) - \mathcal{P}_{\mathbb{T}}(\mathcal{X}))_{a,b,c} \geq \frac{1}{2} \|\mathcal{P}_{\mathbb{T}}(\mathcal{X})\|_{\infty} \right] \\ &\leq 2 \exp \left(\frac{-\|\mathcal{P}_{\mathbb{T}}(\mathcal{X})\|_{\infty}^2 / 8}{\frac{(n_1 + n_2)\mu_0 r}{pn_1 n_2} \|\mathcal{P}_{\mathbb{T}}(\mathcal{X})\|_{\infty}^2 + \frac{(n_1 + n_2)\mu_0 r}{6pn_1 n_2} \|\mathcal{P}_{\mathbb{T}}(\mathcal{X})\|_{\infty}^2} \right) \\ &= 2 \exp \left(\frac{-3pn_1 n_2}{28(n_1 + n_2)\mu_0 r} \right). \end{aligned}$$

Using the union bound on every (a, b, c) -th entry, we have

$$\|(\mathcal{P}_{\mathbb{T}}\mathcal{R}_{\Omega}\mathcal{P}_{\mathbb{T}} - \mathcal{P}_{\mathbb{T}})(\mathcal{P}_{\mathbb{T}}(\mathcal{X}))\|_{\infty} \leq \frac{1}{2} \|\mathcal{P}_{\mathbb{T}}(\mathcal{X})\|_{\infty}$$

with probability at least $1 - 2n_1n_2n_3 \exp\left(\frac{-3pn_1n_2}{28(n_1+n_2)\mu_{0r}}\right)$. ■

Lastly, to ensure the completeness of our exposition, we provide a detailed proof of Proposition 1 in B.5, as originally presented in [37].

B.5 Proof of Proposition 1

In the following context, the symbol \mathcal{Z} represents the tensor that we aim to recover in (16). Before delving into the detailed proof pipeline, we wish to reiterate the purpose of Proposition 1, which asserts that \mathcal{Z} is a unique minimizer to (16) when Conditions 1 and 2 are satisfied simultaneously. Notice that \mathcal{Z} is a feasible solution to (16). To show that \mathcal{Z} is the unique minimizer, it suffices to show

$$\|\mathcal{X}\|_{\text{TNN}} - \|\mathcal{Z}\|_{\text{TNN}} > 0$$

for any feasible solution \mathcal{X} where $\mathcal{X} \neq \mathcal{Z}$.

First, we show that for any feasible solution \mathcal{X} different from \mathcal{Z} , there exists an auxiliary tensor \mathcal{M} such that

$$\|\mathcal{X}\|_{\text{TNN}} - \|\mathcal{Z}\|_{\text{TNN}} \geq \langle \mathcal{W} * \mathcal{V}^\top + \mathcal{P}_{\mathbb{T}^\perp(\mathcal{Z})}(\mathcal{M}), \mathcal{X} - \mathcal{Z} \rangle.$$

In this way, we can transform the proof of $\|\mathcal{X}\|_{\text{TNN}} - \|\mathcal{Z}\|_{\text{TNN}} > 0$ into showing

$$\langle \mathcal{W} * \mathcal{V}^\top + \mathcal{P}_{\mathbb{T}^\perp(\mathcal{Z})}(\mathcal{M}), \mathcal{X} - \mathcal{Z} \rangle > 0.$$

To prove $\langle \mathcal{W} * \mathcal{V}^\top + \mathcal{P}_{\mathbb{T}^\perp}(\mathcal{M}), \mathcal{X} - \mathcal{Z} \rangle > 0$, we split

$$\langle \mathcal{W} * \mathcal{V}^\top + \mathcal{P}_{\mathbb{T}^\perp}(\mathcal{M}), \mathcal{X} - \mathcal{Z} \rangle$$

into two parts

$$\langle \mathcal{P}_{\mathbb{T}^\perp}(\mathcal{M}), \mathcal{X} - \mathcal{Z} \rangle \text{ and } \langle \mathcal{W} * \mathcal{V}^\top, \mathcal{X} - \mathcal{Z} \rangle.$$

By construction the auxiliary tensor \mathcal{M} , we can show that

$$\langle \mathcal{P}_{\mathbb{T}^\perp}(\mathcal{M}), \mathcal{X} - \mathcal{Z} \rangle = \|\mathcal{P}_{\mathbb{T}^\perp}(\mathcal{X} - \mathcal{Z})\|_{\text{TNN}}.$$

As for the part $\langle \mathcal{W} * \mathcal{V}^\top, \mathcal{X} - \mathcal{Z} \rangle$, we further split it into two parts by introducing the dual certification tensor \mathcal{Y} :

$$\langle \mathcal{P}_{\mathbb{T}(\mathcal{Z})}(\mathcal{Y}) - \mathcal{W} * \mathcal{V}^\top, \mathcal{X} - \mathcal{Z} \rangle, \langle \mathcal{P}_{\mathbb{T}^\perp(\mathcal{Z})}(\mathcal{Y}), \mathcal{X} - \mathcal{Z} \rangle.$$

The reason for this separation is that we can bound these two terms by $\frac{1}{2}\|\mathcal{P}_{\mathbb{T}^\perp}(\mathcal{X} - \mathcal{Z})\|_{\text{TNN}}$ and $\frac{\sqrt{2}}{4}\|\mathcal{P}_{\mathbb{T}^\perp}(\mathcal{X} - \mathcal{Z})\|_{\text{TNN}}$ respectively. By combining the bounds of the above three separations together, we obtain

$$\langle \mathcal{W} * \mathcal{V}^\top + \mathcal{P}_{\mathbb{T}^\perp}(\mathcal{M}), \mathcal{X} - \mathcal{Z} \rangle \geq \frac{1}{8}\|\mathcal{P}_{\mathbb{T}^\perp}(\mathcal{X} - \mathcal{Z})\|_{\text{TNN}}.$$

In the end, we prove that $\|\mathcal{P}_{\mathbb{T}^\perp(\mathcal{Z})}(\mathcal{X} - \mathcal{Z})\|_{\text{TNN}}$ strictly larger than zero by contradiction. Before proceeding to the detailed proof, we will present several useful lemmas which are key to the proof of Proposition 1.

B.5.1 Supporting lemmas for the proof of Proposition 1

First, we state the characterization of the tensor nuclear norm (TNN), which can be described as a duality to the tensor spectral norm.

Lemma 10 ([37]) Given a tensor $\mathcal{T} \in \mathbb{K}^{n_1 \times n_2 \times n_3}$, we have

$$\|\mathcal{T}\|_{\text{TNN}} = \sup_{\{\mathcal{Q} \in \mathbb{K}^{n_1 \times n_2 \times n_3} : \|\mathcal{Q}\| \leq 1\}} \langle \mathcal{Q}, \mathcal{T} \rangle.$$

Next, we present a characterization of the subdifferential of TNN, which is useful for proving the uniqueness of the minimizer to (16).

Lemma 11 (Subdifferential of TNN [37]) Let $\mathcal{Z} \in \mathbb{K}^{n_1 \times n_2 \times n_3}$ and its compact t -SVD be $\mathcal{Z} = \mathcal{W} * \mathcal{S} * \mathcal{V}^\top$. The subdifferential (the set of subgradients) of $\|\mathcal{Z}\|_{\text{TNN}}$ is $\partial \|\mathcal{Z}\|_{\text{TNN}} = \{\mathcal{W} * \mathcal{V}^\top + \mathcal{M} : \mathcal{W}^\top * \mathcal{M} = 0, \mathcal{M} * \mathcal{V} = 0, \|\mathcal{M}\| \leq 1\}$.

For the proof of Proposition 1, a significant challenge is proving the minimizer's uniqueness. To tackle it, based on the result of Lemma 11, we can introduce an auxiliary tensor \mathcal{M} such that

$$\langle \mathcal{W} * \mathcal{V}^\top + \mathcal{P}_{\mathbb{T}^\perp(\mathcal{Z})}(\mathcal{M}), \mathcal{X} - \mathcal{Z} \rangle > 0.$$

Lemma 12 ([64]) Assume that Ω is generated according to the Bernoulli sampling with probability p . If $\|\mathcal{P}_{\mathbb{T}} \mathcal{R}_\Omega \mathcal{P}_{\mathbb{T}} - \mathcal{P}_{\mathbb{T}}\| \leq \frac{1}{2}$, then

$$\|\mathcal{P}_{\mathbb{T}}(\mathcal{X})\|_{\text{F}} \leq \sqrt{\frac{2n_3}{p}} \cdot \|\mathcal{P}_{\mathbb{T}^\perp}(\mathcal{X})\|_{\text{TNN}},$$

for any \mathcal{X} with $\mathcal{P}_\Omega(\mathcal{X}) = 0$.

This lemma shows that $\|\mathcal{P}_{\mathbb{T}}(\mathcal{X})\|_{\text{F}}$ can be bounded above by $\sqrt{\frac{2n_3}{p}} \|\mathcal{P}_{\mathbb{T}^\perp}(\mathcal{X})\|_{\text{TNN}}$, a key element in our analysis. Further details are in B.5.2.

B.5.2 Proof of Proposition 1

Proof Consider any feasible solution $\mathcal{X} \neq \mathcal{Z}$ to (16) with $\mathcal{P}_\Omega(\mathcal{X}) = \mathcal{P}_\Omega(\mathcal{Z})$. By Lemma 10, we have an auxiliary tensor \mathcal{M} with $\|\mathcal{M}\| \leq 1$ such that

$$\|\mathcal{P}_{\mathbb{T}^\perp}(\mathcal{X} - \mathcal{Z})\|_{\text{TNN}} = \langle \mathcal{M}, \mathcal{P}_{\mathbb{T}^\perp}(\mathcal{X} - \mathcal{Z}) \rangle = \langle \mathcal{P}_{\mathbb{T}^\perp}(\mathcal{M}), \mathcal{P}_{\mathbb{T}^\perp}(\mathcal{X} - \mathcal{Z}) \rangle.$$

First, it is easy to check that $\mathcal{W}^\top * \mathcal{P}_{\mathbb{T}^\perp}(\mathcal{M}) = 0$ and $\mathcal{P}_{\mathbb{T}^\perp}(\mathcal{M}) * \mathcal{V} = 0$ by the definition of the operator $\mathcal{P}_{\mathbb{T}^\perp}$. By Lemma 11, we have that $\mathcal{W} * \mathcal{V}^\top + \mathcal{P}_{\mathbb{T}^\perp}(\mathcal{M})$ is a subgradient of \mathcal{Z} in terms of tensor nuclear norm. Therefore, we have

$$\|\mathcal{X}\|_{\text{TNN}} - \|\mathcal{Z}\|_{\text{TNN}} \geq \langle \mathcal{W} * \mathcal{V}^\top + \mathcal{P}_{\mathbb{T}^\perp}(\mathcal{M}), \mathcal{X} - \mathcal{Z} \rangle.$$

To prove $\|\mathcal{X}\|_{\text{TNN}} - \|\mathcal{Z}\|_{\text{TNN}} \geq 0$, it is sufficient to show

$$\langle \mathcal{W} * \mathcal{V}^\top + \mathcal{P}_{\mathbb{T}^\perp}(\mathcal{M}), \mathcal{X} - \mathcal{Z} \rangle \geq 0.$$

Notice that for any \mathcal{Y} where $\mathcal{P}_\Omega(\mathcal{Y}) = \mathcal{Y}$, we have

$$\langle \mathcal{Y}, \mathcal{X} - \mathcal{Z} \rangle = \langle \mathcal{P}_\Omega(\mathcal{Y}), \mathcal{X} - \mathcal{Z} \rangle = \langle \mathcal{P}_\Omega(\mathcal{Y}), \mathcal{P}_\Omega(\mathcal{X} - \mathcal{Z}) \rangle = 0.$$

Thus, we have

$$\langle \mathcal{W} * \mathcal{V}^\top + \mathcal{P}_{\mathbb{T}^\perp}(\mathcal{M}), \mathcal{X} - \mathcal{Z} \rangle = \langle \mathcal{W} * \mathcal{V}^\top + \mathcal{P}_{\mathbb{T}^\perp}(\mathcal{M}) - \mathcal{Y}, \mathcal{X} - \mathcal{Z} \rangle.$$

Furthermore, we have

$$\begin{aligned} & \langle \mathcal{W} * \mathcal{V}^\top + \mathcal{P}_{\mathbb{T}^\perp}(\mathcal{M}) - \mathcal{Y}, \mathcal{X} - \mathcal{Z} \rangle \\ &= \langle \mathcal{W} * \mathcal{V}^\top + \mathcal{P}_{\mathbb{T}^\perp}(\mathcal{M}) - \mathcal{P}_{\mathbb{T}^\perp}(\mathcal{Y}) - \mathcal{P}_{\mathbb{T}}(\mathcal{Y}), \mathcal{X} - \mathcal{Z} \rangle \end{aligned}$$

$$\begin{aligned}
&= \langle \mathcal{P}_{\mathbb{T}^\perp}(\mathcal{M}), \mathcal{X} - \mathcal{Z} \rangle - \langle \mathcal{P}_{\mathbb{T}}(\mathcal{Y}) - \mathcal{W} * \mathcal{V}^\top, \mathcal{X} - \mathcal{Z} \rangle - \langle \mathcal{P}_{\mathbb{T}^\perp}(\mathcal{Y}), \mathcal{X} - \mathcal{Z} \rangle \\
&= \|\mathcal{P}_{\mathbb{T}^\perp}(\mathcal{X} - \mathcal{Z})\|_{\text{TNN}} - \langle \mathcal{P}_{\mathbb{T}}(\mathcal{Y}) - \mathcal{W} * \mathcal{V}^\top, \mathcal{P}_{\mathbb{T}}(\mathcal{X} - \mathcal{Z}) \rangle - \langle \mathcal{P}_{\mathbb{T}^\perp}(\mathcal{Y}), \mathcal{P}_{\mathbb{T}^\perp}(\mathcal{X} - \mathcal{Z}) \rangle \\
&\geq \|\mathcal{P}_{\mathbb{T}^\perp}(\mathcal{X} - \mathcal{Z})\|_{\text{TNN}} - \|\mathcal{P}_{\mathbb{T}}(\mathcal{Y}) - \mathcal{W} * \mathcal{V}^\top\|_{\text{F}} \|\mathcal{P}_{\mathbb{T}}(\mathcal{X} - \mathcal{Z})\|_{\text{F}} \\
&\quad - \|\mathcal{P}_{\mathbb{T}^\perp}(\mathcal{Y})\| \|\mathcal{P}_{\mathbb{T}^\perp}(\mathcal{X} - \mathcal{Z})\|_{\text{TNN}} \\
&\geq \frac{1}{2} \|\mathcal{P}_{\mathbb{T}^\perp}(\mathcal{X} - \mathcal{Z})\|_{\text{TNN}} - \frac{1}{4} \sqrt{\frac{p}{n_3}} \cdot \sqrt{\frac{2n_3}{p}} \|\mathcal{P}_{\mathbb{T}^\perp}(\mathcal{X} - \mathcal{Z})\|_{\text{TNN}} \tag{33} \\
&\geq \frac{1}{8} \|\mathcal{P}_{\mathbb{T}^\perp}(\mathcal{X} - \mathcal{Z})\|_{\text{TNN}},
\end{aligned}$$

where Inequality (33) results from Condition 1 ($\|\mathcal{P}_{\mathbb{T}}\mathcal{R}_\Omega\mathcal{P}_{\mathbb{T}} - \mathcal{P}_{\mathbb{T}}\| \leq \frac{1}{2}$), Condition 2 ($\|\mathcal{P}_{\mathbb{T}}(\mathcal{Y}) - \mathcal{W} * \mathcal{V}^\top\|_{\text{F}} \leq \frac{1}{4}\sqrt{\frac{p}{n_3}}$, $\|\mathcal{P}_{\mathbb{T}^\perp}(\mathcal{Y})\| \leq \frac{1}{2}$), and Lemma 12.

Next, we need to show that $\|\mathcal{P}_{\mathbb{T}^\perp}(\mathcal{X} - \mathcal{Z})\|_{\text{TNN}}$ is strictly positive. We show this by contradiction. Suppose $\|\mathcal{P}_{\mathbb{T}^\perp}(\mathcal{X} - \mathcal{Z})\|_{\text{TNN}} = 0$. Then, $\mathcal{P}_{\mathbb{T}}(\mathcal{X} - \mathcal{Z}) = \mathcal{X} - \mathcal{Z}$ and $\mathcal{P}_{\mathbb{T}}\mathcal{R}_\Omega\mathcal{P}_{\mathbb{T}}(\mathcal{X} - \mathcal{Z}) = 0$. Therefore, we have

$$\|\mathcal{X} - \mathcal{Z}\| = \|(\mathcal{P}_{\mathbb{T}}\mathcal{R}_\Omega\mathcal{P}_{\mathbb{T}} - \mathcal{P}_{\mathbb{T}})(\mathcal{X} - \mathcal{Z})\| \leq \|\mathcal{P}_{\mathbb{T}}\mathcal{R}_\Omega\mathcal{P}_{\mathbb{T}} - \mathcal{P}_{\mathbb{T}}\| \|\mathcal{X} - \mathcal{Z}\|,$$

which implies that $\|\mathcal{P}_{\mathbb{T}}\mathcal{R}_\Omega\mathcal{P}_{\mathbb{T}} - \mathcal{P}_{\mathbb{T}}\| \geq 1$. This contradicts with the assumption that $\|\mathcal{P}_{\mathbb{T}}\mathcal{R}_\Omega\mathcal{P}_{\mathbb{T}} - \mathcal{P}_{\mathbb{T}}\| \leq \frac{1}{2}$. Thus, \mathcal{Z} is the unique minimizer to (16). \blacksquare

B.5.3 Proof of Lemma 12

Proof Let \mathcal{X} be a tensor satisfying $\mathcal{P}_\Omega(\mathcal{X}) = 0$. Using the self-adjoint property of the operator $\mathcal{P}_{\mathbb{T}}$, we have

$$\begin{aligned}
\|\mathcal{R}_\Omega\mathcal{P}_{\mathbb{T}}(\mathcal{X})\|_{\text{F}}^2 &= \langle \mathcal{R}_\Omega\mathcal{P}_{\mathbb{T}}(\mathcal{X}), \mathcal{R}_\Omega\mathcal{P}_{\mathbb{T}}(\mathcal{X}) \rangle \\
&= \left\langle \mathcal{R}_\Omega\mathcal{P}_{\mathbb{T}}(\mathcal{X}), \sum_{i,j,k} \frac{1}{p} \delta_{i,j,k} [\mathcal{P}_{\mathbb{T}}(\mathcal{X})]_{i,j,k} \cdot \mathbf{e}_i * \mathbf{e}_k * \mathbf{e}_j^\top \right\rangle \\
&= \frac{1}{p} \left\langle \mathcal{R}_\Omega\mathcal{P}_{\mathbb{T}}(\mathcal{X}), \sum_{i,j,k} \delta_{i,j,k} [\mathcal{P}_{\mathbb{T}}(\mathcal{X})]_{i,j,k} \cdot \mathbf{e}_i * \mathbf{e}_k * \mathbf{e}_j^\top \right\rangle \\
&= \frac{1}{p} \langle \mathcal{R}_\Omega\mathcal{P}_{\mathbb{T}}(\mathcal{X}), \mathcal{P}_\Omega(\mathcal{P}_{\mathbb{T}}(\mathcal{X})) \rangle = \frac{1}{p} \langle \mathcal{P}_{\mathbb{T}}\mathcal{R}_\Omega\mathcal{P}_{\mathbb{T}}(\mathcal{X}), \mathcal{X} \rangle \\
&= \frac{1}{p} \langle \mathcal{P}_{\mathbb{T}}\mathcal{R}_\Omega\mathcal{P}_{\mathbb{T}}(\mathcal{X}) - \mathcal{P}_{\mathbb{T}}(\mathcal{X}), \mathcal{X} \rangle + \frac{1}{p} \langle \mathcal{P}_{\mathbb{T}}(\mathcal{X}), \mathcal{X} \rangle \\
&= \frac{1}{p} \|\mathcal{P}_{\mathbb{T}}(\mathcal{X})\|_{\text{F}}^2 + \frac{1}{p} \langle (\mathcal{P}_{\mathbb{T}}\mathcal{R}_\Omega\mathcal{P}_{\mathbb{T}} - \mathcal{P}_{\mathbb{T}})(\mathcal{X}), \mathcal{P}_{\mathbb{T}}(\mathcal{X}) \rangle \\
&\geq \frac{1}{p} \|\mathcal{P}_{\mathbb{T}}(\mathcal{X})\|_{\text{F}}^2 - \frac{1}{p} \|\mathcal{P}_{\mathbb{T}}\mathcal{R}_\Omega\mathcal{P}_{\mathbb{T}} - \mathcal{P}_{\mathbb{T}}\| \cdot \|\mathcal{P}_{\mathbb{T}}(\mathcal{X})\|_{\text{F}}^2 \geq \frac{1}{2p} \|\mathcal{P}_{\mathbb{T}}(\mathcal{X})\|_{\text{F}}^2.
\end{aligned}$$

Notice that if $\mathcal{P}_\Omega(\mathcal{X}) = 0$, then $\mathcal{R}_\Omega(\mathcal{X})$ must be the zero tensor. Thus, we have

$$\|\mathcal{R}_\Omega\mathcal{P}_{\mathbb{T}}(\mathcal{X})\|_{\text{F}} = \|\mathcal{R}_\Omega\mathcal{P}_{\mathbb{T}^\perp}(\mathcal{X})\|_{\text{F}} \leq \frac{1}{p} \|\mathcal{P}_{\mathbb{T}^\perp}(\mathcal{X})\|_{\text{F}}$$

$$= \frac{1}{p\sqrt{n_3}} \left\| \overline{\mathcal{P}_{\mathbb{T}^\perp}(\mathcal{X})} \right\|_{\text{F}} \leq \frac{1}{p\sqrt{n_3}} \left\| \overline{\mathcal{P}_{\mathbb{T}^\perp}(\mathcal{X})} \right\|_* = \frac{\sqrt{n_3}}{p} \|\mathcal{P}_{\mathbb{T}^\perp}(\mathcal{X})\|_{\text{TNN}}.$$

As a result, we have $\|\mathcal{P}_{\mathbb{T}}(\mathcal{X})\|_{\text{F}} \leq \sqrt{2p} \|\mathcal{R}_\Omega \mathcal{P}_{\mathbb{T}}(\mathcal{X})\|_{\text{F}} \leq \sqrt{\frac{2n_3}{p}} \|\mathcal{P}_{\mathbb{T}^\perp}(\mathcal{X})\|_{\text{TNN}}$. \blacksquare

Next we present a detailed proof of Theorem 2, our main theoretical result, demonstrating that our model ensures tensor recovery in high-probability.

Appendix C. Proof of Theorem 2

In this section, we provide a detailed proof of our main theoretical result Theorem 2. The proof is based on our Two-Step Tensor Completion (TSTC) algorithm. For the ease of the reader, we state the TSTC algorithm in Algorithm 3. This algorithm focuses on subtensor completion before combining results with t-CUR.

Algorithm 3 Two-Step Tensor Completion (TSTC)

- 1: **Input:** $[\mathcal{T}]_{\Omega_{\mathcal{R}} \cup \Omega_{\mathcal{C}}}$: observed data; $\Omega_{\mathcal{R}}, \Omega_{\mathcal{C}}$: observation locations; I, J : lateral and horizontal indices; r : target rank; TC: the chosen tensor completion solver.
 - 2: $\tilde{\mathcal{R}} = \text{TC}([\mathcal{T}]_{\Omega_{\mathcal{R}}}, r)$
 - 3: $\tilde{\mathcal{C}} = \text{TC}([\mathcal{C}]_{\Omega_{\mathcal{C}}}, r)$
 - 4: $\tilde{\mathcal{U}} = [\tilde{\mathcal{C}}]_{I, :, :}$
 - 5: $\tilde{\mathcal{T}} = \tilde{\mathcal{C}} * \tilde{\mathcal{U}}^\dagger * \tilde{\mathcal{R}}$
 - 6: **Output:** $\tilde{\mathcal{T}}$: approximation of \mathcal{T}
-

Based on the idea of TSTC, it is crucial to understand that how the tensor incoherence properties of the original low tubal-rank tensor transfer to subtensors.

C.1 Incoherence passes to subtensors

Inspired by [9, Theorem 3.5], we explore how subtensors inherit the tensor incoherence conditions from the original tensor, differing from [46] in tensor norm and the definition of the tensor incoherence condition. Our focus is on subtensor incoherence due to its impact on the required sampling rate for accurate low tubal-rank tensor recovery (Theorem 4) and our emphasis on completing subtensors in tensor completion. We begin by examining the relationship between the tensor incoherence properties of subtensors and the original low tubal-rank tensor.

Lemma 13 *Let $\mathcal{T} \in \mathbb{K}^{n_1 \times n_2 \times n_3}$ satisfy the tensor μ_0 -incoherence condition. Suppose that \mathcal{T} has a compact t-SVD $\mathcal{T} = \mathcal{W} * \Sigma * \mathcal{V}^\top$ and a condition number κ . Consider the subtensors $\mathcal{C} = [\mathcal{T}]_{:, J, :}$ and $\mathcal{R} = [\mathcal{T}]_{I, :, :}$, each maintaining the same tubal-rank as \mathcal{T} . Their compact t-SVDs are represented as*

$$\mathcal{C} = \mathcal{W}_{\mathcal{C}} * \Sigma_{\mathcal{C}} * \mathcal{V}_{\mathcal{C}}^\top \text{ and } \mathcal{R} = \mathcal{W}_{\mathcal{R}} * \Sigma_{\mathcal{R}} * \mathcal{V}_{\mathcal{R}}^\top,$$

then the following results hold:

$$\mu_{\mathcal{C}} \leq \kappa^2 \left\| [\mathcal{V}]_{J,::}^\dagger \right\|^2 \frac{|J|}{n_2} \mu_0, \quad \text{and} \quad \mu_{\mathcal{R}} \leq \kappa^2 \left\| [\mathcal{W}]_{I,::}^\dagger \right\|^2 \frac{|I|}{n_1} \mu_0.$$

Proof First, let's prove that

$$\max_i \left\| [\widehat{\mathcal{W}}_{\mathcal{C}}^\top]_{::,k} \cdot \mathbf{e}_i \right\|_{\mathbb{F}} \leq \sqrt{\frac{\mu_0 r}{n_1}}.$$

Notice that $\mathcal{C} = \mathcal{T}_{:,J,:} = \mathcal{W} * \Sigma * [\mathcal{V}]_{J,::}^\top$. Assume the compact t-SVD of $\Sigma * ([\mathcal{V}]_{J,::}^\top)^\top$ is $\Sigma * ([\mathcal{V}]_{J,::}^\top)^\top = \mathcal{P} * \mathcal{S} * \mathcal{Q}^\top$. Thus, $\mathcal{P} \in \mathbb{K}^{r \times r \times n_3}$ is an orthonormal tensor, leading to $\mathcal{W}_{\mathcal{C}} = \mathcal{W} * \mathcal{P}$ based on the relationship that $\mathcal{C} = \mathcal{W} * \mathcal{P} * \mathcal{S} * \mathcal{Q}^\top$. $\mathcal{P}^\top * \mathcal{P} = \mathcal{I}$ implies that $[\widehat{\mathcal{P}}]_{::,k}^\top \cdot [\widehat{\mathcal{P}}]_{::,k} = \mathbb{I}_r$, where \mathbb{I}_r is the $r \times r$ identity matrix for all $k \in [n_3]$. Therefore, we can establish that for $k \in [n_3]$,

$$\max_i \left\| \widehat{\mathcal{W}}_{\mathcal{C}}^\top_{::,k} \cdot \mathbf{e}_i \right\|_{\mathbb{F}} = \max_i \left\| [\widehat{\mathcal{W}}]_{::,k}^\top \cdot \mathbf{e}_i \right\|_{\mathbb{F}} \leq \sqrt{\frac{\mu_0 r}{n_1}}. \quad (34)$$

Next, let's prove $\max_i \left\| [\widehat{\mathcal{V}}_{\mathcal{C}}^\top]_{::,k} \cdot \mathbf{e}_i \right\|_{\mathbb{F}} \leq \kappa(\mathcal{T}) \left\| ([\mathcal{V}]_{J,::}^\top)^\dagger \right\| \sqrt{\frac{\mu_0 r}{n_2}}$. The compact t-SVD of \mathcal{C} implies $\mathcal{V}_{\mathcal{C}}^\top = \Sigma_{\mathcal{C}}^\dagger * \mathcal{W}_{\mathcal{C}}^\top * \mathcal{C}$. Thus, for each $k \in [n_3]$, $[\widehat{\mathcal{V}}_{\mathcal{C}}^\top]_{::,k} = [\widehat{\Sigma}_{\mathcal{C}}^\dagger]_{::,k} \cdot [\widehat{\mathcal{W}}_{\mathcal{C}}^\top]_{::,k} \cdot [\widehat{\mathcal{C}}]_{::,k}$ holds and $\left\| [\widehat{\mathcal{V}}_{\mathcal{C}}^\top]_{::,k} \cdot \mathbf{e}_i \right\|_{\mathbb{F}}$ can be bounded by

$$\begin{aligned} \left\| [\widehat{\mathcal{V}}_{\mathcal{C}}^\top]_{::,k} \cdot \mathbf{e}_i \right\|_{\mathbb{F}} &= \left\| [\widehat{\Sigma}_{\mathcal{C}}^\dagger]_{::,k} \cdot [\widehat{\mathcal{W}}_{\mathcal{C}}^\top]_{::,k} \cdot [\widehat{\mathcal{C}}]_{::,k} \cdot \mathbf{e}_i \right\|_{\mathbb{F}} \\ &\leq \left\| [\widehat{\Sigma}_{\mathcal{C}}^\dagger]_{::,k} \right\| \left\| [\widehat{\mathcal{W}}_{\mathcal{C}}^\top]_{::,k} \cdot [\widehat{\mathcal{W}}]_{::,k} \cdot [\widehat{\Sigma}]_{::,k} \cdot [\widehat{\mathcal{V}}]_{J,::}^\top \cdot \mathbf{e}_i \right\|_{\mathbb{F}} \\ &\leq \left\| \widehat{\Sigma}_{\mathcal{C}}^\dagger \right\| \left\| \widehat{\Sigma} \right\| \left\| [\widehat{\mathcal{V}}]_{J,::}^\top \cdot \mathbf{e}_i \right\|_{\mathbb{F}} \\ &\leq \left\| \mathcal{C}^\dagger \right\| \left\| \mathcal{T} \right\| \left\| [\widehat{\mathcal{V}}]_{::,k}^\top \cdot \mathbf{e}_i \right\|_{\mathbb{F}} \\ &= \left\| ([\mathcal{V}]_{J,::}^\top)^\dagger * \Sigma^\dagger * \mathcal{W}^\top \right\| \left\| \mathcal{T} \right\| \left\| [\widehat{\mathcal{V}}]_{::,k}^\top \cdot \mathbf{e}_i \right\|_{\mathbb{F}} \\ &\leq \left\| ([\mathcal{V}]_{J,::}^\top)^\dagger \right\| \left\| \mathcal{T}^\dagger \right\| \left\| \mathcal{T} \right\| \left\| [\widehat{\mathcal{V}}]_{::,k}^\top \cdot \mathbf{e}_i \right\|_{\mathbb{F}} \leq \kappa \left\| ([\mathcal{V}]_{J,::}^\top)^\dagger \right\| \sqrt{\frac{\mu_0 r}{n_2}}. \end{aligned}$$

That is,

$$\max_i \left\| [\widehat{\mathcal{V}}_{\mathcal{C}}^\top]_{::,k} \cdot \mathbf{e}_i \right\|_{\mathbb{F}} \leq \kappa \left\| [\mathcal{V}]_{J,::}^\dagger \right\| \sqrt{\frac{\mu_0 |J|}{n_2}} \sqrt{\frac{r}{|J|}}. \quad (35)$$

Combining (34) and (35), we can conclude that $\mu_{\mathcal{C}} \leq \kappa^2 \left\| [\mathcal{V}]_{J,::}^\dagger \right\|^2 \frac{|J|}{n_2} \mu_0$.

Applying above process on \mathcal{R} , we can get $\mu_{\mathcal{R}} \leq \kappa^2 \left\| [\mathcal{W}]_{I,::}^\dagger \right\|^2 \frac{|I|}{n_1} \mu_0$. \blacksquare

Following Lemma 13, we explore the incoherence properties of uniformly sampled subtensors, with summarized results below.

Lemma 14 *Let $\mathcal{T} \in \mathbb{K}^{n_1 \times n_2 \times n_3}$ with multi-rank \vec{r} , and let $\mathcal{T} = \mathcal{W} * \Sigma * \mathcal{V}^\top$ be its compact t-SVD. Additionally, \mathcal{T} satisfies the tensor μ_0 -incoherence condition, and*

κ denotes the condition number of \mathcal{T} . Suppose $I \subseteq [n_1]$ and $J \subseteq [n_2]$ are chosen uniformly at random with replacement. Then

$$\text{rank}_m(\mathcal{R}) = \text{rank}_m(\mathcal{C}) = \text{rank}_m(\mathcal{T}), \mu_{\mathcal{C}} \leq \frac{25}{4}\kappa^2\mu_0 \text{ and } \mu_{\mathcal{R}} \leq \frac{25}{4}\kappa^2\mu_0$$

hold with probability at least $1 - \frac{1}{n_1^\beta} - \frac{1}{n_2^\beta}$ provided that $|I| \geq 2\beta\mu_0\|\vec{r}\|_\infty \log(n_1\|\vec{r}\|_1)$ and $|J| \geq 2\beta\mu_0\|\vec{r}\|_\infty \log(n_2\|\vec{r}\|_1)$.

Proof According to Lemma 2 by setting $\delta = 0.815$ and $\beta_1 = \beta_2 = \beta$, we can easily get that

$$\begin{aligned} \mathbb{P}\left(\|[\mathcal{V}]_{J, :, :}^\dagger\| \leq \sqrt{\frac{25n_2}{4|J|}}, \text{rank}_m(\mathcal{C}) = \text{rank}_m(\mathcal{T})\right) &\geq 1 - \frac{1}{n_2^\beta}, \\ \mathbb{P}\left(\|[\mathcal{W}]_{I, :, :}^\dagger\| \leq \sqrt{\frac{25n_1}{4|I|}}, \text{rank}_m(\mathcal{R}) = \text{rank}_m(\mathcal{T})\right) &\geq 1 - \frac{1}{n_1^\beta}. \end{aligned}$$

Therefore,

$$\mathbb{P}\left(\mu_{\mathcal{C}} \leq \frac{25}{4}\kappa^2\mu_0, \text{rank}_m(\mathcal{C}) = \text{rank}_m(\mathcal{T})\right) \geq 1 - \frac{1}{n_2^\beta}, \quad (36)$$

$$\mathbb{P}\left(\mu_{\mathcal{R}} \leq \frac{25}{4}\kappa^2\mu_0, \text{rank}_m(\mathcal{R}) = \text{rank}_m(\mathcal{T})\right) \geq 1 - \frac{1}{n_1^\beta}. \quad (37)$$

Combining (36) and (37), we can conclude that

$$\text{rank}_m(\mathcal{R}) = \text{rank}_m(\mathcal{C}) = \text{rank}_m(\mathcal{T}), \mu_{\mathcal{C}} \leq \frac{25}{4}\kappa^2\mu_0 \text{ and } \mu_{\mathcal{R}} \leq \frac{25}{4}\kappa^2\mu_0$$

with probability at least $1 - \frac{1}{n_1^\beta} - \frac{1}{n_2^\beta}$ provided that

$$|I| \geq 2\beta\mu_0\|\vec{r}\|_\infty \log(n_1\|\vec{r}\|_1) \text{ and } |J| \geq 2\beta\mu_0\|\vec{r}\|_\infty \log(n_2\|\vec{r}\|_1). \quad \blacksquare$$

C.2 Proof of Theorem 2

Proof Note that $I \subseteq [n_1]$ and $J \subseteq [n_2]$ are chosen uniformly with replacement. According to Lemma 14, we thus have

$$\text{rank}_m(\mathcal{R}) = \text{rank}_m(\mathcal{C}) = \text{rank}_m(\mathcal{T}), \mu_{\mathcal{C}} \leq \frac{25}{4}\kappa^2\mu_0 \text{ and } \mu_{\mathcal{R}} \leq \frac{25}{4}\kappa^2\mu_0$$

hold with probability at least

$$\begin{aligned} &1 - \frac{1}{n_1^{800\beta\kappa^2 \log(n_1n_3+n_2n_3)}} - \frac{1}{n_2^{800\beta\kappa^2 \log(n_1n_3+n_2n_3)}} \\ &= 1 - \frac{1}{(n_1n_3 + n_2n_3)^{800\beta\kappa^2 \log(n_1)}} - \frac{1}{(n_1n_3 + n_2n_3)^{800\beta\kappa^2 \log(n_2)}} \end{aligned}$$

provided that

$$\begin{aligned} |I| &\geq 3200\beta\mu_0r\kappa^2 \log^2(n_1n_3+n_2n_3) \geq 800\kappa^2 \log(n_1n_3+n_2n_3)\beta \cdot (2\mu_0\|\vec{r}\|_\infty \log(n_1\|\vec{r}\|_1)), \\ |J| &\geq 3200\beta\mu_0r\kappa^2 \log^2(n_1n_3+n_2n_3) \geq 800\kappa^2 \log(n_1n_3+n_2n_3)\beta \cdot (2\mu_0\|\vec{r}\|_\infty \log(n_2\|\vec{r}\|_1)). \end{aligned}$$

Additionally, the following statements hold by Theorem 4 and the condition that $\mu_{\mathcal{C}} \leq \frac{25}{4}\kappa^2\mu_0$ and $\mu_{\mathcal{R}} \leq \frac{25}{4}\kappa^2\mu_0$:

i) Given $\mathcal{C} \in \mathbb{K}^{n_1 \times |J| \times n_3}$ with $\text{rank}(\mathcal{C}) = r$,

$$p_{\mathcal{C}} \geq \frac{1600\beta(n_1 + |J|)\mu_0 r \kappa^2 \log^2(n_1 n_3 + |J|n_3)}{n_1 |J|}$$

for some $\beta > 1$ ensures that \mathcal{C} is the unique minimizer to

$$\min_{\mathcal{X} \in \mathbb{K}^{n_1 \times |J| \times n_3}} \|\mathcal{X}\|_{\text{TNN}}, \quad \text{subject to } \mathcal{P}_{\Omega_{\mathcal{C}}}(\mathcal{X}) = \mathcal{P}_{\Omega_{\mathcal{C}}}(\mathcal{C}).$$

with probability at least $1 - \frac{3 \log(n_1 n_3 + |J|n_3)}{(n_1 n_3 + |J|n_3)^{4\beta-2}}$.

ii) Given $\mathcal{R} \in \mathbb{K}^{|I| \times n_2 \times n_3}$ with $\text{rank}(\mathcal{R}) = r$,

$$p_{\mathcal{R}} \geq \frac{1600\beta(n_2 + |I|)\mu_0 r \kappa^2 \log^2(n_2 n_3 + |I|n_3)}{n_2 |I|}$$

for some $\beta > 1$ ensures that \mathcal{R} is the unique minimizer to

$$\min_{\mathcal{X} \in \mathbb{K}^{|I| \times n_2 \times n_3}} \|\mathcal{X}\|_{\text{TNN}}, \quad \text{subject to } \mathcal{P}_{\Omega_{\mathcal{R}}}(\mathcal{X}) = \mathcal{P}_{\Omega_{\mathcal{R}}}(\mathcal{R}).$$

Once \mathcal{C} and \mathcal{R} are uniquely recovered from $\Omega_{\mathcal{C}}$ and $\Omega_{\mathcal{R}}$, respectively. Then t-CUR decomposition can provide the reconstruction of \mathcal{T} via $\mathcal{T} = \mathcal{C} * \mathcal{U}^\dagger * \mathcal{R}$ with the condition $\text{rank}_m(\mathcal{R}) = \text{rank}_m(\mathcal{C}) = \text{rank}_m(\mathcal{T})$.

Combining all the statements above, we can conclude that \mathcal{T} can be uniquely recovered from $\Omega_{\mathcal{C}} \cup \Omega_{\mathcal{R}}$ with probability at least

$$1 - \frac{2}{(n_1 n_3 + n_2 n_3)^{800\beta\kappa^2 \log(n_2)}} - \frac{3 \log(n_1 n_3 + |J|n_3)}{(n_1 n_3 + |J|n_3)^{4\beta-2}} - \frac{3 \log(n_2 n_3 + |I|n_3)}{(n_2 n_3 + |I|n_3)^{4\beta-2}}.$$

■

Appendix D. More numerical experiments

In this section, we include further empirical data demonstrating the convergence behavior of the ITCURTC algorithm within the t-CCS model framework. In this experiment, we form a low tubal-rank tensor $\mathcal{T} = \mathcal{A} * \mathcal{B} \in \mathbb{R}^{n_1 \times n_2 \times n_3}$ using two Gaussian random tensors, where $\mathcal{A} \in \mathbb{R}^{n_1 \times r \times n_3}$ and $\mathcal{B} \in \mathbb{R}^{r \times n_2 \times n_3}$. Our objective is to examine the convergence behavior of the ITCURTC algorithm under different conditions. For the simulations, we set $n_1 = n_2 = 768$ and $n_3 = 256$, and generate partial observations using the t-CCS model by adjusting the rank r and configuring the concentrated subtensors as $\mathcal{R} \in \mathbb{R}^{\delta n_1 \times n_2 \times n_3}$ and $\mathcal{C} \in \mathbb{R}^{n_1 \times \delta n_2 \times n_3}$, with $0 < \delta < 1$. For each fixed r , we maintain a constant overall sampling rate α .

Utilizing the observed data, the ITCURTC algorithm is then employed to approximate the original low tubal-rank tensor. The algorithm continues until the stopping criterion $\varepsilon_k \leq 10^{-6}$ is met, where ε_k represents the relative error between the estimate at the k -th iteration and the actual tensor, defined as $\varepsilon_k = \frac{\|\mathcal{T} - \hat{\mathcal{T}}_k\|_{\text{F}}}{\|\mathcal{T}\|_{\text{F}}}$.

For each specified set of parameters (r, δ, α) , we generate 10 different tensor completion scenarios. The mean relative errors ε_k , along with the specific configurations, are reported in Figure 8. One can see that ITCURTC can achieve an almost linear convergence rate.

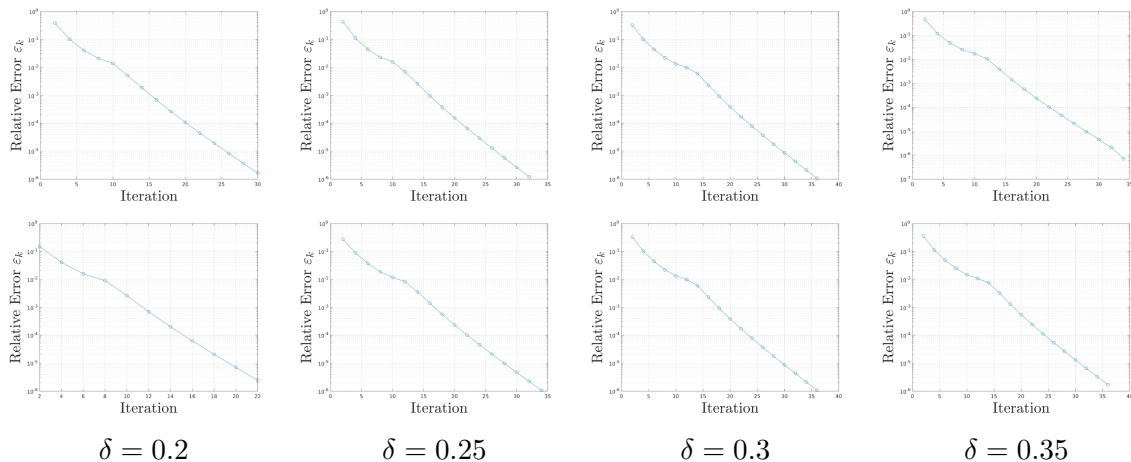


Figure 8: The averaged relative error of ITCURTC under the t-CCS model with respect to iterations over 10 independent trials. **1st row**: the overall sampling rate $\alpha = 0.15$ and tubal-rank $r = 2$. **2nd row**: $\alpha = 0.25$ and $r = 5$.

References

- [1] Benefits and risks of MRI. Benefits and Risks of MRI. Accessed: 2023-12-19.
- [2] Salman Ahmadi-Asl, Anh Huy Phan, Andrzej Cichocki, Anastasia Sozykina, Zaher Al Aghbari, Jun Wang, and Ivan Oseledets. Adaptive cross tubal tensor approximation. *arXiv:2305.05030*, 2023.
- [3] Andreas Argyriou, Theodoros Evgeniou, and Massimiliano Pontil. Convex multi-task feature learning. *Machine learning*, 73(3):243–272, 2008.
- [4] Haim Avron and Christos Boutsidis. Faster subset selection for matrices and applications. *SIAM Journal on Matrix Analysis and Applications.*, 34(4):1464–1499, 2013.
- [5] Aditya Bhaskara, Afshin Rostamizadeh, Jason Altschuler, Morteza Zadimoghaddam, Thomas Fu, and Vahab Mirrokni. Greedy column subset selection: New bounds and distributed algorithms. International Conference on Machine Learning, 2016.
- [6] Christos Boutsidis and David Woodruff. Optimal CUR matrix decompositions. *SIAM Journal on Computing*, 46(2):543–589, 2017.
- [7] HanQin Cai, Jian-Feng Cai, and Ke Wei. Accelerated alternating projections for robust principal component analysis. *Journal of Machine Learning Research*, 20(1):685–717, 2019.

- [8] HanQin Cai, Keaton Hamm, Longxiu Huang, and Deanna Needell. Mode-wise tensor decompositions: Multi-dimensional generalizations of CUR decompositions. *Journal of Machine Learning Research*, 22(185):1–36, 2021.
- [9] HanQin Cai, Keaton Hamm, Longxiu Huang, and Deanna Needell. Robust CUR decomposition: Theory and imaging applications. *SIAM Journal on Imaging Sciences*, 14(4):1472–1503, 2021.
- [10] HanQin Cai, Longxiu Huang, Pengyu Li, and Deanna Needell. Matrix completion with cross-concentrated sampling: Bridging uniform sampling and CUR sampling. *IEEE Transactions on Pattern Analysis and Machine Intelligence*, 2023.
- [11] Jian-Feng Cai, Raymond H Chan, and Zuowei Shen. A framelet-based image inpainting algorithm. *Applied and Computational Harmonic Analysis*, 24(2): 131–149, 2008.
- [12] Emmanuel Candès, Xiaodong Li, Yi Ma, and John Wright. Robust principal component analysis? *Journal of the ACM*, 58(3):1–37, 2011.
- [13] Juefei Chen, Yimin Wei, and Yanwei Xu. Tensor CUR decomposition under t-product and its perturbation. *Numerical Functional Analysis and Optimization*, 43(6):698–722, 2022. doi: 10.1080/01630563.2022.2056198.
- [14] Jiawei Chiu and Laurent Demanet. Sublinear randomized algorithms for skeleton decompositions. *SIAM Journal on Matrix Analysis and Applications.*, 34(3): 1361–1383, 2013.
- [15] Petros Drineas, Michael Mahoney, and S Muthukrishnan. Relative-error CUR matrix decompositions. *SIAM Journal on Matrix Analysis and Applications.*, 30(2):844–881, 2008.
- [16] Gregory Ely, Shuchin Aeron, Ning Hao, and Misha Kilmer. 5D seismic data completion and denoising using a novel class of tensor decompositions. *Geophysics*, 80:V83 – V95, 2015. ISSN 00168033.
- [17] Ajai Gaur and Sanjaya S Gaur. *Statistical methods for practice and research: A guide to data analysis using SPSS*. Sage, 2006.
- [18] Lars Grasedyck. Hierarchical singular value decomposition of tensors. *SIAM Journal on Matrix Analysis and Applications.*, 31(4):2029–2054, 2010.
- [19] Lars Grasedyck and Sebastian Krämer. Stable ALS approximation in the tt-format for rank-adaptive tensor completion. *Numerische Mathematik*, 143(4): 855–904, 2019.

- [20] Wolfgang Hackbusch and Stefan Kühn. A new scheme for the tensor representation. *Journal of Fourier analysis and applications*, 15(5):706–722, 2009.
- [21] Keaton Hamm. Generalized pseudoskeleton decompositions. *Linear Algebra and Its Applications*, 664:236–252, 2023.
- [22] Keaton Hamm and Longxiu Huang. Perspectives on CUR decompositions. *Applied and Computational Harmonic Analysis*, 48(3):1088–1099, 2020.
- [23] Keaton Hamm and Longxiu Huang. Stability of sampling for CUR decompositions. *Foundations of Data Science*, 2(2):83, 2020.
- [24] Frank Hitchcock. The expression of a tensor or a polyadic as a sum of products. *Journal of Mathematical Physics*, 6(1-4):164–189, 1927.
- [25] Yao Hu, Debing Zhang, Jieping Ye, Xuelong Li, and Xiaofei He. Fast and accurate matrix completion via truncated nuclear norm regularization. *IEEE Transactions on Pattern Analysis and Machine Intelligence*, 35(9):2117–2130, 2012.
- [26] Prateek Jain and Sewoong Oh. Provable tensor factorization with missing data. In *Advances in Neural Information Processing Systems*, volume 2, page 1431 – 1439, 2014.
- [27] Taixiang Jiang, Tingzhu Huang, Xile Zhao, Tengyu Ji, and Liangjian Deng. Matrix factorization for low-rank tensor completion using framelet prior. *Information Sciences*, 436:403–417, 2018.
- [28] Taixiang Jiang, Tingzhu Huang, Xile Zhao, and Liangjian Deng. Multi-dimensional imaging data recovery via minimizing the partial sum of tubal nuclear norm. *Journal of Computational and Applied Mathematics*, 372:112680, 2020.
- [29] Taixiang Jiang, Michael Kwok Po Ng, Xile Zhao, and Tingzhu Huang. Framelet representation of tensor nuclear norm for third-order tensor completion. *IEEE Transactions on Image Processing*, 29:7233–7244, 2020.
- [30] Hastad Johan. Tensor rank is NP-complete. *Journal of Algorithms*, 4(11):644–654, 1990.
- [31] Misha Kilmer and Carla Martin. Factorization strategies for third-order tensors. *Linear Algebra and Its Applications*, 435(3):641–658, 2011.
- [32] Misha Kilmer, Karen Braman, Ning Hao, and Randy C Hoover. Third-order tensors as operators on matrices: A theoretical and computational framework with applications in imaging. *SIAM Journal on Matrix Analysis and Applications.*, 34(1):148–172, 2013.

- [33] Misha Kilmer, Lior Horesh, Haim Avron, and Elizabeth Newman. Tensor-tensor products for optimal representation and compression. *arXiv:2001.00046*, 2019.
- [34] Xuelong Li and Yawei Pang. Deterministic column-based matrix decomposition. *IEEE Transactions on Knowledge and Data Engineering*, 22(1):145–149, 2010.
- [35] Ji Liu, Przemyslaw Musialski, Peter Wonka, and Jieping Ye. Tensor completion for estimating missing values in visual data. *IEEE Transactions on Pattern Analysis and Machine Intelligence*, 35(1):208–220, 2013. doi: 10.1109/TPAMI.2012.39.
- [36] Canyi Lu, Jiashi Feng, Yudong Chen, Wei Liu, Zhouchen Lin, and Shuicheng Yan. Tensor robust principal component analysis: Exact recovery of corrupted low-rank tensors via convex optimization. In *Proceedings of the IEEE conference on computer vision and pattern Recognition*, pages 5249–5257, 2016.
- [37] Canyi Lu, Jiashi Feng, Zhouchen Lin, and Shuicheng Yan. Exact low tubal rank tensor recovery from Gaussian measurements. In *Proc. 27th International Joint Conference on Artificial Intelligence*, pages 2504–2510, 2018.
- [38] Canyi Lu, Jiashi Feng, Yudong Chen, Wei Liu, Zhouchen Lin, and Shuicheng Yan. Tensor robust principal component analysis with a new tensor nuclear norm. *IEEE Transactions on Pattern Analysis and Machine Intelligence*, 42(04):925–938, apr 2020. ISSN 1939-3539. doi: 10.1109/TPAMI.2019.2891760.
- [39] Michael Mahoney and Petros Drineas. CUR matrix decompositions for improved data analysis. *Proceedings of the National Academy of Sciences of the United States of America*, 106(3):697–702, 2009.
- [40] Larsson Omberg, Gene H Golub, and Orly Alter. A tensor higher-order singular value decomposition for integrative analysis of DNA microarray data from different studies. *Proceedings of the National Academy of Sciences of the United States of America*, 104(47):18371–18376, 2007.
- [41] Ivan Oseledets. Tensor-train decomposition. *SIAM Journal on Scientific Computing*, 33(5):2295–2317, 2011.
- [42] Roger Peng and Elizabeth Matsui. *The Art of Data Science: A guide for anyone who works with Data*. Skybrude Consulting, LLC, 2015.
- [43] Jonathan Popa, Susan Minkoff, and Yifei Lou. An improved seismic data completion algorithm using low-rank tensor optimization: Cost reduction and optimal data orientation. *Geophysics*, 86(3):V219–V232, 2021.
- [44] Wenjin Qin, Hailin Wang, Feng Zhang, Jianjun Wang, Xin Luo, and Tingwen Huang. Low-rank high-order tensor completion with applications in visual data. *IEEE Transactions on Image Processing*, 31:2433–2448, 2022.

- [45] Benjamin Recht. A simpler approach to matrix completion. *Journal of Machine Learning Research*, 12(12), 2011.
- [46] Mohammad Mohammadpour Salut and David Anderson. Tensor robust CUR for compression and denoising of hyperspectral data. *IEEE Access*, 2023.
- [47] Parikshit Shah, Nikhil Rao, and Gongguo Tang. Sparse and low-rank tensor decomposition. In *Advances in Neural Information Processing Systems*, volume 28, 2015.
- [48] Andrews Sobral and Elhadi Zahzah. Matrix and tensor completion algorithms for background model initialization: A comparative evaluation. *Pattern Recognition Letters*, 96:22–33, 2017.
- [49] Guangjing Song, Michael Kwok Po Ng, and Xiongjun Zhang. Robust tensor completion using transformed tensor singular value decomposition. *Numerical Linear Algebra with Applications*, 27(3):e2299, 2020.
- [50] Guangjing Song, Michael Kwok Po Ng, and Xiongjun Zhang. Tensor completion by multi-rank via unitary transformation. *Applied and Computational Harmonic Analysis*, 65:348–373, 2023. ISSN 1063-5203. doi: <https://doi.org/10.1016/j.acha.2023.03.007>. URL <https://www.sciencedirect.com/science/article/pii/S1063520323000283>.
- [51] Davoud Ataee Tarzanagh and George Michailidis. Fast randomized algorithms for t-product based tensor operations and decompositions with applications to imaging data. *SIAM Journal on Imaging Sciences*, 11(4):2629–2664, 2018. doi: 10.1137/17M1159932.
- [52] Tian Tong, Cong Ma, Ashley Prater-Bennette, Erin Tripp, and Yuejie Chi. Scaling and scalability: Provable nonconvex low-rank tensor estimation from incomplete measurements. *Journal of Machine Learning Research*, 23(163):1–77, 2022.
- [53] Joel Tropp. Column subset selection, matrix factorization, and eigenvalue optimization. In *Proceedings of the Twentieth Annual ACM-SIAM Symposium on Discrete Algorithms*, pages 978–986. Society for Industrial and Applied Mathematics, 2009.
- [54] Joel Tropp. User-friendly tail bounds for sums of random matrices. *Foundations of Computational Mathematics*, 12:389–434, 2010.
- [55] Ledyard Tucker. Some mathematical notes on three-mode factor analysis. *Psychometrika*, 31(3):279–311, 1966.

- [56] Andong Wang and Zhong Jin. Near-optimal noisy low-tubal-rank tensor completion via singular tube thresholding. In *2017 IEEE International Conference on Data Mining Workshops (ICDMW)*, pages 553–560, 2017. doi: 10.1109/ICDMW.2017.78.
- [57] Shusen Wang and Zhihua Zhang. Improving CUR matrix decomposition and the nystrom approximation via adaptive sampling. *The Journal of Machine Learning Research*, 14(1):2729–2769, 2013.
- [58] Zhou Wang, Alan C Bovik, Hamid R Sheikh, and Eero P Simoncelli. Image quality assessment: from error visibility to structural similarity. *IEEE Transactions on Image Processing*, 13(4):600–612, 2004.
- [59] Yangyang Xu, Ruru Hao, Wotao Yin, and Zhixun Su. Parallel matrix factorization for low-rank tensor completion. *Inverse Probl Imaging*, 9(2):601–624, 2015. ISSN 1930-8337. doi: 10.3934/ipi.2015.9.601.
- [60] Shengke Xue, Wenyuan Qiu, Fan Liu, and Xinyu Jin. Low-rank tensor completion by truncated nuclear norm regularization. In *2018 24th International Conference on Pattern Recognition (ICPR)*, pages 2600–2605. IEEE, 2018.
- [61] Jinghua Yang, Xile Zhao, Tianhui Ma, Yong Chen, Tingzhu Huang, and Meng Ding. Remote sensing images destriping using unidirectional hybrid total variation and nonconvex low-rank regularization. *Journal of Computational and Applied Mathematics*, 363:124–144, 2020.
- [62] Feng Zhang, Jianjun Wang, Wendong Wang, and Chen Xu. Low-tubal-rank plus sparse tensor recovery with prior subspace information. *IEEE Transactions on Pattern Analysis and Machine Intelligence*, 43(10):3492–3507, 2020. doi: 10.1109/TPAMI.2020.2986773.
- [63] Lefei Zhang, Liangchen Song, Bo Du, and Yipeng Zhang. Nonlocal low-rank tensor completion for visual data. *IEEE Trans Cybern*, 51(2):673–685, 2019.
- [64] Zemin Zhang and Shuchin Aeron. Exact tensor completion using t-SVD. *IEEE Trans. Signal Process.*, 65(6):1511–1526, 2017. doi: 10.1109/TSP.2016.2639466.
- [65] Zemin Zhang, Gregory Ely, Shuchin Aeron, Ning Hao, and Misha Kilmer. Novel methods for multilinear data completion and de-noising based on tensor-SVD. In *Proceedings of the IEEE conference on computer vision and pattern Recognition*, pages 3842–3849, 2014.
- [66] Qibin Zhao, Liqing Zhang, and Andrzej Cichocki. Bayesian CP factorization of incomplete tensors with automatic rank determination. *IEEE transactions on pattern analysis and machine intelligence*, 37(9):1751–1763, 2015.

- [67] Xile Zhao, Jinghua Yang, Tianhui Ma, Taixiang Jiang, Michael Kwok Po. Ng, and Tingzhu Huang. Tensor completion via complementary global, local, and nonlocal priors. *IEEE Transactions on Image Processing*, 31:984–999, 2022. doi: 10.1109/TIP.2021.3138325.
- [68] Yubang Zheng, Tingzhu Huang, Xile Zhao, Taixiang Jiang, Tianhui Ma, and Tengyu Ji. Mixed noise removal in hyperspectral image via low-fibered-rank regularization. *IEEE Transactions on Geoscience and Remote Sensing*, 58(1): 734–749, 2019.
- [69] Pan Zhou, Canyi Lu, Zhouchen Lin, and Chao Zhang. Tensor factorization for low-rank tensor completion. *IEEE Transactions on Image Processing*, 27(3): 1152–1163, 2017.